



***IN VIVO* QUANTIFICATION OF METABOLIC ACTIVITY
IN AORTIC ANEURYSMS USING PET**

**A thesis submitted as part of the requirements for degree of MD (Res), University
College London**

Carl Willem Kotze MBChB, MRCS

January 2015



DECLARATION OF ORIGINALITY

I, Carl Willem Kotze, confirm that the work presented in this thesis is my own. Where information has been derived from other sources, I confirm that this has been indicated in the thesis.

Carl Willem Kotze [MD (Res) candidate]

Table of Contents

DECLARATION OF ORIGINALITY	2
ABSTRACT	8
THE AIMS OF THE THESIS	10
PUBLICATIONS, PRESENTATIONS & AWARDS	11
DEDICATION	15
ACKNOWLEDGEMENTS.....	16
LIST OF ABBREVIATIONS.....	18
LIST OF FIGURES	23
LIST OF TABLES	25
SECTION I INTRODUCTION	26
CHAPTER 1. AORTIC ANEURYSM PATHOGENESIS	26
1.1. MORPHOLOGY OF AORTIC ANEURYSM.....	29
1.1.1. <i>Classification.....</i>	29
1.1.2. <i>Shape and tortuosity.....</i>	29
1.1.3. <i>Diameter.....</i>	29
1.1.4. <i>Expansion rates.....</i>	30
1.1.5. <i>Calcification.....</i>	31
1.2. STRUCTURAL CONSIDERATIONS IN AORTIC ANEURYSM	32
1.2.1. <i>Elastin</i>	34
1.2.2. <i>Collagen.....</i>	34
1.2.3. <i>Vascular smooth muscle cells (VSMCs).....</i>	34
1.2.4. <i>Experimental and clinical studies</i>	35
1.3. MOLECULAR GENETICS IN AORTIC ANEURYSM.....	36
1.3.1. <i>Historical background</i>	37
1.3.2. <i>Genetics considerations</i>	37
1.4. HAEMODYNAMIC FACTORS AND BIOMECHANICAL WALL STRESS	
CONSIDERATIONS IN AORTIC ANEURYSM	38
1.4.1. <i>Haemodynamic forces.....</i>	38
1.4.2. <i>Haemodynamic forces effect on aneurysm expansion.....</i>	39

1.4.3.	<i>Haemodynamic forces effect on aneurysm rupture</i>	40
1.4.4.	<i>Current limitations</i>	40
1.5.	ENZYMATIC ACTIVITY IN AORTIC ANEURYSM	40
1.5.1.	<i>Experimental and clinical studies</i>	41
1.5.2.	<i>Gelatinases</i>	41
1.5.3.	<i>Elastases</i>	42
1.5.4.	<i>Collagenases</i>	43
1.5.5.	<i>Inhibition of MMPs</i>	43
1.6.	INFLAMMATORY CHANGES IN AORTIC ANEURYSM.....	44
1.6.1.	<i>Experimental and clinical studies</i>	45
1.6.2.	<i>Inflammatory cells involved in aortic aneurysm</i>	46
1.6.3.	<i>Infection and aortic aneurysm</i>	49
1.6.4.	<i>Vasculitides and aortic aneurysm</i>	49
1.6.5.	<i>Aortitis</i>	50
1.6.6.	<i>Inflammatory aortic aneurysm</i>	50
1.6.7.	<i>Rupture and inflammation</i>	51
1.6.8.	<i>Reactive oxygen species and aortic aneurysm</i>	52
1.7.	RISK FACTORS IN AORTIC ANEURYSM.....	52
1.7.1.	<i>Family history</i>	52
1.7.2.	<i>Age</i>	52
1.7.3.	<i>Gender</i>	53
1.7.4.	<i>Hypertension</i>	53
1.7.5.	<i>Diabetes</i>	53
1.7.6.	<i>Smoking</i>	54
1.7.7.	<i>Aortic dissection</i>	55
1.7.8.	<i>Atherosclerosis</i>	55
1.8.	INTRALUMINAL THROMBUS (ILT) IN AORTIC ANEURYSM.....	56
1.9.	SUMMARY OF AORTIC ANEURYSM PATHOBIOLOGY	57
CHAPTER 2. IMAGING VESSEL WALLS		59
2.1.	INTRODUCTION.....	59
2.1.1.	<i>Nuclear based molecular application</i>	60
2.1.2.	<i>Ultrasound-based molecular imaging applications</i>	62
2.1.3.	<i>MRI-based molecular application</i>	63

2.1.4.	<i>Spectral CT molecular imaging</i>	64
2.1.5.	<i>Summary of vascular imaging techniques</i>	65
2.2.	HISTORY OF PET / HYBRID PET/CT.....	65
2.3.	PET TRACERS IN RELATION TO ATHEROMA.....	67
2.3.1.	<i>¹⁸F-fluorodeoxyglucose (¹⁸F-FDG)</i>	68
2.3.2.	<i>¹¹C or ¹⁸F-choline</i>	69
2.3.3.	<i>Radiogallium-labelled compounds</i>	69
2.3.4.	<i>Tracers in experimental phase</i>	70
2.4.	STANDARDIZED UPTAKE VALUE (SUV).....	73
2.5.	SUVMAX , SUVMEAN AND TARGET-TO-BACKGROUND RATIO.....	74
2.6.	WHOLE-VESSEL SUV.....	74
2.7.	PET/CT LIMITATIONS.....	75
2.8.	ETHICAL APPROVAL.....	76
SECTION II ORIGINAL WORK		77
CHAPTER 3. ABDOMINAL AORTIC ANEURYSM METABOLIC ACTIVITY DETECTED BY 18F-FLUORODEOXYGLUCOSE (18F-FDG) POSITRON EMISSION TOMOGRAPHY/COMPUTED TOMOGRAPHY (PET/CT)		77
3.1.	INTRODUCTION.....	77
3.2.	MATERIALS AND METHODS.....	78
3.2.1.	<i>Patients</i>	78
3.2.2.	<i>Protocol for ultrasound surveillance</i>	81
3.2.3.	<i>Protocol for FDG-PET/CT</i>	82
3.2.4.	<i>Image analysis</i>	82
3.2.5.	<i>Calcification quantification</i>	83
3.2.6.	<i>Statistical analysis</i>	83
3.3.	RESULTS.....	84
3.3.1.	<i>Relationship between clinical characteristics and ¹⁸F-FDG Uptake</i>	84
3.3.2.	<i>Relationship between anatomical characteristics and ¹⁸F-FDG Uptake</i>	85
3.3.3.	<i>Optimum circulation time for ¹⁸F-FDG</i>	85
3.4.	DISCUSSION.....	86

CHAPTER 4. RELATIONSHIP BETWEEN ¹⁸F-FDG AORTIC ANEURYSM UPTAKE ON PET/CT AND ANEURYSM GROWTH RATE 92

4.1. INTRODUCTION..... 92

4.2. MATERIAL AND METHODS 93

 4.2.1. *Patients*..... 93

 4.2.2. *Duplex ultrasound image acquisition* 93

 4.2.3. *PET/CT image acquisition*..... 94

 4.2.4. *Image analysis*..... 95

 4.2.5. *Statistical analysis*..... 96

4.3. RESULTS..... 96

 4.3.1. *Aortic ¹⁸F-FDG uptake and ultrasound measurements* 96

 4.3.2. *PET interobserver agreement* 98

4.4. DISCUSSION..... 98

CHAPTER 5. INVESTIGATING AA CT TEXTURAL ANALYSIS AND ¹⁸F-FDG UPTAKE ON PET/CT AND FUTURE GROWTH RATE..... 102

5.1. INTRODUCTION..... 102

5.2. MATERIALS AND METHODS 103

 5.2.1. *Patients*..... 103

 5.2.2. *PET/CT image acquisition*..... 103

 5.2.3. *CT texture analysis*..... 104

 5.2.4. *PET/CT image analysis*..... 107

 5.2.5. *Duplex ultrasound image acquisition* 108

 5.2.6. *Statistical analysis*..... 108

5.3. RESULTS..... 109

 5.3.1. *Texture-metabolic association for AAA* 110

 5.3.2. *Aortic CTTA and future AAA expansion* 112

 5.3.3. *Texture analysis comparison between aneurysmal and normal aorta.* 115

 5.3.4. *Inter-observer variability for whole aneurysm CTTA*..... 116

 5.3.5. *Aortic ¹⁸F-FDG uptake and future AAA expansion* 117

 5.3.6. *Diagnostic criteria for imaging parameters to identify significant AAA expansion*..... 117

5.4. DISCUSSION..... 118

CHAPTER 6. RELATIONSHIP BETWEEN SERUM BIOMARKERS AND ¹⁸F-FDG AORTIC ANEURYSM UPTAKE ON PET/CT	123
6.1. INTRODUCTION.....	123
6.2. MATERIALS AND METHODS	124
6.2.1. <i>Patients and baseline characteristics</i>	124
6.2.2. <i>PET/CT image acquisition</i>	125
6.2.3. <i>PET/CT image analysis</i>	125
6.2.4. <i>Biomarker measurements</i>	126
6.2.5. <i>Statistical analysis</i>	127
6.3. RESULTS.....	127
6.3.1. <i>Clinical factors and associations with serum biomarkers</i>	127
6.3.2. <i>Increased levels of hsMMP-9 & hsMMP-2 were observed in AAA subjects compared to controls</i>	129
6.3.3. <i>AAA wall FDG uptake does not correlate with levels of circulating inflammatory biomarkers</i>	130
6.4. DISCUSSION.....	130
CHAPTER 7. DISCUSSION	135
7.1. VASCULAR METABOLISM - ¹⁸ F-FDG HYBRID PET/CT UPTAKE IN AAA ...	135
7.2. RELATIONSHIP BETWEEN ¹⁸ F-FDG AORTIC ANUERYSM UPTAKE ON PET/CT AND ANUERYSM GROWTH RATE.....	136
7.3. INVESTIGATING AAA TEXTURE ANALYSIS AND ¹⁸ F-FDG UPTAKE ON PET/CT AND FUTURE GROWTH RATE.....	136
7.4. SERUM BIOMARKERS AND ¹⁸ F-FDG AAA UPTAKE ON PET/CT	137
CHAPTER 8. CONCLUSION AND FUTURE WORK.....	138
APPENDIX	139
REFERENCES	143

ABSTRACT

Objective:

To investigate the role of hybrid ^{18}F -FDG PET/CT as a potential risk-stratification tool of aneurysm expansion by measuring metabolic activity on PET and textural analysis on CT in abdominal aortic aneurysm (AAA). Histological markers of AAA wall inflammatory cell infiltrate and enzymatic degradation have been associated with increased ^{18}F -Fluorodeoxyglucose (^{18}F -FDG)-Positron Emission Tomography /Computed Tomography (PET/CT) uptake.

Methods:

Fifty patients with asymptomatic infrarenal AAA enrolled under surveillance at one of our institutions underwent ^{18}F -FDG-PET/CT. Seventeen subjects were investigated for increased glycolysis in the AAA wall and optimal circulation imaging time for ^{18}F -FDG. In 25 subjects the relationship between aneurysm metabolic activity and expansion was explored. Forty subjects had AAA CT textural analysis (CTTA) parameters performed on the CT component of PET/CT and were studied in relation to aneurysm expansion. Twenty-four subjects had circulating biomarkers analysed. Whole vessel assessment, region of interest analysis and the role of correcting for background blood pool activity were explored.

Results:

Thirteen of seventeen subjects investigated for increased ^{18}F -FDG uptake had an AAA wall SUVmax > 2.5. In 17 subjects assessed for optimal circulation imaging time for ^{18}F -FDG, no significant advantage in imaging at 3h over 1h after ^{18}F -FDG injection was observed. ^{18}F -FDG uptake correlated inversely with future AAA expansion in the preliminary group of 25 patients and in 40 subjects who also had CTTA. In subjects who had CTTA, coarse texture showed an inverse association with ^{18}F -FDG uptake and medium coarse texture correlated with future AAA expansion. In 24 AAA patients who had serum biomarker assays, significantly higher levels of high sensitivity matrix metalloproteinase-9 (hsMMP-9) and hsMMP-2 compared to healthy controls were found. There was no correlation between AAA ^{18}F -FDG uptake and levels of hsMMP-9, hsMMP-2, hs-interferon- γ and hs-C-reactive protein.



Conclusions:

In-vivo ^{18}F -FDG PET/CT data indicated that small AAA show increased glucose metabolism. Relationships between AAA ^{18}F -FDG uptake, CTTA and future expansion were identified. AAA ^{18}F -FDG PET/CT shows potential to identify subjects at risk of significant expansion. AAA metabolism may not relate to serum levels of certain inflammatory biomarkers.



THE AIMS OF THE THESIS

The pathobiology of aortic aneurysm is both complex and multifactorial with inflammation suggested as a major central factor in AAA formation and progression. FDG PET/CT of metabolic activity currently represents a promising imaging modality for detecting vascular metabolic activity. However the optimum tracer and technique of PET/CT and its clinical role remains to be established.

The primary aim of the thesis was to explore the role of hybrid PET/CT in imaging AAA metabolic activity. The secondary aims were to investigate the relationships between aneurysmal wall tracer uptake and textural analysis of CT, serum biomarkers of inflammation and aneurysm growth rate.

PUBLICATIONS, PRESENTATIONS & AWARDS

Oral presentation

European Society for Vascular Surgery meeting, Amsterdam, Netherlands 6-9 September 2010 and published in ESVS Abstract Book 2010, p 125

¹⁸F-FDG aortic uptake on PET/CT is inversely associated with future growth rate.

(**Kotze CW**, Groves AM, Menezes LJ, Harvey R, Endozo R, Kayani IA, Ell PJ, Yusuf SW.)

Posters

ASGBI Meeting, Liverpool, 9-13 May 2012

Investigating Abdominal Aortic Aneurysms Texture Analysis, ¹⁸F-FDG PET Uptake and Future Growth Rate.

(**Kotze CW**, Menezes L, Endozo R, Hutton B, Ell P, Yusuf SW, Groves AM.)

International Society of Magnetic Resonance meeting, Stockholm, Sweden, 1-7 May 2010

Diffusion weighted imaging of carotid atherosclerotic plaque in symptomatic patients at 3-tesla: correlation with MRI, CT & histopathological predictors of plaque vulnerability.

(Taylor NJ, Goh VJ, Stirling JJ, Simcock I, Orton M, Collins DJ, Strecker R, Menezes L, Cross J, **Kotze CW**, Yusuf SW, Groves AM.)

ASGBI meeting, Liverpool, 14-16 April 2010

Assessing Abdominal Aortic Aneurysms Using ¹⁸F-FDG PET/CT. Comparison of ¹⁸F-FDG Uptake in Patients Undergoing Routine Surveillance *Versus* Patients Presenting with Large Aneurysms Prior to Surgery.

(**Kotze CW**, Harvey R, Groves AM, Menezes L, Endozo R, Hutton B, Shastry M, Ell P, Yusuf SW.)

Vascular Society Annual Scientific Meeting, Liverpool, 18-20 November 2009.

Study on carotid plaque with dynamic contrast enhanced 3-T MRI scan.

(Menezes L, **Kotze CW**, Goh V, Taylor J, Cross J, Rodriguez-Justo M, Collins D, Stirling J, Rocha R, Orton M, Wong W, Mohan H, Ell P, Groves A, Yusuf S.)

International Society of Magnetic Resonance meeting, Honolulu, Hawaii, 7-9 May 2009

Assessment of the Neovascularisation of Carotid Atherosclerotic Plaque in Symptomatic Patients at 3T by DCE-MRI: Feasibility Study.

(Taylor NJ, Goh VJ, Stirling JJ, Simcock I, Orton M, Collins DJ, Strecker R, Menezes L, Cross J, **Kotze CW**, Yusuf SW, Groves AM.)

European Society for Vascular Surgery meeting, Nice, France 4-7 September 2008

(Winner of Poster Prize)

Abdominal Aortic Aneurysm Inflammation Detected by ¹⁸F-fluorodeoxyglucose (¹⁸F-FDG) Positron Emission Tomography/ Computed Tomography.

(**Kotze CW**, Menezes LJ, Endozo R, Groves AM, Ell PJ, Yusuf SW.)

Book chapter

Etiology, Pathogenesis and Pathophysiology of Aortic Aneurysms and Aneurysm rupture. Etiology and Pathogenesis of Aortic Aneurysm July 2011.

InTech Publishers

Kotze CW; Ahmed IG.

Original papers

CT signal heterogeneity of abdominal aortic aneurysm as a possible predictive biomarker for expansion.

Atherosclerosis. 2013 [In Press].

(Kotze CW, Rudd JHR, Ganeshan B, Menezes LJ, Brookes J, Agu O, Yusuf SW, Groves AM.)

Investigating Vulnerable Atheroma Using Combined ¹⁸F-FDG PET/CT Angiography of Carotid Plaque with Immunohistochemical Validation.

J Nucl Med. 2011 Nov; **52**(11): 1698-1703

(Menezes LJ, **Kotze CW**, Agu O, Richardson T, Brookes J, Goh V, Harvey R, Endozo R, Kayani IA, Yusuf SW, Ell PJ, Groves AM.)

What is the relationship between ^{18}F -FDG aortic aneurysm uptake on PET/CT and future growth rate?

Eur J Nucl Med Mol Imaging. 2011 Aug; **38** (8): 1493-9.

(**Kotze CW**, Groves AM, Menezes LJ, Harvey R, Endozo R, Kayani IA, Ell PJ, Yusuf SW.)

Abdominal Aortic Aneurysm Inflammation Detected by ^{18}F -fluorodeoxyglucose (^{18}F -FDG) Positron Emission Tomography/ Computed Tomography (PET/CT).

Eur J Vasc Endovasc Surg. 2009 Jul; **38** (1):93-9.

(**Kotze CW**, Menezes L J, Endozo R, Groves AM, Ell P J, Yusuf SW.)

Vascular Inflammation Imaging with ^{18}F -FDG PET/CT: When to Image?

J Nucl Med. 2009 Jun; **50** (6):854-7.

(Menezes LJ, **Kotze CW**, Endozo R, Groves A M, Ell PJ, Yusuf SW.)

Abstracts

Peri-operative anti-platelet therapy guided by point of care (POC) platelet function tests in patients undergoing cardiac or vascular surgery.

Br J Surg 2009; **96** (Suppl 1): 2

(**Kotze CW**, Sepehrpour S, Harvey NH, Cheek E, Harper MC, Hutchinson NP, Kong RC, Yusuf SW.)

Letter

Letter to J Nucl Med in response to: ‘Vascular Imaging with FDG PET/CT - optimal FDG circulation time?’

J Nucl Med. 2009 Aug; E-pub

(**Kotze CW**, Menezes LJ, Endozo R, Groves AM, Ell PJ, Yusuf SW.)

Submitted

Serum biomarkers and ^{18}F -FDG aortic aneurysm uptake on PET/CT assessing relationships

(**Kotze CW**, Mohamed-Ali V, Menezes LJ, Ell PJ, Yusuf SW, Groves AM.)



Correlation of aortic inflammation assessed by ^{18}F -FDG, macrophage activity by ^{68}Ga -Dotatate PET, and vascular calcification: a dual tracer PET/CT study
(**Kotze CW**, Rudd JHF, Menezes LJ, Shortman RI, Yusuf SW, Groves AM.)



DEDICATION

I thank my God and Father for this opportunity to grow and for the strength and ability throughout this journey to complete this work.

I dedicate this thesis to my loving beautiful wife, Belinda, and our two sons, Joel and Judah, born to us during preparation of this work. Belinda, I thank you for your love and support in this season, your encouragement, words of wisdom and belief, that inspired me to be who I am. I value you and thank our God for you. Joel and Judah, you are the joy of my heart. I love you both dearly.

ACKNOWLEDGEMENTS

The work was carried out during my appointment as Surgical Research and Teaching Fellow affiliated to Brighton and Sussex Medical School, Royal Sussex University Hospitals NHS Trust and in the Department of Nuclear Medicine, University College Hospital, London. Supervision of the thesis was carried out by Prof Ashley M Groves, professor in nuclear medicine (Metabolism and Experimental Therapeutics) and consultant radiologist, Prof Brian Hutton, professor in nuclear medicine (Biomedical Imaging) at University College Hospital, and external supervisor, Mr S Waqar Yusuf, consultant vascular surgeon at Royal Sussex County Hospital, Brighton.

I thank my primary and secondary supervisors, Prof Ashley Groves and Prof Brian Hutton, for their input, guidance and support. You have challenged me to think laterally and have led by example. Furthermore, I thank my external supervisor, Mr Yusuf, for mentoring me through his coaching leadership style, and inspiring me to excel. I respect and value your input and advice. You have inspired belief and confidence in me.

Under the direction of my supervisors, I designed and conducted the work. I recruited most of the study patients. The PET/CT scans were performed by dedicated nuclear medicine radiographers at UCLH. I performed all the PET/CT uptake measurements of AAA apart from the initial preliminary work measurements.

I thank Dr Menezes, a dual accredited radiologist/nuclear medicine physician with a special interest in cardiovascular imaging, who supervised me in performing PET/CT uptake measurements. Dr Menezes also repeated measurements to record inter-observer variation for the chapter on ^{18}F -FDG and future aneurysm growth. I thank Balaji Ganeshan for familiarizing me with CT textural analysis and his support in answering my questions.

I also thank Dr. Vidya Mohamed-Ali, senior lecturer, Adipokines and Metabolism Research Group and her team, who helped me perform the serum biomarkers assays.



Specialist vascular scientists, with greater than three years' experience, performed the surveillance ultrasound scans (Philips, HDI 5000, C5-2, Curved Linear Probe).

I am grateful to Mrs Stephanie Goubet, biostatistician, BSMS Research & Development Department, Mr David Crook, principal research advisor, Health and Social Sciences, Mrs Elizabeth Cheek, senior lecturer, Computing, Engineering & Mathematics, University of Brighton and Dr Gareth Ambler, biostatistician, Joint UCLH/UCL Research & Development Department, for statistical support and advice.

I thank all the team members of the Vascular Unit, Royal Sussex County Hospital, Brighton, and of the Nuclear Medicine Unit, University College Hospital, London, for contributing to this work.

This work was part funded by the Sussex Stroke and Circulation Fund and the Royal College of Radiologists. UCLH/UCL receives a proportion of funding from the Department of Health's NIHR Biomedical Research Centre's funding scheme.

LIST OF ABBREVIATIONS

AA = aortic aneurysm
AAA = abdominal aortic aneurysm
ABPI = ankle brachial pressure index
ACE = angiotensin converting enzyme
ADAM = aneurysm detection and management
ANA = antinuclear antibody
ANOVA = analysis of variance
AOD = aortic occlusive disease
AP = anteroposterior
APC = antigen presenting cell
Apo-A1 = apolipoprotein A1
ApoE = apolipoprotein E
AR = arbitrary units
ARE = antioxidant response element
AUC = area under the curve
B-blockers = beta blockers
BGO = bismuth-germanate
C pneumoniae = Chlamydomphila pneumoniae
CABG = coronary artery bypass grafting
CAD = coronary heart disease
CI = confidence interval
CK = Carl Kotze
cm = centimetre
CMR = contrast-enhanced magnetic resonance
COPD = chronic obstructive pulmonary disease
CRP = C-reactive protein
CT = computed tomography
CTTA = computer tomography texture analysis
CVA = cerebral vascular accident
df = degrees of freedom
DTC = well-differentiated thyroid tumours

ECM = extracellular matrix
EGFR = epidermal growth factor receptor
ELISA = enzyme-linked immunosorbent assay
ESR = erythrocyte sedimentation rate
F = female
 ^{18}F -DOPA = ^{18}F -fluorodihydroxyphenyl-L-alanine
 ^{18}F -FBM = ^{18}F -fluorobromo-methane
 ^{18}F -FCH = fluoromethyl-dimethyl-2-hydroxyethyl-ammonium or ^{18}F - choline
FDA = Food and Drug Administration
FDG = fluorodeoxyglucose
 ^{18}F -FDG = ^{18}F -fluorodeoxyglucose
FEA = finite element analysis
 ^{18}F -FMCH = ^{18}F -fluoromethylcholine
 ^{18}F -FMISO = ^{18}F – fluoromisonidazole
 ^{18}F galacto- RGD = ^{18}F - glycosylated RGD-peptide
 ^{67}Ga -citrate = gallium citrate
 ^{68}Ga = gallium 68
GCA = giant cell arteritis
GLUT = glucose transporter
h = hour
HCFA = Health Care Financing Administration
Her2Neu = human epidermal growth factor receptor 2
HO-1 = hemoxygenase
HU = Hounsfield units
hsCRP = high sensitivity C-reactive protein
hsIFN- γ = high sensitivity interferon-gamma
hsMMP-2 = high sensitivity MMP-2
hsMMP-9 = high sensitivity MMP-9
HSS = highest single site
IAAA = inflammatory abdominal aortic aneurysm
ICAM-1 = intercellular adhesion molecule-1
ID = identification
IEL = internal elastic lamina

IgG = immunoglobulin
IHC = immunohistochemistry
IL = interleukin
ILD = inflammatory lung disease
ILT = intraluminal thrombus
IFN- γ = interferon gamma
IQR = interquartile range
IV = intravenous
K = kurtosis
kBq/g = kilobecquerel per gram
kVp = peak kilovoltage
LDL = low-density lipoprotein
LS = laminar shear stress
LSO = lutetium oxyorthosilicate
M = male
mA = milliamperage
MBq = megabecquerel
mg/dL = milligrams per decilitre
MHC = major histocompatibility
MI = mechanical index
mm = millimetre
MMP = matrix metalloproteinase
MRI = magnetic resonance imaging
mSv = millisievert
n = sample size
N = population size
NET = neuroendocrine tumour
NIHR = National Institute for Health Research
O₂⁻ = superoxide
OS = oscillatory and low mean shear stresses
OSEM = ordered subsets expectation maximization
ox-LDL-c = oxidized low-density cholesterol
p = probability p-value
PAI-1 = plasminogen activator inhibitor-1

PET = positive emission tomography
PET/CT = positron emission tomography / computed tomography
PG = prostaglandin
POC = point of care
PPARS = peroxisome proliferator-activated receptor agonists
PVD = peripheral vascular disease
Q = average activity per unit volume
r = Pearson correlation coefficient
 r_s = Spearman rank correlation
ROC = receiver-operating-characteristic
ROI = region of interest
ROS = reactive oxygen species
rpm = revolutions per minute
s = second
SD = standard deviation
SE = standard error
SMC = smooth muscle cell
SMS = somatostatin
SSTR-2 = somatostatin receptor
SUV = standardized uptake value
 SUV_{max} = maximum standardized uptake value
 SUV_{mean} = mean standardized uptake value
SPIO = superparamagnetic iron oxide
SPECT = single photon emission computed tomography
SPSS = Statistical Product and Service Solutions
SSTR = somatostatin receptor
t = Student's t distribution
TA = Takayasu's arteritis
TAA = thoracic aortic aneurysm
TBR = target to background ratio
 TBR_{max} = maximum target to background ratio
 TBR_{mean} = mean target to background ratio
TGF- β 1 = transforming growth factor beta-1
TGV = total glycolytic volume

TIMP-1 = tissue inhibitor of metalloproteases-1
TNF- α = tumour necrosis factor alpha
tPA = tissue plasminogen activator
TSPO = translocator protein/peripheral benzodiazepine receptor
UCA = ultrasound contrast agent
UCL = University College London
UCLH = University College London Hospital
UK = United Kingdom
UKSAT = the UK Small Aneurysm Trial
U/S = ultrasound
USPIO = ultra-small superparamagnetic particles of iron oxide
uPA = urokinase-type plasminogen activator
VCAM-1 = vascular cell adhesion molecule-1
VSMC =vascular smooth muscle cell
WBC = white blood cell
WI = Wisconsin
y = years
2D = two-dimensional
3D = three-dimensional
4D = four-dimensional

LIST OF FIGURES

FIGURE 1.1 CHAIN OF BIOLOGICAL EVENTS LEADING TO ABDOMINAL AORTIC ANEURYSM RUPTURE	33
FIGURE 1.2 SCHEMATIC DIAGRAM OF THE MECHANISMS IMPLICATED IN ABDOMINAL AORTIC ANEURYSM, WHICH PRIMARILY INVOLVE TWO MAIN PROCESSES: INFLAMMATION AND EXTRACELLULAR MATRIX TURNOVER	48
FIGURE 3.1 AXIAL PET IMAGE OF AN ABDOMINAL AORTIC ANEURYSM WITH REGIONS OF INTEREST (ROI) PLACED ON THE LUMEN (ROI1) AND THE WALL OF THE AORTA (ROI0)	83
FIGURE 3.2 SCATTER PLOT OF MAXIMUM STANDARD UPTAKE VALUES (SUV_{MAX}) OF ^{18}F -FLUORODEOXYGLUCOSE (^{18}F -FDG) ILLUSTRATING NO ASSOCIATION BETWEEN AAA SIZE AND FDG UPTAKE ($R_S=-0.006$; $P=0.96$)	85
FIGURE 3.3 AXIAL (A) UNENHANCED CT, (B) PET, AND (C) PET/CT FUSION OF AN AAA DEMONSTRATING ^{18}F -FDG CIRCULATING IN THE ARTERIAL AND VENOUS LUMENS AND NO UPTAKE IN THE WALL OF THE AORTA	90
FIGURE 3.4 AXIAL (A) UNENHANCED CT, (B) PET, AND (C) PET/CT FUSION OF AN AAA SHOWING UPTAKE IN THE LUMEN AND INCREASED UPTAKE IN THE WALL OF THE AORTA	91
FIGURE 4.1 AXIAL FUSED PET/CT (A) AND PET (B) IMAGES OF AN AAA SHOWING ^{18}F -FDG UPTAKE IN THE WALL OF THE AORTA (WHOLE VESSEL $SUV_{MAX}=3.35$; WHOLE VESSEL $TBR_{MAX}=1.60$)	94
FIGURE 4.2 AXIAL FUSED PET/CT (A) AND PET (B) IMAGES OF AN AAA SHOWING MINIMAL ^{18}F -FDG UPTAKE IN THE WALL OF THE AORTA	95
FIGURE 4.3 BAR CHART SHOWING THE CONSECUTIVE SERIES OF INDIVIDUAL SUBJECT'S AA EXPANSION OVER 12 MONTHS	97
FIGURE 4.4 SCATTER PLOT SHOWING RANKED CORRELATION BETWEEN ^{18}F -FDG UPTAKE ON BASELINE STUDY AGAINST EXPANSION AT 12 MONTHS ($R_S=-0.501$; $P=0.011$)....	98
FIGURE 5.1 COMPUTER TOMOGRAPHY TEXTURE ANALYSIS OF AAA WALL AND CONTENT - (A) CONVENTIONAL INFRA RENAL AAA CT IMAGE. (B-D) CORRESPONDING IMAGES SELECTIVELY DISPLAYING FILTRATION OF THE HISTOGRAM AT (B) FINE (2MM IN WIDTH), (C) MEDIUM (3-5MM IN WIDTH), AND (D) COARSE (6MM IN WIDTH) TEXTURE.	106

FIGURE 5.2 COMPUTER TOMOGRAPHY TEXTURE ANALYSIS OF AAA LUMINAL CONTENT INCLUDING THE BLOOD POOL AND INTRALUMINAL THROMBUS (AAA WALL EXCLUDED). (A) CONVENTIONAL INFRA RENAL AAA CT IMAGE. (B–D) CORRESPONDING IMAGES SELECTIVELY DISPLAYING FILTRATION OF THE HISTOGRAM AT (B) FINE (2MM IN WIDTH), (C) MEDIUM (3-5MM IN WIDTH), AND (D) COARSE (6MM IN WIDTH) TEXTURE.....	107
FIGURE 5.3 SCATTER PLOT OF WHOLE AAA METABOLIC ACTIVITY MEASURED AS SUV_{MAX} AND COARSE TEXTURE PARAMETER STANDARD DEVIATION (SD) (N=40). SPEARMAN CORRELATION COEFFICIENT R_s (WITH P-VALUE) BETWEEN THE TWO VARIABLES IS PRESENTED AT TOP RIGHT.....	111
FIGURE 5.4 SCATTER PLOT OF AAA EXPANSION AT 1Y AND MEDIUM COARSENESS TEXTURE PARAMETER KURTOSIS (K) (N=40). SPEARMAN CORRELATION COEFFICIENT R_s (WITH P-VALUE) BETWEEN THE TWO VARIABLES IS PRESENTED AT TOP RIGHT...	114
FIGURE 5.5 BOX PLOT SHOWING A SIGNIFICANT DIFFERENCE BETWEEN COARSE TEXTURE PARAMETER SD OF ANEURYSMAL COMPARED TO NORMAL AORTA (WILCOXON SIGNED RANK TEST, P=0.001)	116
FIGURE 5.6 SCATTER PLOT OF AAA EXPANSION AT 1Y ADJUSTED FOR BASELINE ANEURYSM SIZE AND WHOLE AAA METABOLIC ACTIVITY MEASURED AS SUV_{MAX} (N=40). SPEARMAN CORRELATION COEFFICIENT R_s (WITH P-VALUE) BETWEEN THE TWO VARIABLES IS PRESENTED AT TOP RIGHT.	117
FIGURE 6.1 SAGITTAL FUSED PET/CT IMAGE OF AN AAA SHOWING ^{18}F -FDG UPTAKE IN THE ANEURYSM	125
FIGURE 6.2 AORTIC WALL METABOLIC ACTIVITY VARIATIONS AMONG DIFFERENT RISK FACTOR GROUPS	128
FIGURE 6.3 HIGH SENSITIVITY METALLOPROTEINASE-9 VARIATIONS AMONG DIFFERENT RISK FACTOR GROUPS	129
FIGURE 6.4 BOX PLOT SHOWING HIGHER LEVELS OF CIRCULATING HIGH SENSITIVITY METALLOPROTEINASE-9 IN SUBJECTS COMPARED TO CONTROLS (P<0.001).....	130
FIGURE A1 THE 2-D FORMS OF THE LOG FILTER IN THE SPATIAL AND FREQUENCY DOMAIN AT EXTRACT MEDIUM TEXTURE	142
FIGURE A2 THE 2-D FORMS OF THE LOG FILTER IN THE SPATIAL AND FREQUENCY DOMAIN AT FILTER VALUE OF 2.0 (EXTRACT MEDIUM TEXTURE).....	142

LIST OF TABLES

TABLE 1.1 ANNUAL ESTIMATED RUPTURE RISK.....	30
TABLE 1.2 GENETIC DISEASE AND AORTIC ANEURYSM.....	38
TABLE 3.1 PATIENT DEMOGRAPHIC DATA	80
TABLE 3.2 PATIENT CHARACTERISTICS WITH NON-SPECIFIC AAAs UNDERGOING SURVEILLANCE.....	81
TABLE 3.3 DATA FOR SUV_{MAX} OF AORTIC WALL, AORTIC LUMEN, AND TBR_{MAX} AT EACH TIME-POINT AFTER INJECTION OF ^{18}F -FDG.....	86
TABLE 4.1 SUMMARY OF THE MEDICAL DETAILS OF THE PATIENT POPULATION	93
TABLE 5.1 SUMMARY OF THE MEDICAL DETAILS OF THE PATIENT POPULATION	109
TABLE 5.2 THE MEDIAN WHOLE AAA TEXTURE PARAMETERS AT FINE, MEDIUM AND COARSE FILTER LEVELS FOR STANDARD DEVIATION (SD) AND KURTOSIS (K)	110
TABLE 5.3 THE CORRELATION OF TEXTURE PARAMETERS KURTOSIS (K) AND STANDARD DEVIATION (SD) WITH METABOLIC ACTIVITY MEASURED AS FDG UPTAKE BEFORE AND AFTER ADJUSTING FOR CONFOUNDING CLINICAL FACTORS (BACK PAIN).....	112
TABLE 5.4 UNIVARIATE ANALYSIS OF CLINICAL FACTORS TO IDENTIFY CONFOUNDING FACTORS FOR AAA EXPANSION ADJUSTED FOR BASELINE AAA SIZE AND ANNUAL EXPANSION > 2MM	113
TABLE 5.5 THE CORRELATION OF TEXTURE PARAMETERS KURTOSIS (K) AND STANDARD DEVIATION (SD) WITH FUTURE GROWTH BEFORE AND AFTER ADJUSTING FOR CONFOUNDING CLINICAL FACTORS	115
TABLE 6.1 SUMMARY OF THE MEDICAL DETAILS OF THE PATIENT POPULATION AND CONTROL GROUP	124
TABLE 6.2 SUMMARY OF THE MEAN LEVELS OF STUDIED CIRCULATING BIOMARKERS ...	127
TABLE A1 FILTER VALUES AND THE CORRESPONDING WIDTHS OF THE FILTER IN MM	141

SECTION I INTRODUCTION

CHAPTER 1. AORTIC ANEURYSM PATHOGENESIS

Technological advances in molecular imaging have increased the possibilities for enhancing our understanding of the pathogenesis of abdominal aortic aneurysms (AAAs). AAA continues to pose a substantial health and economic burden, and is present in up to 10% of men between the ages of 65 and 79 years¹. Aneurysm rupture is associated with 80% mortality for patients reaching emergency hospital services and 50% for those deemed fit for emergency repair¹. Mortality rates for patients with ruptured aneurysms undergoing repair have remained unchanged for more than a decade². The current recommendation is for aneurysms larger than 5.5 cm to have elective intervention to prevent rupture¹.

Aortic aneurysm (AA) is defined as a localized dilation of the aorta greater than 50 % of its diameter, involving all the layers of the vessel wall³ or maximum external diameter of $\geq 3\text{cm}$ ⁴. Most AAAs are asymptomatic (although back pain and tenderness over the aneurysm have been described) and are detected as an incidental finding on ultrasonography, abdominal computed tomography or magnetic resonance imaging performed for other purposes. Approximately 30% of AAAs are diagnosed through clinical examination of the abdomen. Rupture and thromboembolic events are the complications most feared, with only approximately 20% of ruptured AA patients reaching emergency services alive. Peri-operative mortality for open and endovascular repair of AAA in the UK was reported at 7.9 % and 1.7 % respectively⁵.

An attempt has been made to improve peri-operative AAA repair mortality with the introduction in 2009 of a framework for improving the results of elective AAA repair⁶. The framework, which emphasizes the importance of risk stratification, advised that all patients should undergo standard preoperative assessment and risk scoring. Certainly, in the last decade we have witnessed a decrease in peri-operative mortality, predominantly as a result of endovascular repair being established as a preferred treatment for AA when feasible. Yet this comes at the cost of patients needing lifelong follow-up and higher re-intervention rates being reported.

The introduction of aneurysm screening programmes in North America and Europe has led to a greater awareness of this disease, with an increased number of new diagnoses. The United States Preventive Services Task Force recommended that men between the ages of 65 and 75 years who have ever smoked should be screened at least once for AAAs by abdominal ultrasonography⁷. The increase in surveillance is creating demand for further risk stratification whilst intensifying the need to develop strategies for retarding growth rate in small aneurysms.

In 2001, the Vascular Biology Research Program of the National Heart, Lung and Blood Institute summarized AAA pathogenic mechanisms into four broad areas: “proteolytic degradation of the aortic wall connective tissue, inflammation and immune response, molecular genetics and biomechanical wall stress”⁸. More recently, Nordon and colleagues investigated three possible models of AAA pathogenesis not mutually exclusive: “AAAs secondary to a local disease process confined to the abdominal aorta resulting from atherosclerosis; a systemic dilating diathesis primarily governed by genotype; and diseased vascular tree as a consequence of a chronic inflammatory process. They concluded that the evidence points to AAA disease being a systemic disease of the vasculature, with a predetermined genetic susceptibility leading to a phenotype governed by environmental factors”⁹. AAAs are therefore referred to by some researchers as a degenerative disease.

AAAs are associated with atherosclerosis, transmural degenerative processes, neovascularization, degeneration of vascular smooth muscle cells (VSMC), and chronic inflammation, mainly located in the outer aortic wall¹⁰. The variability of local haemodynamic factors and intrinsic characteristics along the arterial segment of aorta have also been suggested as important factors in aneurysm disease and progression¹¹. Observational evidence also suggests that intraluminal thrombus (ILT), together with adventitial angiogenic and immune responses, play important roles in the evolution of atherothrombosis from the initial stages through to clinical complications, which include the formation of aneurysms¹². The role of ILT in AA pathogenesis merits further discussion and will be explored later in this chapter.

The influence of reported AA risk factors is unknown. More AAAs are being diagnosed than ever before, despite efforts in smoking cessation and an increased incidence of

diabetes with a suggested protective benefit. Other factors commonly associated with aneurysm formation include family history, advanced age, male sex, hypertension, aortic dissection and arteriosclerosis. The significance of AA risk factors will be further explored in this chapter.

In developing the background to this thesis the following review will fall into nine areas:

- 1.1 Morphology
- 1.2 Structural considerations
- 1.3 Genetic concepts
- 1.4 Biomechanical concepts
- 1.5 Proteolytic considerations
- 1.6 Inflammation
- 1.7 Risk factors
- 1.8 Intraluminal thrombus
- 1.9 Summary

1.1. MORPHOLOGY OF AORTIC ANEURYSM

1.1.1. Classification

In general aneurysms are classified into true and false aneurysms. True aneurysms involve dilatation of all three layers of the vessel wall, namely, the intima, media and adventitia. All layers of the vessel wall are not involved with false or pseudo aneurysms, in which often an association with trauma has been described.

1.1.2. Shape and tortuosity

The most prevalent aneurysms are characterized by symmetrical enlargement of the whole circumference and are therefore referred to as *fusiform* aneurysms. Aneurysms that affect only segments of the arterial circumference are named *saccular* aneurysms. These eccentric aneurysms are more likely to rupture than fusiform aneurysms. Therefore, some researchers advocate that the evaluation of AAA rupture risk should be based on the accurate quantification of aneurysmal sac shape and size¹³. Interestingly, FEA analysis of an axisymmetric and fusiform AAA model found that maximum stress was a function of the shape of the AAA wall rather than its diameter¹⁴. In an FEA analysis of a non-aneurysmal model, Vorp *et al* also confirmed that wall stress was greatly dependent on the shape as well as the size of the aneurysm¹⁵. Fillinger *et al* observed that ruptured AAAs (matched for age, gender and diameter) are less tortuous with greater cross-sectional diameter asymmetry¹⁶. Furthermore, existent calcifications may influence AAA shape, thus AAA calcification should be considered in computational wall stress analyses¹⁷.

1.1.3. Diameter

Currently, the maximum diameter of the aneurysm is the cardinal determinant of AAA rupture and therefore used as surrogate for intervention. Contemporary information on the rupture risk of larger aneurysms has been derived from the non-surgical arm of the US aneurysm detection and management (ADAM) Veteran Affairs Cooperative Study¹⁸. In this study, which reported a substantial rupture rate for high-operative-risk patients with AAA of at least 5.5cm, the participant numbers were small (n=198). A

statement from the Joint Council of the American Association for Vascular Surgery and Society for Vascular Surgery¹⁹ estimated the annual rupture risk according to AAA diameter.

Table 1.1 Annual estimated rupture risk

<i>Initial aneurysm diameter</i>	<i>Annual risk of rupture (%)</i>
< 4.0	0
4.0-4.9	0.5 – 5
5.0–5.9	3 – 15
6.0–6.9	10 – 20
7.0–7.9	20 – 40
>8.0	30 – 50

A recent systematic review concluded that rupture rates of small AAAs appear to be low with a range between 0 to 1.61 ruptures per 100 person-years²⁰. However, most studies have been poorly reported and lacked clear ascertainment and diagnostic criteria for aneurysm rupture²⁰.

1.1.4. Expansion rates

A recent study identified a bimodal growth pattern for AAA, with a significant association between annual AAA expansion of 2 mm or more and future intervention or rupture²¹. Choke *et al* reviewed and reported on AAA expansion rates²². Risk of aortic rupture relates to both aneurysm size and the rate of expansion²³. This finding was confirmed by demonstrating a significantly greater mean AAA enlargement rate in patients with probable rupture than patients without rupture (75 vs 41 mm per year)¹⁸. Other researchers also reported increased mean and median expansion rates in patients with ruptured AAA compared to patients without rupture (84 vs 39 mm per year)²⁴. Expansion rate as an exponential function of initial aneurysm diameter has been suggested²⁵, and supported by other researchers^{23, 26-28}. It was observed that final aneurysm size was predicted by initial size, suggesting expansion rate was dependent on initial AAA diameter, so that 3–6cm diameter aneurysms expanded by 10% of their diameter per year²⁵. Limet *et al*²³ also reported more rapid growth in larger diameter

aneurysms (5.3mm/year for AAA diameters less than 40mm *versus* 7.4mm/year for AAA diameters of 50mm or more). Conversely, a large observational study of AAAs of 3.0cm to 3.9cm reported slow expansion with no rupture detected in 1445 patients²⁹. A large series of patients with similar aneurysm sizes but varying expansion rates would need to be followed without intervention in order to establish if expansion rate independently predicts rupture. Furthermore, it is well recognized that AAAs have periods of stability, and of gradual and accelerated growth, increasing the difficulty of predicting individual expansion rates³⁰. Other variables that have been shown to have a positive correlation with expansion rate are pulse pressure²⁵, systolic and diastolic blood pressures³¹ and smoking³². Interestingly, the ADAM (2002) study reported that diabetes was negatively associated with aneurysm expansion. A large cohort study reported lipid-lowering drug treatment and initial AAA diameter appear to be independently associated with lower AAA growth rates³³. Furthermore, A PET stand-alone study observed a possible association between increased ¹⁸F-FDG uptake and AAA expansion and rupture³⁴. This suggests that inflammation may be an important factor in aneurysm progression.

1.1.5. Calcification

Maier and co-workers defined calcifications as “heterogeneously distributed, non-fibrous, stiff plaques which are most commonly found near the luminal surface in between the intima and the media layer of the vessel wall”¹⁷. The relationship between atherosclerosis and vascular calcification is well known³⁵. A study of the thoracic aorta in cancer patients demonstrated ¹⁸F-FDG vascular uptake was common on PET/CT and correlated with vascular calcifications, although the specific sites rarely overlapped³⁶. This could suggest inflammation and calcification as different stages in the evolution of atheroma. Lindholt suggested that the calcification content in small AAA predicts the natural history of small AAA³⁷. This study conducted with serial ultrasound found the mean annual growth rate to be significantly lower in men with an AAA wall calcification above 50% compared with those having below 50% (1.72mm *versus* 2.97mm, p=0.001)³⁸. Other researchers have found no influence of aortic calcification on AAA expansion³⁹.

The relationship between calcification and AAA peak wall stress has been described⁴⁰.⁴¹. Calcification may decrease the biomechanical stability of aneurysmal aorta, since AAA calcification increases peak wall stress⁴⁰. However, some researchers are not convinced of an increased rupture risk for AAAs with a high calcium burden¹⁷. In contrast, it is also suggested that intraluminal thrombus decreases maximum wall stress in AAA. Therefore, calcification and intraluminal thrombus should both be taken into account when wall stress for risk assessment of AAA rupture is evaluated⁴⁰.

Furthermore, the location and shape of the calcified regions, not only the relative amount, are considerations that influence wall stress in AAA⁴¹. AAA calcification not only possibly influences expansion but also affects sac regression after repair⁴². The correlation between MMP-mediated elastin degradation and vascular calcification suggests inflammation as a major role-player in AAA calcification and pathogenesis⁴³.

1.2. STRUCTURAL CONSIDERATIONS IN AORTIC ANEURYSM

Multiple factors rather than a single process are implicated in AA pathogenesis. These factors result in damaging structural changes involving the media and adventitia of the aneurysm wall that eventually progress to aneurysm formation and potential rupture (Figure 1.1). The media consists of several elastic laminae and vascular smooth muscle cells (VSMCs) embedded in a ground substance, whereas fibroblasts, loose connective tissue, collagen fibres and vasa vasorum collectively form the adventitia. AAA wall integrity is dependent on a balanced remodelling of elastin, collagen and VSMCs as predominant constituents of the extracellular matrix (ECM)^{44, 45}.

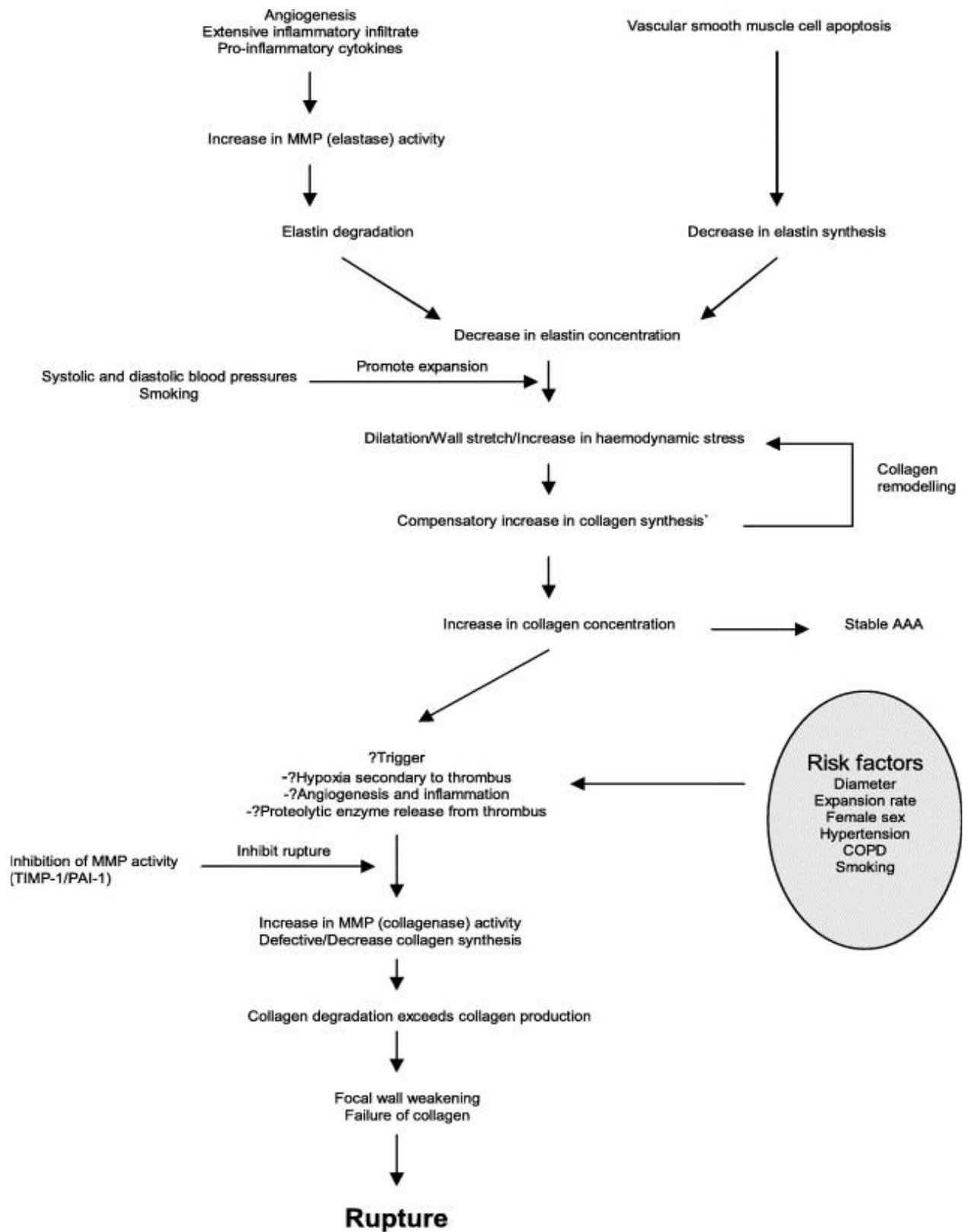


Figure 1.1 Chain of biological events leading to abdominal aortic aneurysm rupture

[Reproduced with kind permission from the Elsevier Publishing Group, Alexander et al. Figure 1.⁴⁶]

1.2.1. Elastin

The chief component of the media is elastin, a lamellar ECM protein consisting of soluble tropoelastin monomers. Elastin production by the VSMCs ceases when a patient reaches maturity, therefore these soluble tropoelastin monomers, which are cross-linked by lysine residues, have a half-life of 40 to 70y⁴⁷. This could explain the elderly predisposition to AA formation. Normally, more than 99% of total elastin in arteries is found in an insoluble cross-linked form that can be stretched as much as 70% of its initial length⁴⁸. Elastin is responsible for the load-bearing property that behaves uniformly in both the circumferential and longitudinal directions at different locations across the wall thickness, thereby absorbing oscillating arterial shock waves, providing recoil and maintaining arterial structure⁴⁹. Treatment with elastase causes lamellar disruption and, results in aneurysmal dilatation, thus emphasizing the importance of the lamellar structure in providing resilience to the aortic wall⁴⁸.

1.2.2. Collagen

Collagen is the dominant structural component of the arterial adventitia and to a lesser extent is found in the media. It is a stable triple helix composed of three polypeptide chains with repeating tripeptide sequences and is responsible for tensile strength and resistance of the vessel wall⁵⁰. In contrast to elastin, collagen is synthesized on a continual basis throughout life, so collagen content represents the net effect of synthesis and degradation⁵¹. Type 1 fibrillar collagen accounts for aortic wall load-bearing capability (over 20 times greater than that of elastin), while Type 3 collagen provides some extensile stretch⁵². Arterial distension in response to increasing intraluminal pressures is limited through the recruitment of inextensible collagen fibres⁵³. Structural damage occurs when collagen is extended beyond 2–4% from its uncoiled form⁵⁴.

1.2.3. Vascular smooth muscle cells (VSMCs)

VSMCs are important structural elements of the ECM that govern AA disease by producing transforming growth factor-beta (TGF-beta1), components of ECM and proteases^{55, 56}. VSMCs undergo morphological cell changes from a contractile to a synthetic phenotype to produce substances important in remodelling the vascular wall⁵⁵. This change in morphology is associated with a loss of myofilaments and the formation

of extensive rough endoplasmic reticulum and a large Golgi complex. This was verified by an experimental study that reported cultured VSMCs from AAAs exhibited greater elastolytic activity than VSMCs from aortic occlusive disease (AOD)⁵⁷. VSMC density depends on patient age, patient gender and the location of quantification in non-atherosclerotic aneurysms. Conversely, loss of VSMCs is a characteristic of atherosclerotic aortic aneurysms^{11, 58}. In particular VSMC apoptosis has been associated with fibrous cap thinning, enlargement of the necrotic core, plaque calcification, medial expansion and degeneration, elastin breaks, and failure of outward remodelling⁵⁹. In addition, chronic VSMC apoptosis may mimic multiple features of medial degeneration seen in a variety of human pathologies⁵⁹.

1.2.4. Experimental and clinical studies

Histological examination of aneurysms reveals a thinning of the media, disruption of the medial connective tissue structure, and the loss of elastin⁶⁰ culminating in the effacement of the lamellar architecture⁶¹. The role of the aortic media in contributing to wall stability is emphasized through studies demonstrating AA formation following media destruction with surgical resection, freezing, or the injection of acetrizate or other noxious agents⁶².

Other studies confirmed that both elastin and collagen content is decreased in AA walls with increased collagen cross-links⁶³ and an increased collagen to elastin ratio⁶⁴. Loss of elastin appears to be accompanied by an increase in the collagen content of the arterial wall, resulting in an overall decrease in the elastin to collagen ratio⁶⁵. This reflects in experimental studies that suggest that aortic elastase secretion is significantly higher in patients with AAAs, multiple aneurysms, and ruptured AAAs compared with occlusive aorta disease⁶⁴. Also different expressions of aortic wall elastase and its major serum inhibitor, alpha 1-antitrypsin are found in various types of infrarenal aortic disease⁶⁴.

AA development is characterized by initial elastin fragmentation responsible for aneurysmal elongation and tortuosity. Researchers agree that remodelling causes aneurysmal wall thickening as a result of aorta dilation secondary to elastin loss and media structural changes. Early stages of aneurysm formation are characterized by

increased collagen synthesis, which suggests a repair process⁶⁶. As the load bearing increases, more uncoiled collagen is recruited to load bear circumferentially⁶⁷ resulting in a less distensible vessel. Collagen, because of its structural properties, must fail for significant dilatation and rupture to occur. This is confirmed as patients who are post aortic endarterectomy rarely incur AA disease. Dobrin *et al* concluded that both elastin and collagen are possibly critical in AA dilatation with collagen failure resulting in gross expansion and rupture⁴⁴. This work confirmed experimental studies demonstrating that application of elastase caused arterial dilatation and stiffening, whereas application of collagenase leads to arterial rupture without dilatation⁶⁴. Cohen suggested that elastin degradation is a key step in the development of aneurysms, but that collagen degradation is responsible for aneurysm rupture⁶⁴.

It has been shown that certain disease states, such as inflammation, arterial trauma, medial stress, and normal ageing, can induce elastolysis, which results in reduced compliance of the aorta, increased wall stiffness, and increased stress^{68, 69}. It is suspected that persistent haemodynamic, oxidant, or other forms of stress could induce elastin damage and initiate dysfunctional remodelling of the wall through the stretch-induced production of atypical collagen and elastin by VSMCs. Ineffective elastogenesis by VSMCs and macrophages is demonstrated in an experimental study where the AA group showed 9-fold lower levels of desmosine, a marker of mature, cross-linked elastin, and a 4- to 6-fold increase in levels of tropoelastin as compared with normal aortas⁴⁵. Impairment of the remodelling of new collagen and elastin may render these components more susceptible to further enzymatic degradation^{70, 71}. The integral role of VSMCs in AA disease is confirmed by an animal study that observed AAA prevention and regression after infusion with VSMCs⁷².

1.3. MOLECULAR GENETICS IN AORTIC ANEURYSM

Genetic factors have been shown to play a role in the aetiology of AA even when they are not associated aortic syndromes⁷³. The genetic basis of aortic aneurysms was reviewed in 1991⁷⁴. The major determining factor in the appearance of aortic aneurysms may be an inborn defect of collagen type III or of another component of the connective tissue matrix. At least 20% of aneurysms result from inherited disorders⁷⁵.

1.3.1. Historical background

Coady and co-workers summarized the historical background of AA⁷⁶. The majority of work on the genetic factors involved in AA is from AAA studies. Clifton was the first to identify a familial aggregation of AAA, describing 3 male siblings who presented and were treated for ruptured aneurysms⁷⁷. A later paper reported 1 or more first-degree relatives in 50 families with AAA⁷⁸. Several AAA genetic models were studied to underpin the familial nature of the disease⁷⁸⁻⁸¹. These studies confirmed AAA as a common familial disease with 18 out of 100 patients having a first-degree relative with the disease⁸². For most patients, however, the cause of the aortic aneurysm remains unknown^{76, 83}.

1.3.2. Genetics considerations

Genetic factors in AAAs have been implicated by the above-mentioned and other studies, the presence of multiple aneurysms and by systemic abnormalities in AA patients such as association with connective tissue disease. AAA genetic screening studies suggest an odds ratio of 1.9 to 2.4 with 20% of males likely to develop AAA if they have a first-degree relative with the disease⁸⁴. To a lesser extent, researchers have focussed on AAA families with at least 2 affected members and suggested genes located on chromosome 19q13 and 4q31.47^{85, 86}. Genes implicated in these territories include interleukin (IL)-15, endothelin receptor A, programmed cell death 5, and LDL receptor-related protein 3.47⁷³. AA and association with genetic disease is summarized in Table 1.2.

Table 1.2 Genetic disease and aortic aneurysm

Affected Aortic Segment	Familial disorder	Mode of inheritance	Gene linked
Ascending, thoracic or abdominal	Ehlers-Danlos syndrome type IV	Autosomal dominant	COLA3A1
Ascending	Marfan Syndrome	Autosomal dominant	FBN1 TGF β R2
Thoracic	Turner Syndrome	Chrosomal	
	Osteogenesis imperfecta	Autosomal dominant	COLA1A1
Abdominal	Autosomal dominant adult polycystic kidney disease	Autosomal dominant	PKD1,PKD2
	Homocystinuria	Autosomal recessive	CBS
	Pseudoxanthoma elasticum	Autosomal recessive	ABCC6

1.4. HAEMODYNAMIC FACTORS AND BIOMECHANICAL WALL STRESS CONSIDERATIONS IN AORTIC ANEURYSM

Contrary to current understanding of certain biological, biochemical and morphological factors, the role of biomechanical factors in AA pathobiology is poorly understood. Researchers recognize that when the stress acting on the AAA wall exceeds the strength of the wall it can cause continuous expansion, dissection and rupture. Li and co-workers advocate wall-stress simulation based on a patient-specific AAA model as a more accurate rupture risk stratificator than AAA diameter alone⁸⁷.

1.4.1. Haemodynamic forces

Sprouse *et al* identified three distinct fluid-induced forces on the artery wall: (1) pressure created by hydrostatic forces, (2) circumferential stretch exerting longitudinal forces, and (3) shear stress created by the movement of blood⁸⁸. The net force includes a component perpendicular to the wall, the pressure, and a component along the wall, the

shear stress. Endothelium damage and accelerating degeneration of the arterial wall as a result of turbulence and other flow factors contribute to aneurysm expansion. Furthermore, high and low shear stress and areas of flow oscillation are implicated in aortic atherosclerosis development⁸⁹. Although clinical studies demonstrate that blood flow within AAAs can be smooth and laminar or irregular and turbulent, the effects of wall shear stress in aneurysms remain to be established⁹⁰.

Zeng and co-workers identified factors affecting intra-aneurysmal flow such as the geometry of the aneurysm sac and surrounding vasculature, including the existence, size, and symmetry of branches arising near the aneurysm, and the position of the aneurysm sac relative to the parent vessel (eg, sidewall, terminal, or bifurcation). Effort has been made to correlate rupture with these various geometric features⁹¹.

1.4.2. Haemodynamic forces effect on aneurysm expansion

Aneurysm endothelium is constantly exposed to dragging force of blood shear stress. The focal development of atherosclerosis in haemodynamically defined areas (regions of branched and curved arteries exposed to disturbed flow conditions as opposed to straight arteries) emphasizes the role of shear stress in vascular pathophysiology⁹². A dominating factor identified in vessel remodelling is alteration in blood flow⁹³. Arterial remodelling is hampered by wall shear stress increases (causing vascular inflammation and wall thickening) but encouraged by decreases in arterial wall shear stress^{94, 95}. Also, degradation of the internal elastic lamina (IEL) is caused by a low wall shear stress⁹⁶. However, this process of how proteases are influenced by wall shear stress remains to be defined⁹³.

Furthermore, mechanical forces can increase or decrease gene activation in the blood vessel wall. For example, in cultured human endothelial cells, laminar shear stress increases expression of superoxide dismutase and endothelial nitric oxide synthase, whereas turbulent shear stress does not induce these protective genes⁹⁷. Mechanically induced genes contain positive and negative shear stress responsive elements in their promoter regions, such as antioxidant response element (ARE) that functions to protect cells against oxidant stress⁹⁸.

The increase in shear stress has been linked with a decrease in reactive oxidative stress (ROS). The pathway of this reduction in ROS is mediated by haemoxygenase (HO-1) in macrophages rather than by the inflammatory response. In order to survive exposure to environmental stresses this adaptive cellular response HO-1 expression exists⁹⁹.

Given the beneficial effects of flow loading on vessel remodelling in AAA, it may be surprising that shear stress does not reduce expression of MMP-2 or MMP-9. However, because ROS activates latent proforms of MMPs in the vascular interstitium, reduction in oxidative stress may nonetheless result in decreased MMP activity¹⁰⁰.

To overcome biomechanical design limitations of *in vitro* AAA models, Miller *et al* suggested experiments in animal models. Unfortunately, controversy exists regarding appropriate animal models of human AAAs⁹⁸.

1.4.3. Haemodynamic forces effect on aneurysm rupture

Rupture of the aneurysm has been described as a structural failure when the induced mechanical wall stresses exceed aneurysmal wall integrity. Several concomitant factors (including aneurysm shape and tortuosity, wall constituents, ILT characteristics and the interaction between the fluid and solid domains) associated with blood pressure and shear stress are indicated in AA rupture⁸⁷ and have been evaluated in the past^{15, 101-103}.

1.4.4. Current limitations

Accurate wall strength measurement *in vivo* is currently not possible. This may affect computed wall stress estimation, since wall stress at a certain time point is dependent on wall strength at that point for rupture to occur. However, wall stress analysis based on serial images may be more useful in depicting aneurysm stability⁸⁷.

1.5. ENZYMATIC ACTIVITY IN AORTIC ANEURYSM

Proteolytic degeneration is known to cause AA formation and lead to disease progression. Proteases identified in excess in AA and other aortic diseases include matrix metalloproteinases (MMPs), cathepsins, chymase and tryptase, neutrophil-

derived serine elastase, tissue plasminogen activator (tPA), urokinase-type plasminogen activator (uPA) and plasmin¹⁰⁴. These proteolytic enzymes are involved in regulating and remodelling the ECM.

1.5.1. Experimental and clinical studies

Pioneering work in animal models has demonstrated the role of proteolysis in AA. These experimental studies showed elongation and dilatation following treatment with elastase, and rupture post collagenase infusion. More recently, an *in vivo* study of aortic wall treated with doxycycline-loaded, controlled-release, biodegradable fibre led to preservation of elastin content, decreased MMPs (most notably MMP-2 and MMP-9) and increased tissue inhibitor of metalloproteases (TIMP-1)¹⁰⁵. The media of the AAA host increased levels of several MMPs, including elastases, collagenases, gelatinases and stromelysin. The release of these proteases (derived from macrophages and VSMCs into ECM is caused by stimulation by the products of elastin degradation¹⁰⁶. Inflammatory infiltrates and invading neovessels are relevant sources of MMPs in the AAA wall and may substantially contribute to aneurysm wall instability¹⁰⁷. Histological studies reported elastases MMP-2, MMP-9, and MMP-12 have increased expression in aneurysmal aortic tissue¹⁰⁸. Also higher levels of collagenases MMP-1 and MMP-13 in human AAAs have been linked with structural collagen degradation¹⁰⁹. Despite evidence in animal models of the crucial involvement of MMP-9 in AAA formation and growth, the pivotal role of MMP-9 in driving human AAA growth is debated. It has been suggested that additional proteases such as MMP-8 and the cysteine proteases cathepsin K, L, and S may also play central roles¹¹⁰. These and other studies confirm the significant role that MMPs and their substrates play in AA formation. In AA disease evidence suggests that the equilibrium of vessel wall remodelling between MMPs, TIMPS and other protease inhibitors is disrupted, resulting in elastin and collagen degradation, with the net pathobiological effect of ECM destruction.

1.5.2. Gelatinases

1.5.2.1. MMP-9 (92-kd gelatinase)

MMP-9, predominantly secreted by macrophages, monocytes and VSMCs, is the most comprehensively studied of the metalloproteases. MMP-9 concentrations are higher in

patients with AAA compared to subjects without AAA or AOD. Interestingly, Takagi observed that increased MMP-9 serum levels return to normal after aneurysm repair¹¹¹. Furthermore, an experimental study showed that targeted gene disruption of MMP-9 prevented aneurysmal degeneration in murine models¹¹². More recently, a correlation was found between AAA rupture and elevated plasma levels of MMP-9 and MMP-1¹¹³.

1.5.2.2. **MMP-2 (72-kd gelatinase)**

Evidence suggests MMP-2 may be the most integral protease in ECM degeneration. MMP-2, found predominantly in its active form (62-kd), is sourced by adventitial VSMCs and fibroblasts and is uniquely activated by membrane type (MT)-MMPs. MMP-2 can degrade both elastin and collagen and may be responsible for early AA development. MMP-2 also complements and facilitates MMP-9 activity in transgenic murine models. However, some researchers suggest that MMP-2 may have greater elastolytic activity compared to MMP-9. Increased MMP-2 expression has been observed in subjects with AAA compared to those with AOD or without AAA disease¹¹⁴. Convincing evidence from a rat aneurysm model demonstrated that the inhibition of AA formation following TIMP-1 over-expression, resulted in an activation blockade of both MMP-2 and MMP-9¹¹⁵. Furthermore, other researchers concluded patients with larger aortic diameters have increased MMP-2/TIMP-1 ratios¹¹⁶.

1.5.3. **Elastases**

1.5.3.1. **MMP- 3**

Matrix metalloproteinase-3 (MMP-3) also degrades the ECM and perhaps aids ascending thoracic aorta development¹¹⁷. MMP-3 gene inactivation in mice demonstrated that MMP-3 possibly causes degradation of matrix components, and promotes aneurysm formation by degradation of the elastica lamina¹¹⁸.

1.5.3.2. **MMP-12(54-kd macrophage metalloelastase)**

MMP-12 is involved in AA pathogenesis and shows a high affinity for elastin. In its active form the 22-kd enzyme degrades elastin¹¹⁹. A study on AA development in apolipoprotein E-knockout mice reported MMP-12 predominance in elastolytic activity.

Deficiency of MMP-12 in the mice conferred protection against medial destruction and ectasia¹²⁰.

1.5.4. Collagenases

Increasing collagenolytic activity has been identified in AAs; however, collagen proteolysis is mostly associated with the terminal event of AA rupture. This is confirmed by greater levels of activity measured in specimens of ruptured aneurysms¹²¹.

1.5.4.1. MMP-1 (Collagenase-1)

MMP-1 localizes within the mesenchymal cells (VSMCs, fibroblasts and endothelial cells) and is up-regulated by inflammatory mediators; however, macrophage involvement has been described. Increased pro-MMP-1, MMP-1 protein and mRNA levels have been reported in AAA compared to healthy aorta¹²².

1.5.4.2. MMP-8 (Collagenase-2) (matrilysin)

Studies report inconsistent expression of MMP-8 in AOD and AAA tissue; however, MMP-8 is stored as pre-formed protein in granules. Therefore MMP-8 mRNA may not accurately reflect protein concentration. Prominent expression of MMP-8 has been described in acute aortic dissection¹²³.

1.5.4.3. MMP-13 (Collagenase-3)

MMP-13 is closely spatially related to VSMCs and collagen. Mao *et al* observed higher expression of MMP-13 in AAA compared to AOD tissue¹⁰⁹.

1.5.5. Inhibition of MMPs

Primary control of the activity of MMPs is achieved through tissue inhibitor of metalloproteinase (TIMP), by the formation of non-covalent complexes²². TIMP-2, a broad-spectrum MMP inhibitor, and PAI-1, an inhibitor of tPA and uPA, are less expressed in AAA walls than in AOD, suggesting that ECM destruction is caused by a decrease in inhibitors and an increase in proteases¹⁰⁴. Alpha-1-antitrypsin and alpha-2-

macroglobulin may suppress elastolysis, which is responsible for 90% of the inhibition of circulating MMPs¹²⁴. Treatment with atorvastatin decreases MMP expression and activity and leads to a reduction of TGF-beta signalling in the central region of human AAAs¹²⁵. Also ezetimibe combination therapy decreases aortic wall inflammation implicated in AAA expansion¹²⁶.

1.6. INFLAMMATORY CHANGES IN AORTIC ANEURYSM

AA is best described as a chronic inflammatory condition with an associated proteolytic imbalance. The most important pathological feature of human AA is probably the presence of a chronic inflammatory infiltrate consisting predominantly of macrophages, plasma cells and lymphocytes. These inflammatory cells and others mediate this chronic inflammatory process through the release of cytokines that allow for increased protease expression, expression of cell adhesion molecules, and the release of ROS causing degradation of the ECM through the activation of MMPs and TIMP¹²⁷.

The recruitment of macrophages by chemotactic agents is possibly triggered by exposed elastin degradation products, whereas lymphocyte stimulation may be triggered by micro-organisms and auto-antigens from structural degradation. Interferon (INF)-gamma and tumour necrosis factor (TNF)-alpha appear to be the most consistently expressed cytokines in patients with large AAAs¹²⁸. Furthermore, these inflammatory cytokines play multiple roles in regulating mesenchymal cell matrix metabolism, endothelial cell growth and proliferation, lymphocyte activation, antigen presenting cell (APC) function, major histocompatibility (MHC) class II molecule expression, vascular adhesion molecule expression, and even matrix degrading protease expression of surrounding cells¹²⁹.

Although AA and AOD are characterized by underlying inflammation, immunohistological studies have concluded that T- and B-cell predominance is localized to the outer media and adventitia in AA, compared to largely T-cell involvement localized to the intima and inner media in AOD. Furthermore, an autoimmune component to AA disease has been suggested after localization of B-lymphocytes in the media and considerable deposits of immunoglobulins (IgG) and complement proteins in the wall of AA¹⁰.

1.6.1. Experimental and clinical studies

Key features of human AA include intense inflammation, increased expression of MMP-2 and -9, and local ECM destruction. Inflammation as integral role player in aneurysm pathogenesis was identified following breakthrough experimental animal models that demonstrated key features of human aneurysm following transmural chemical injury induced by calcium chloride treatment of the adventitia layer of the vessel. Interestingly, researchers advocate that aneurysm development secondary to chemical and mechanical injury is caused by inflammation, rather than direct elastolysis since aneurysm formation only developed after the inflammatory response was present. The calcium chloride murine model further indicates that CD4+ lymphocytes may be central in orchestrating production of MMP-2 and MMP-9 through interferon gamma^{130, 131}. Researchers recognized that elastase exposure of the aorta wall caused elastin degradation with up to a 421% increase in AA diameter six days post treatment¹³². This aorta diameter increase was also associated with media infiltration of a large number of activated macrophages and T-cells¹³². From the elastase infusion model we also learned that the inflammatory cell infiltrate is accompanied by greater expression of MMP-2 and MMP-9. Inhibition of the arachidonic acid metabolites by indomethacin has proved inhibition of both recognized MMPs in AA formation and progression. Doxycycline, a tetracycline derivative, is also found to be effective in inhibiting these integral MMPs. It has been shown to reduce aneurysm formation in both the calcium chloride and elastase infusion animal models; however, additional clinical studies are needed to clarify its role in the progression of human AA¹³³. Interestingly, Choke and co-workers observed that ruptured areas on immunohistochemistry have significantly increased amounts of immature micro-vessels, with an excess of MMPs and to a much lesser extent infiltration of macrophages and T-lymphocytes¹³⁴.

Furthermore, the influence of prostaglandins and leukotrienes in the 5-lipoxygenase pathway has been suggested as a potential mechanism in AAA formation, since deficiency of 5-lipoxygenase attenuates aneurysm formation of atherosclerotic apolipoprotein E-deficient mice⁶⁶.

1.6.2. Inflammatory cells involved in aortic aneurysm

1.6.2.1. Lymphocytes

It is suggested that T-helper (Th)1 and Th2-restricted T lymphocyte are the most commonly found immunological cells in AAA walls and are activated by antigen presenting cells such as macrophages, VSMCs, and endothelial cells¹⁰. These inflammatory cells are integral for mediation of the immune response in AAA. However, the specific regulatory traits of components of the inflammatory cascades and of proteases that cause aneurysmal growth remain largely unresolved. This reflects in earlier mouse studies which designated AAA disease as a Th-2-type inflammatory disease and identified Th-2-restricted CD3C T as the dominant influx. Later human studies suggested differently with AAA disease labelled as Th1-dominated or as a general pro-inflammatory condition¹³⁵. Local secretion of Th1 cytokines INF-gamma, Interleukin-2 (IL-2), IL-12, IL-15 and IL-18) may enhance macrophage expression of MMPs, whereas Th2 cytokines (IL-4, 5, 8, and 10, TNF-alpha, INF-gamma and CD40 ligand) possibly inhibit macrophage MMP production and may constrain disease progression¹⁰. In addition, T-helper (Th)-2 cells secrete an FAS-ligand and Fas-associated phosphatase-1 resulting in apoptosis of VSMCs and Th1 cells¹³⁶. Cytokines TNF-alpha and IL-8 cause inflammatory cell recruitment that is responsible for stimulating neoangiogenesis. INF-gamma stimulates cathepsin production for further Th2 activation, B-cell differentiation and Ig secretion¹⁰.

In addition to regulating the immune response and cell apoptosis, Th2-cells also produce IFN-gamma, as well as CD40 ligand¹³⁷. This is supported by animal studies showing that mice lacking IL-4, IL-10 or CD4 develop larger elastase induced aneurysms compared to common mice. However, no significant effect on AAAs has been observed in mice with IFN-gamma deficiency. Others have found that CD4-deficient mice do not develop experimental aneurysms, unless IFN-gamma is administered. This could indicate that Th1-type immune responses are essential in aneurysmal disease, and that shifting the cellular immune response from domination of Th1 cytokines to one that favours Th2 cytokines, could in theory suppress aneurysmal degeneration¹³⁷.

In most cases, the default pathway will be a Th1-dominant for stenotic arterial lesions;

however, when the local environment is skewed toward Th2 predominance, aneurysms will develop⁶⁶. More recently a study comparing inflammatory and proteolytic processes in AAA and popliteal artery aneurysm, characterized degenerative aneurysmal disease as a general inflammatory condition that is dominated by profound activation of the nuclear factor-kappa-B and activator protein-1 pathways with over-expression of IL-6 and IL-8, and neutrophil involvement¹³⁵.

1.6.2.2. **Macrophages**

Inflammation is characterized by macrophage migration from the onset of AA formation. Elastin degradation products are possibly responsible for the recruitment of macrophages by chemotactic agents (Figure 1.2). Haemodynamic forces may regulate macrophage adhesion, transmural migration and survival¹³⁸. A recent animal study confirmed that MT1-MMP acts directly to regulate macrophage secretion¹³⁹. This antigen presenting cell is suggested to be a central role player in the immune response and subsequent ECM destruction. It is mostly localized in the adventitia of the AA wall. Through the secretion of cytokines (IL-1b, IL-6, IL-8, and TNF-alpha) and proteases (in particular MMP-9) these macrophages recruit inflammatory cells and stimulate cytokine production, protease production, B-cell differentiation, Ig secretion, cytotoxic T-cell differentiation and neovascularization¹⁰. In addition to producing cytokines and proteases, these cells also produce TIMP, confirming the governing role of macrophages in AA immune response. Animal studies confirmed the paramount role of macrophages in AA inflammatory response by demonstrating human-like aortic aneurysmal degradation without further manipulation following the application of macrophages and plasmin to the aorta¹⁴⁰.

1.6.2.3. **Endothelial cells**

Endothelial cells have been localized in AA and are found proximate to neovascularization. A prominent role for endothelial cells in the inflammatory response has been suggested following histological study reports of a positive association between the degree of inflammation and the degree of neovascularization. It is suggested that these inflammatory cells play a role in ECM remodelling through the secretion of IL-1b and IL-8, which stimulate intercellular adhesion molecule-1 (ICAM-

1) presentation, thus causing recruitment of additional inflammatory cells, attraction of lymphocytes, stimulation of endothelial proliferation, stimulation of B-cell differentiation and Ig secretion. In addition, like macrophages, the proliferating endothelium also produces various MMPs and TIMP¹⁰. To this end an experimental study has demonstrated that doxycycline not only inhibits MMP-8 and MMP-9 activity, but also the synthesis of MMPs in human endothelial cells¹⁴¹.

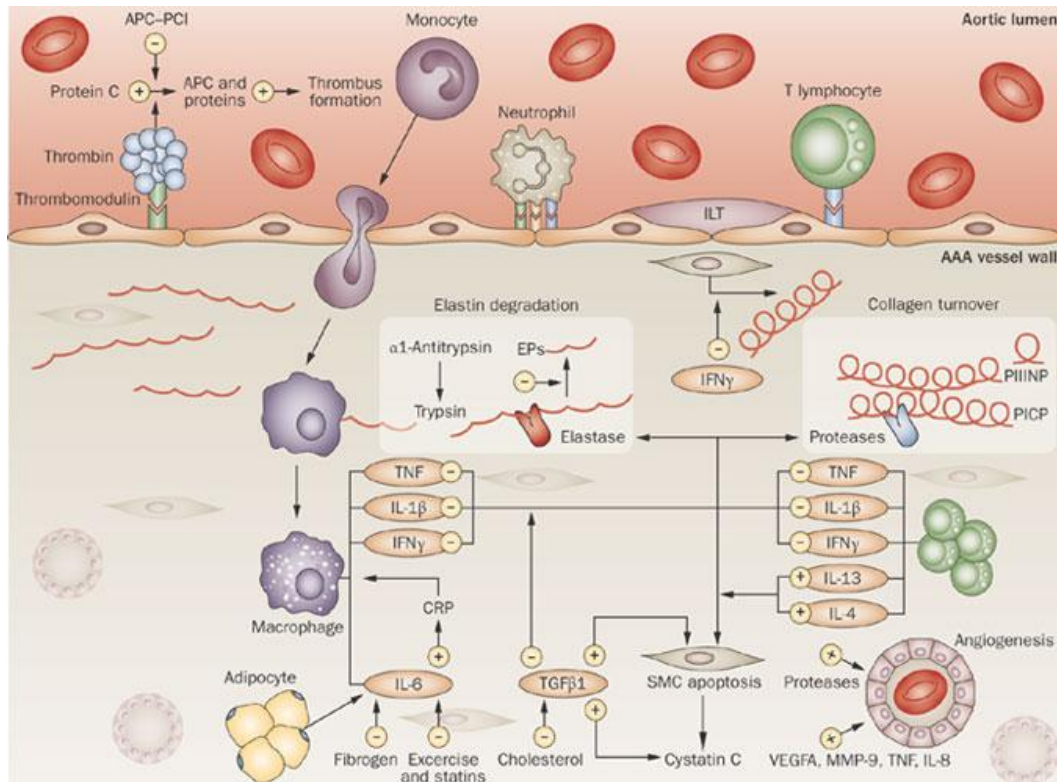


Figure 1.2 Schematic diagram of the mechanisms implicated in abdominal aortic aneurysm, which primarily involve two main processes: inflammation and extracellular matrix turnover

Onset of AAA is associated with recruitment of inflammatory cells to the aortic media, macrophage activation, and the production of proinflammatory molecules. The aortic lumen shows intraluminal thrombus formation and adhesion of inflammatory cells. Within the AAA vessel wall, inflammatory cell infiltration promotes smooth muscle cell apoptosis, elastin degradation, and collagen turnover either directly or indirectly (via the production of proinflammatory molecules). The AAA vessel wall architecture shows typical changes, including loss of elastin, collagen deposition, depletion of smooth muscle cells, and neovascularization. Abbreviations: +, promotes; -, inhibits; APC-PCI, activated protein C-protein C inhibitor complex; CRP, C-reactive protein; EP, elastin peptide; IFN, interferon; IL, interleukin; ILT, intraluminal thrombus; MMP, matrix metalloproteinase; PICP, carboxy-terminal propeptide of type I procollagen; PIINP, amino-terminal propeptide of type III procollagen; SMC, smooth muscle cell; TGF, transforming growth factor; TNF, tumor necrosis factor; VEGFA, vascular endothelial growth factor A.

[Reproduced with kind permission from the Nature Publishing Group, Hellenthal et al. Figure 1.¹⁴²]

1.6.2.4. **Fibroblasts**

Although fibroblasts are commonly identified in the adventitia of AAA and have a recognized function in atherosclerosis, the role of the fibroblast in aneurysm pathogenesis is uncertain. Fibroblasts secrete cytokine IL-6 which is suggested to cause a stimulatory cascade of B-cell and cytotoxic T-cell differentiation and MMP stimulation¹⁴³.

1.6.3. **Infection and aortic aneurysm**

An infectious cause responsible for aneurysm formation has also been advocated. Between 30% and 50% of AAAs are associated with *Chlamydia* and *Herpes* virus infections. *Chlamydia* has been shown to induce AAA in rabbits and antichlamydial antibodies are commonly detected in AAA patients; however, a causal relationship remains to be established. Studies have suggested that these infections play a role in elastolysis, possibly creating and augmenting an autoimmune response through particle mimicking. Lindholt *et al* found that serum antibodies against *Chlamydomytila pneumoniae* have been associated with AAA expansion and cross-reaction with AAA structural proteins. Thus, immune responses mediated by microorganisms and autoantigens may play a pivotal role in AAA pathogenesis¹⁴⁴.

1.6.4. **Vasculitides and aortic aneurysm**

Vasculitides that affect the aorta are predominantly giant cell arteritis (GCA) and Takayasu's arteritis (TA). These are idiopathic systemic inflammatory conditions characterized by granulomatous inflammation of large and medium-sized arteries¹⁴⁵. The pathogenesis of GCA and TA is poorly understood. It is suggested that cell-mediated autoimmunity plays an important role, possibly triggered by infectious agents. The histological appearance is of a focal panarteritis. The transmural inflammatory infiltrate is largely composed of lymphocytes, macrophages and multinucleated giant cells, which may be organized into granulomas. The cellular infiltrate in TA tends to localize to the adventitia and outer parts of the media can lead to aneurysmal dilation. Ultimately, intimal proliferation and dense scarring can compromise the vascular lumen resulting in arterial stenosis. In GCA, the centre of tissue damage lies at the internal elastic lamina. Concentric intimal thickening, partly resulting from oedema, narrows the

vessel and luminal thrombosis can occur¹⁴⁵. Aortitis due to GCA may lead to destruction of the elastic lamina and muscular media causing late aneurysms even in those individuals responding well to medical treatment. Aneurysm development may also be secondary to isolated necrotizing aortitis. Aneurysm formation as a complication is more frequent than vessel stenosis or occlusion¹⁴⁶.

New imaging modalities such as colour Doppler ultrasound and positron-emission tomography are providing further insights into the extent and pathobiology of large vessel vasculitis. It allows for the detection of vessel alterations early on and a better control of the disease progression. However, at present temporal artery biopsy and angiography remain the gold standards for diagnosis¹⁴⁵.

1.6.5. Aortitis

Chronic periaortitis is characterized by an inflammatory process involving fibrous tissue that arises from the abdominal aorta and the iliac arteries. Historically, chronic periaortitis was suggested to be a localized inflammation as part of a severe degree of aortic atherosclerosis, however, involvement often extended beyond the aorta including other large vessels with or without aneurysmal dilatation. Histopathologic characteristics of chronic periaortitis include adventitial inflammation and fibrosis, vasculitis of vasa vasorum, and adventitial lymphoid follicles with germinal centres, which suggest a primary nature to chronic aortitis¹⁴⁷. Recently identified IgG4-related inflammatory AAAs (IAAAs) may be part of IgG4 related systemic disease and therefore IAAA should be ruled out in patients diagnosed with aortitis or periaortitis¹⁴⁸.

1.6.6. Inflammatory aortic aneurysm

Since the first description of inflammatory abdominal aortic aneurysm (IAAA)¹⁴⁹, it has been estimated that IAAA accounts for 2 – 10% of all AAAs^{150, 151}. Patients with IAAA are younger in relation to the rest of the AAA population¹⁵¹ with a strong male predominance¹⁵². Some researchers have suggested that IAAA and non-inflammatory AAA is one pathological process with varying degrees of inflammation¹⁵³⁻¹⁵⁵, whereas others have postulated an autoimmune and or infectious cause with *Chlamydia pneumoniae* or *Helicobacter pylori*¹⁵⁶⁻¹⁵⁸. Elevated serum IgG levels and autoantibodies

such as antinuclear antibody (ANA) are also detected in patients with IAAA¹⁵⁹ suggesting an autoimmune role in the pathobiology¹⁶⁰. Systemic inflammatory markers, such as erythrocyte sedimentation rate (ESR), C-reactive protein levels and white blood counts are commonly elevated in IAAA¹⁴⁹. Symptoms of back pain and, weight loss in a patient with an AAA and an elevated ESR, is highly suggestive of an inflammatory component¹⁶¹. IAAA radiological characteristics include aortic dilatation, periaortic mantle zone, and adhesions to adjacent organs¹⁶². This periaortic mantle zone microscopically characterizes IAAA and is described as white, glistening, perianeurysmal fibrosis^{149, 163}. Histopathological studies observed extensive fibrosis with marked thickening of the aortic wall and severe lymphoplasmacytic infiltration that predominantly involves the adventitia with extension into adjacent soft tissues^{164, 165}.

Inflammatory cell infiltrates are characterized by macrophages, T-lymphocytes and B-lymphocytes^{153, 166, 167}. Furthermore, it is suggested that an imbalance in the ratio of T-helper cells to T-suppressor cells, with the predominance of T-helper cells stimulating macrophages, results in activation and proliferation of B-lymphocytes. Macrophages may also act as antigen presenting cells and thus govern the immune response¹⁵³. Therefore, it is not surprising that *in vivo* imaging modalities are explored in AAA assessment, in particular PET/ CT, to detect inflammatory or metabolic activity in the aneurysmal wall and to further delineate the role of chronic inflammation in aneurysm pathobiology.

1.6.7. Rupture and inflammation

MMP activity has been linked with AAA rupture; however, the exact mechanism remains to be found. A quantitative immunohistochemistry study demonstrated that expression of MMP-8 and -9 was dependent on mesenchymal cells native to the aorta, either VSMCs, fibroblasts, or myofibroblasts, rather than inflammatory infiltrate¹⁶⁸. Furthermore, another immunohistochemistry study found increased medial neovascularization and overexpression of alpha(v)-integrin, VEGF, vascular endothelial-cadherin, MCP-1, and vimentin at the edge of the site of AAA rupture¹⁶⁹.

These inflammatory changes may involve more than just the rupture site. A recent immunohistochemistry study observed inflammatory changes in aneurysm biopsies

from three distinct sites: 1) stable non-ruptured aneurysms, 2) a non-ruptured site within the ruptured aneurysm and 3) the actual site of AAA rupture. Wilson *et al* concluded the biological events leading to AAA rupture may not be dependent on an up-regulation in the inflammatory process¹⁷⁰. This finding is in keeping with a quantitative analysis of macrophages and generic lymphocytes which failed to show an increase at the site of aneurysm rupture, suggesting inflammation may have little bearing on the terminal process of aneurysm rupture¹⁶⁸.

1.6.8. Reactive oxygen species and aortic aneurysm

Increased concentrations of ROS such as superoxide (O_2^-) have been observed in human AAAs. Increased nitric oxide synthase expression and lower levels of the antioxidant, O_2^- dismutase following experimental aneurysm induction with elastase infusion were identified. O_2^- levels in human aneurysmal tissue are 2.5-fold higher than in adjacent non-aneurysmal aortic tissue and 10-fold higher than in control aorta¹⁷¹.

1.7. RISK FACTORS IN AORTIC ANEURYSM

1.7.1. Family history

Familial aggregation studies have confirmed a positive family history for AAA in approximately 15% of patients with AAA who do not have any recognizable connective tissue disorder¹⁷².

1.7.2. Age

The process of ageing is known to cause an estimated 15-20% increase in the diameter of major arteries at age 65 compared to younger controls¹⁷³. This change can be influenced by factors such as hypertension, body size and sex; and has been linked to matrix degeneration. The prevalence of AAA post adjustment for confounding factors shows an almost two-fold increase from 2.7% in ages 65-69y to 4.4% at 75-79y, with a peak incidence at 65y¹⁷⁴.

1.7.3. Gender

Men are 5.6 times more likely to develop an AAA compared to females, therefore confirming that male sex is the greatest risk factor for AAA¹⁷⁴. The prevalence of AAA amongst men aged 65-79y was 6.8 per cent. In the pathogenesis of AAA, oestrogen may play an inhibitory role by decreasing the expression of MMP-2 and MMP-9 synthesis¹⁷⁵, thus providing a possible explanation for the lower incidence in the female sex. Nevertheless, there is a three-fold higher risk of rupture in women compared to men when non-randomized patients were included in analysis¹⁷⁶. A smaller study found the risk of rupture in women with AAAs of 5.0–5.9cm to be four times that of men with AAAs of 5.0–5.9cm²⁴. Also, the mean diameter preceding rupture was decreased in women (5.0±0.8 cm) compared to men (6.0±1.4cm). Furthermore, McPhee and co-workers reported a higher percentage of female patients presenting with rupture, and a higher mortality rate during hospital stay for both intact and ruptured aneurysm presentations¹⁷⁷.

1.7.4. Hypertension

Hypertension alongside chemical induced elastic lamina degradation is used to induce aneurysms in murine models¹⁷⁸. Clinical studies concluded that hypertension may be a factor predisposing to AAA, or it may affect the growth rate or risk of rupture of an existing aneurysm¹⁷⁴. However, the effect is more pronounced in larger aneurysms. Multivariate analysis in one study revealed a marginally significant correlation between hypertension and AAA¹⁷⁹. UK Small Aneurysm Trial (UKSAT) furthermore reported that aneurysm rupture was associated with higher mean blood pressure¹⁷⁶. Researchers have also emphasized that diastolic blood pressure was a more accurate predictor of aneurysm rupture than systolic blood pressure. Another study reported that of 157 patients hypertension (>150/100 mmHg) was present in 67% who had ruptured, but in only 23% of those without rupture¹⁸⁰.

1.7.5. Diabetes

This cardiovascular risk factor demonstrates a significantly negative association with AAA expansion¹⁷⁹ with a reduction of over 30% of aneurysm diameter observed by some¹⁸¹. Furthermore a large study found a significantly lower prevalence of AAA

amongst patients known to have diabetes¹⁸². Decreased aneurysm expansion associated with diabetes is explained by three suggested theories. Firstly, hyperinsulinaemia causes reduced fibrinolysis with less renewal of mural thrombosis, thus affecting progression. Secondly, hyperglycaemia causes increased collagen synthesis. This leads to decreased synthesis and activity of MMP, resistance to MMP digestion and altered VSMC phenotype, facilitating increased wall stiffness. Lastly, therapeutic agents decrease inflammation, MMP activity and blood pressure, with a resultant reduction of AA expansion. This rather paradoxical association of diabetes with AAA may help to explain differing pathogeneses between aneurysmal and atherosclerotic disease.

1.7.6. Smoking

Cigarette smoking is recognized as one of the most prevalent risk factors and certainly the largest avoidable risk factor associated with AA formation, expansion and rupture. Lifetime male smokers are 2.5 times more likely to develop AAA than male non-smokers^{18, 174}. The strength and dose-response of the correlation between the cumulative lifetime history of being a smoker and AAA, suggests a causative role in aneurysm aetiology. In a hypertension-induced ApoE (-/-) mice study mainstream smoke was responsible for both the formation and severity of AAA¹⁸³. Furthermore, increased protease activity was shown when the mice were exposed to a combination of angiotensin-II treatment and cigarette smoke¹⁸³, thereby increasing the degradation of aortic connective tissue.

Shimizu *et al* studied a subset of patients with aortic atherosclerosis, smoking and/or genetic predilection, and found inhibition of local IFN-signalling and/or eliciting Th2-dominant cytokine environments, thus inducing macrophage elastolytic activity, which resulted in AAA formation⁶⁶. Brady *et al* furthermore reported a 15-20% increase in AAA growth rate in current smokers¹⁸¹. Although highly significant, this effect is insufficient to warrant the recommendation of different screening intervals for smokers. The UKSAT did measure COPD specifically, and reported that aneurysm rupture risk was independently and significantly related to current cigarette smoking. The benefit of smoking cessation is demonstrated through a clinical study showing a significant difference between ex-smoker and current smoker AAA rupture rates¹⁷⁴.

1.7.7. Aortic dissection

Aortic dissection has been related to aneurysm formation. An autopsy study of 84 consecutive cases observed that 5 patients had associated aneurysms¹⁸⁴. Chronic aortic dissections have a tendency to increase in size over time. All mechanisms weakening the media layer of the aorta will lead to higher wall stress with subsequent dilatation, aneurysm formation, aortic dissection or rupture. Chronic aortic dissection results in an overall weakened affected aortic wall through an instability due to the dissection in the first instance, and a weaker outer wall of the false lumen caused by the intima dissecting away. Therefore, patients with chronic aortic dissections are at high risk for aneurysm formation¹⁸⁵.

1.7.8. Atherosclerosis

The relationship between atherosclerosis and AA remains to be established. Three non-dominant theories have been suggested. Most aneurysms are associated with atherosclerosis¹⁸⁶, hence in the past atherosclerosis was advocated as a causative factor, and the hypothesis of AAA development secondary to atherosclerosis was supported by principles governing arterial remodelling. This theory is opposed by some researchers as 3 out of 4 patients with AAA do not demonstrate occlusive vascular disease of the aortoiliiofemoral segments. Animal studies which have aimed to induce AAA through atherogenic diet have not been predictable, and attempts to regress experimental atheromas in monkeys have caused aneurysm formation. An alternative theory suggests atherosclerosis and AAA formation to be independent entities with shared environmental and genetic risk factors. A large Tromso study designed to understand the relationship between atherosclerosis and AAA suggested that atherosclerosis and AAA develop in parallel, rather than atherosclerosis leading to AAA⁸². However, this study did not consider important confounding factors (for example diabetes), thereby not completely refuting the part atherosclerosis play in AAA formation¹⁸⁷. Also, excessive remodelling as result of atherosclerosis may provide the stimulation causing the chronic inflammatory response identified in AAA. Hence, others adopt the view that either aortic atherosclerosis or AAA can develop first, and both form part of the interactive process that stimulates the other's development. In fact, Brady and colleagues reported a negative association between atherosclerotic burden as measured with ankle brachial pressure index (ABPI) and aneurysm growth, suggesting that

atherosclerosis has a minimal role in the continuing expansion that characterizes the natural history of AAA¹⁸¹. The bulk of the evidence points to AAA disease being a systemic disease of the vasculature that may more accurately be described as degenerative rather than atherosclerotic. Nevertheless, atherosclerosis plays a role in the pathogenesis of AAA as demonstrated by the association of AAA formation and progression with atherosclerosis risk factors¹⁸⁸, atherosclerotic vascular disease and systemic inflammatory markers.

1.8. INTRALUMINAL THROMBUS (ILT) IN AORTIC ANEURYSM

Intraluminal thrombus is found in an estimated 3 out of 4 AAAs¹⁸⁹. The presence of an ILT has been associated with both expansion and rupture of AA. ILT is described as a biologically active laminated structure, containing several layers of fibrin clot, underlying a fresh, red haematic luminal layer containing undegraded cross-linked fibrin, and an actively fibrinolyzed abluminal layer. Proteolytic and oxidative degradation of the arterial wall is caused by this biofunctional unit. The damage occurs through fibrin formation, platelet activation, the binding of plasminogen and its activators and the entrapment of erythrocytes and neutrophils. This occurs mainly at the ILT/circulating blood interface.

Vorp and co-workers demonstrated that ILT attenuated oxygen flow from the lumen to the aortic wall, and that a hypoxic environment is more pronounced in aneurysms with greater thrombus volume (>4mm). This environment may be responsible for an increase in MMP activity in the AA wall, with subsequent weakening, decrease in tensile strength and ultimately rupture¹⁹⁰. Also, ILT has been shown to be associated with a thinner arterial wall, more extensive elastolysis, a lower density of VSMCs in the media and a higher level of immuno-inflammation in the adventitia¹⁹¹. This suggests that an important part of protease activity originates from the ILT, rather than being directly generated within the aneurysm wall¹⁹¹. This work confirms earlier research reporting that ILT enhances proteolysis in AAA¹⁹². Furthermore, Folkesson *et al* observed that neutrophil gelatinase-associated lipocalin in complex with activated MMP-9 is found in AAA walls and thrombi. This relationship may enhance the enzymatic activity associated with AAA¹⁹³. More recently a study observed the differentiation of protease

activity within the same AAA wall and its enhancement within the thin thrombus-covered aneurysm wall¹⁹⁴. Experimental models confirm that ILT may contribute to AAA progression via its influence on the level of aneurysmal wall protease activity¹⁹⁵. Increased inflammatory activity correlated to the abundance of leukocytes has made *in vivo* imaging of superparamagnetic iron oxide (SPIO) uptake at the luminal interface of the thrombus with MR imaging a possibility¹⁹⁶.

Bleeding into the thrombus as suggested by higher attenuation levels and a ‘crescent sign’ is associated with AAA rupture¹⁹⁷. Leading on from this work, Polzer and his colleagues observed ILT fissures increase the stress in the underlying wall, whereas other regions remain unaffected. If ILT fissures reach the wall or involve large parts of the ILT, the resulting increase in wall stress could possibly cause AAA rupture¹⁹⁸.

Infrarenal aortic thrombus volume is linked with the incidence of cardiovascular events and AAA progression¹⁹⁹. Some researchers speculate weakening of the AAA wall, under the influence of thrombus, might play a more imminent role in AAA expansion than wall stress²⁰⁰. This conclusion followed an observation by Speelman and colleagues, suggesting that larger thrombus in AAA was associated with a higher AAA growth rate, but also with a lower wall stress²⁰¹.

Nevertheless, wall stress plays a central role in AAA pathobiology and the relationship between ILT and wall stress is important. The presence of ILT causes a reduction in the peak wall stress. This correlation was mainly observed in smaller aneurysms. Geometric configurations of the AAA may influence wall stress in larger aneurysms²⁰².

1.9. SUMMARY OF AORTIC ANEURYSM PATHOBIOLOGY

Interaction of multiple factors is responsible for the failure of the structural integrity of the aneurysm wall, which results in aneurysm formation and progression. Current areas of interest include proteolytic degradation of the arterial wall, inflammation and the immune response, biomechanical wall stress, and molecular genetics. Insight into the pathobiology of AA has led to more targeted imaging methods and treatment trial design to investigate various pathobiological mechanisms of AA regression. As it

stands, surgical treatment of AA disease continues to be the most effective means of addressing the majority of factors involved in AA formation and progression. Non-invasive *in vivo* imaging of AA inflammation may offer solutions and yield valuable information on the role that inflammation plays in AA pathobiology. This could also have potential clinical application such as estimation of growth and rupture risk to help with decision about repair.

CHAPTER 2. IMAGING VESSEL WALLS

2.1. INTRODUCTION

Inflammation is prevalent at several stages of atherosclerotic plaque development²⁰³. Inflammation marked by the pathological feature of the infiltration of inflammatory cells plays a central role in AA formation and progression. Although the relationship between atherosclerosis and AA remains to be established, atherosclerosis plays a role in the pathogenesis of AAA as demonstrated by the association of AAA formation and expansion with atherosclerosis risk factors, atherosclerotic vascular disease and systemic inflammatory markers.

Contemporary imaging techniques can accurately assess vascular wall anatomy and, with targeted probes, depict the metabolic processes central in vascular inflammation. Technology and probe advances allow for imaging of multiple facets related to the vessel wall including expansive ECM remodelling, angiogenesis of the vasa vasorum, atherosclerotic plaque inflammation, and even fibrin deposits on early non-occlusive vascular thrombosis²⁰⁴. Expansive or restrictive vascular remodelling is commonly found in vascular lesions. Extracellular matrix remodelling by proteolytic degradation and cell apoptosis is the predominant characteristic of expansive remodelling²⁰⁴. In atherosclerosis, VSMC migration is observed from the adventitia with transformation into monocytes or macrophages and subsequent lipid-filled core formation. To allow for plaque growth, the ECM adopts an expansive remodelling with inflammation central to this process²⁰⁴. It is suggested that this form of remodelling characterizes aneurysm formation²⁰⁵. AAAs accumulate inflammatory cells, but usually exhibit much more extensive medial damage⁶⁶.

In atherosclerosis and other vascular diseases, molecular imaging provides insight of the disease-specific biological events, enables novel non-invasive strategies for individualized risk assessment, and facilitates monitoring of highly targeted therapies. Molecular imaging is a rapidly developing discipline aimed at depicting cellular and sub-cellular processes using traditional and novel imaging platforms²⁰⁶.

Molecular imaging techniques with ultrasound, MRI, PET and CT individually capture only limited aspects of the vast spectrum of pathobiologic events involved in atherosclerosis. Therefore, based on their unique advantages and disadvantages, these molecular imaging applications may have a complementary, rather than a competitive role in depicting the molecular underpinnings of atherosclerosis²⁰⁷.

2.1.1. Nuclear based molecular application

In the last few years hybrid PET / CT has become an established clinical imaging modality in oncology and clinical cardiology to demonstrate inflammation, ischaemia and other disease-specific molecular process mostly reflected through glucose metabolism. The development of dedicated fusion imaging systems that combine PET imaging or single photon emission computed tomography (SPECT) with either CT or MRI have enabled accurate anatomic localization and functional correlation of metabolic activity.

The main advantage of nuclear imaging is that sensitivity is many orders of magnitude higher than MRI, CT or ultrasound. Compared with MRI and CT, sensitivity for both SPECT and PET are within the picomolar range, allowing for functional imaging of biomolecular targets with the use of less radiopharmaceutical ligands. PET and SPECT, however, have limited spatial resolution (PET 5mm, SPECT 10-15mm) compared to MRI and CT which have superior spatial (1mm) and temporal resolution in comparison. Combining strengths of the various imaging modalities is the rationale behind hybrid PET/CT and PET/MRI²⁰⁴. Furthermore, FDG PET can provide non-invasive quantitative assessment at a functional level indicative of atherosclerotic plaque metabolism, hence for example, reflecting the degree of increased vascular glucose metabolism, distinguishing it from MRI and echo-based techniques.

Non-invasive quantification of metabolism with both SPECT and PET imaging techniques has been extensively described, especially with the ¹⁸F-FDG tracer. Radiolabelled probes are used to depict activated macrophages within the vessel wall. Increased cellular metabolism of glucose forms the principal foundation of deoxyglucose imaging.

Experimental and clinical studies confirmed that macrophages are the main source of FDG uptake in vascular lesions. Newby *et al* observed that inflammatory cytokines trigger MMP induction and subsequent macrophages migration and modulation²⁰⁸. Metabolically active macrophages have enhanced glucose uptake and therefore can be detected as an increased radioactivity using ¹⁸F-FDG as tracer²⁰⁹⁻²¹¹.

Yun *et al* first reported ¹⁸F-FDG uptake in aorta walls in patients with cancer imaged for the purpose of staging^{212, 213}. They further described increased FDG uptake in older patients. Others demonstrated an association between FDG uptake and cardiovascular risk factors^{214, 215} and also the relationship between vessel FDG uptake with levels of inflammatory biomarkers²¹⁶. Tahara *et al* showed that drug therapy can reduce arterial metabolic activity²¹⁷. Similarly, arterial tracer uptake was decreased in patients who adhered to dietary and lifestyle changes²¹⁸. ¹⁸F-FDG PET as a vascular imaging tool was further validated through clinical histological PET studies which confirmed correlation between ¹⁸F-FDG radioactivity and carotid plaque metabolic activity^{210, 219, 220} and AAA wall inflammation^{221, 222}. ¹⁸F-FDG uptake is reproducible²²³, allowing serial non-invasive measurements of the effects of anti-inflammatory drugs on the vasculature, including statins²¹⁷, PPARS (peroxisome proliferator-activated receptor agonists)²²⁴ and drugs still under development²²⁵. Although the association between FDG uptake and inflammatory burden in vascular plaque is well described, a recent histological PET study suggests that glucose uptake and therefore FDG uptake signal may reflect hypoxia-stimulated macrophages rather than mere vascular inflammation²²⁶. At present, to overcome spatial resolution challenges with PET, ¹⁸F-FDG imaging of the aorta may be more reliable than functional imaging of smaller arteries, ie carotid or coronary arteries²²⁷.

Furthermore, radiolabelling of nanoparticles has been attempted in a murine animal study with higher ¹⁸F-labelled carbohydrate-coated nanoparticles uptake reported in TAA 10-12 h after tracer administration²²⁸. Nevertheless, high radiation levels and long clearance times hinder translation of this tracer into clinical practice.

2.1.2. Ultrasound-based molecular imaging applications

This form of molecular imaging relies on the detection of novel site-targeted modern ultrasound contrast agents (UCAs) or other acoustically active particles after ligand-directed binding to the ROI²²⁹. UCAs are gas-filled molecules (or microbubbles) that have an outer shell composed of phospholipids, liposomes or other biodegradable polymers²³⁰. UCAs possess properties that allow ultrasound contrast enhancement so as to perform vessel molecular imaging. They are small (1–5µm) with similar rheologic behaviour to mature red blood cells²³¹. They are intra-vascular tracers without significant retention in the diseased tissue unless selective molecular targeting is induced by structural shell changes, or molecular probes are conjugated in the outer shell. UCAs tend to undergo volumetric oscillation, providing a greater ability to reflect, absorb and re-radiate sound energy²³².

Disruptive changes in the modulation of the periadventitial vasculature may have an active role in atherosclerosis development and progression²³³⁻²³⁵. Microbubbles targeted to various processes involved in atherosclerosis and thrombosis including endothelium adhesion molecules, angiogenesis, thrombus, activated platelets, von Willebrand factor and tissue ischaemia have been applied²²⁹. Plaque neovascularization has been successfully imaged using contrast-enhanced ultrasound and other non-invasive imaging such as microscopic three-dimensional (3D) CT and contrast-enhanced magnetic resonance (CMR)²³⁴. Experimental studies on the use of UCAs with targeted probes suggest these microbubbles may depict endothelial activation and immune cell retention seen in early atherosclerosis²³⁶. However, low microbubble retention at the atherosclerosis site due to high-velocity and high-shear stress, and low specificity of selected targets suggest further research development is necessary before human translation is attempted²³⁶.

The benefit of UCAs for echo-based study is that they remain intravascular, thus making molecular imaging of especially the endothelium of large arteries possible. However, low acoustic signal and difficulty of detection with routine available ultrasound technology and clinical feasibility in vascular imaging is hampered by suboptimal accuracy to differentiate between UCAs signal and tissue back ground when

using conventional probes. Nevertheless, research is focussing on microbubble design and echo-based technology to overcome these issues.

2.1.3. MRI-based molecular application

MRI has been successful in demonstrating vascular inflammation by targeting the phagocytic activity of inflammatory cells. Studies describe the use of ultra-small superparamagnetic particles of iron oxide (USPIO), which are circulating iron oxide nanoparticles (ferumoxtran-10) that metabolize slowly over 24–36h by the reticuloendothelial system. USPIO have a similar molecular size (less than 50nm) to oxidized low-density cholesterol (ox-LDL-c), hence their ability to be retained in the sub-endothelial space of dysfunctional endothelium²³⁷ and their specific affinity for scavenger receptors and other outer cell membrane molecules expressed by activated macrophages²³⁸. USPIO have nonstoichiometric microcrystalline magnetite cores which are mostly coated with dextran or siloxane²³⁹. Experimental studies with hyperlipidaemic rabbits showed spontaneous uptake of USPIO and superparamagnetic iron particles by macrophages in atherosclerotic plaque^{240, 241}. Kooi *et al* subsequently described vascular uptake of USPIO in a clinical study²⁴². This histopathological study demonstrated that up to 75% of the ruptured or rupture-prone lesions contained high concentrations of USPIO, compared to only 7% uptake by the stable plaques²⁴². Furthermore, Trivedi and colleagues described USPIO-enhanced MRI identification of carotid plaque inflammation through accumulation of USPIO within plaque macrophages in 30 patients with symptomatic disease²⁴³. In AAA, a nanoparticle MRI study showed a change in decay of transverse magnetization after 36h, suggesting potential for use in molecular imaging of vascular walls²⁴⁴. Another study identified a subset of patients with distinct USPIO uptake associated with a threefold higher aneurysm expansion rate, advocating use as a risk stratification tool²⁴⁵. Visualization of USPIO particles within activated macrophages is achieved with T2*-weighted gradient echo sequences in which areas of high plaque inflammatory activity are represented by signal hypodensity.

Evidence that macrophage activity assessment by MRI is valid in clinical trials is robust. High spatial resolution, excellent soft tissue contrast and lack of radiation are advantages of this modality. However, the MRI study needs repeating 24-36h after

basal image acquisition for comparison of imaging intensities, and this is sometimes impractical. Furthermore, there is no correlation between USPIO hypodensity and long-term clinical outcome, and the long-term safety of using USPIO is questioned.

Other MRI probes focus predominantly on endothelial dysfunction, eg Apo-A1 mimetic tracers²⁴⁶ and antibodies targeting oxidized-specific epitopes such as the human IK17 or the murine MDA2 and E06²⁴⁷. Platelet activation has also been pursued as potential molecular imaging MRI targets^{248, 249}. In order to overcome some technical challenges with MRI probe imaging, Caruther studied the colloidal iron oxide nanoparticle theranostic platform, a vascular constrained T1-weighted molecular imaging agent, that avoided typical magnetic bloom artifacts, allowed for rapid vascular imaging without blood pool magnetization interference, and supported targeted drug delivery²⁵⁰.

2.1.4. Spectral CT molecular imaging

CT molecular imaging shows promise with evolution of dual-energy and multicoloured or spectral CT derived from properties of the photon-processing detector. Spectral CT recognizes the k-edge of metals, which occurs when the attenuation of photons interacting with a k-shell electron suddenly increases as a result of photoelectric absorption²⁰⁴. Multiple materials can be quantified and differentiated from each other simultaneously using spectral imaging, since each material has a specific measurable X-ray spectrum²⁵¹. Spectral CT scanners allow for traditional CT image and quantitative k-edge image data (based on unique spectral footprints of specific elements, for example, gold, gadolinium, or bismuth)²⁰⁴. Metal nanocolloid k-edge agents that can localize to fibrin fibrils within an intravascular thrombus or other suitable biomarker, have been developed²⁰⁴. Localization of hot spots from intraluminal fibrin to the coronary bed are made possible through image registration of CT images²⁰⁷. At present its role is seen more as an adjunctive imaging tool, with researchers advocating greater efficacy in cancer diagnosis and treatment monitoring when combined with PET/CT. Although this molecular imaging modality is promising, technology, image reconstruction and display soft ware challenges, as well as the identification of suitable biomarkers for the disease in question, all hamper clinical translation²⁵¹.

2.1.5. Summary of vascular imaging techniques

To foresee the clinical application of vascular molecular imaging, technical constraints, safety issues and potential clinical impact regarding managing strategies to reduce clinical events, needs consideration. Cost-effectiveness, non-toxic low-molecular-weight probes with an easy accessible imaging platform to some extent elude us. FDG vascular imaging currently represents a promising vascular imaging modality; however its clinical role remains to be established. Future introduction of 4-D PET and appropriate gating may help overcome recognized technical constraints for PET/CT. Lack of radiation and therefore benefit in serial monitoring, drives the push for widespread clinical use of MRI-based and ultrasound-based molecular imaging techniques. The emergence of multimodal molecular imaging strategies may prove useful, but may not be cost effective.

2.2. HISTORY OF PET / HYBRID PET/CT

Today, PET is recognized as an established major clinical imaging tool. Nutt *et al* summarized the history, which is marked by significant technological advances that shaped modern PET²⁵². Sweet first and later Wrenn *et al* described the medical use of positrons in 1951. The Massachusetts General Hospital study group built the first brain probe using two opposing sodium iodide (NaI(Tl)) detectors²⁵³.

In 1973, following recognized efforts by scientist and physicians including Hounsfield, the first successful PET with a hexatomograph design, known as PETT I, was built at Washington University. PETT I lacked proper reconstructed images because it employed limited sampling, and did not provide for attenuation correction, but nevertheless used a proper filtered Fourier-based image reconstruction algorithm. Collaboration with the EG&G ORTEC group saw the development of PETT II with automatic rotation of 24 NaI detectors, making a fully sampled data set possible. Understanding gained on PET mathematics and physics from studies with PETT I / II marked the beginning of modern PET²⁵².

In 1974, the Washington study group developed PETT III, with 48 NaI(Tl) detectors, for clinical human studies. Shortly thereafter ECAT II, the first commercial PET, was produced. Detectors used in PET are the determining factor in the sensitivity, the image resolution and the count rate capability. In the early eighties the introduction of bismuth-germanate (BGO) as a PET scintillator was observed. This dense crystal has a high effective atomic number, necessary to stop the high energy annihilation photons. The first PET III images were captured at Washington University using ^{11}C -glucose, ^{15}O -water and ^{13}N -ammonia for blood flow, ^{15}O -oxygen for oxygen utilization, and ^{18}F -fluoride for bone scans. The first synthesized FDG led to the first FDG PET image performed in December 1976.

The development in the mid eighties of the 'electronic generator' for automated production of PET tracers and the validation of the match / mismatch principle for determining cardiac viability with ^{13}N - ammonia used for blood flow and FDG for glucose metabolism marked other breakthroughs in PET history. The use of PET for diagnosis and management of cancer treatment in the nineties helped establish PET as a recognized clinical imaging modality. Further advancement of clinical PET came about when Siemens and GE joined the PET market.

Introduction of whole-body PET imaging along with the large amount of clinical research in cancer, cardiac applications and epilepsy has been crucial in the establishment of clinical PET. This resulted in FDA approval of FDG and Health Care Financing Administration (HCFA) reimbursement which furthered the evolution of modern PET.

The introduction of lutetium oxyorthosilicate (LSO) has further revolutionized PET imaging. In comparison it has a slightly greater density, slightly lower effective atomic number, and has 5 times more light output than BGO²⁵⁴. LSO provide for up to 2mm resolution tomographs that will image the torso in less than half an hour (in systems designed for brain studies) or 4-6mm resolution scans in 3-5mins, thereby overcoming criticism of the imaging time factor in PET²⁵⁴.

At present the evolution of modern PET is marked by hybrid PET/CT. Improved diagnostic accuracy, surgery and radiation therapy planning, by merging the anatomy

and functional aspect of disease biology into a single procedure, are amongst several benefits. Fast, low-noise attenuation correction from the CT component also improves the PET component.

2.3. PET TRACERS IN RELATION TO ATHEROMA

The locally changed conditions, such as enhanced blood flow, enhanced vascular permeability and influx of white blood cells (WBCs), promote the accumulation of imaging agents to the site of inflammation²⁵⁵. Several tracers have been studied in the evaluation on vascular inflammation, in particular, atherosclerotic plaque. Single photon emission computed tomography (SPECT) with *in vitro* labelled leukocytes has been suggested as the 'gold standard' for acute inflammation imaging, although the sensitivity is suboptimal²⁵⁵⁻²⁵⁷. ⁶⁷Ga-citrate, radiolabelled WBCs and indium-111(111In) - or technetium-99m(99mTc)-labelled antibodies are used for SPECT assessment of inflammation. In chronic inflammation, limited neutrophils migrate to the inflamed site, so radiolabelled WBCs are not suitable for chronic inflammation imaging²⁵⁸. This is best accomplished with ⁶⁷Ga-citrate and ¹⁸F-FDG tracers which are useful to identify both acute and chronic inflammation^{255, 259}; however, neither is an inflammation specific imaging agent. In cancer studies, enhanced glucose metabolism is detected with FDG-PET scanning utilizing the difference in accumulation of ¹⁸F-FDG tracers which are useful to identify both acute and chronic inflammation between normal and cancerous tissues. The reduced specificity of ¹⁸F-FDG tracers, in particular the inability to discriminate between inflammation and tumour activity, has prompted researchers to investigate alternative tracers in cancer research. Other PET tracers, visualizing specific molecular pathways in tumours such as proliferation (eg ¹¹C-methionine, ¹¹C-choline, ¹⁸F-fluorothymidine), hypoxia (eg ¹⁸F-FMISO) or expression of certain receptors (Her2Neu, EGFR) are being used in the evaluation of malignancies. Some of these, as a result of individual characteristics, have found use as vascular PET tracers. Nevertheless, ¹⁸F-FDG PET remains the most widely studied vascular molecular imaging technique.

2.3.1. ^{18}F -fluorodeoxyglucose (^{18}F -FDG)

Readily available ^{18}F -FDG is a glucose analogue with a half-life of 110 min which decays by β^+ -emission. The active ingredient is 2-deoxy-2- ^{18}F -fluoro-D-glucose which accumulates in metabolic active cells and also has been found to be associated with neovessel content^{219, 260, 261}, a recognized characteristic of atherosclerosis. It is dependent on facilitated glucose transporters (GLUT) and sodium glucose co-transporters found on the walls of metabolic active cells known to metabolize glucose²⁶².

2.3.1.1. **How FDG - PET reflects vascular metabolism**

In a recent review Joshi *et al*²⁶³ described the mechanism of uptake of FDG with PET. FDG directly competes with glucose for cell uptake through GLUT transporter proteins, hence reflecting metabolic activity at the target site. Subsequently, FDG is phosphorylated to FDG-6-phosphate (rendering it resistant to further metabolism) by the hexokinase enzyme and thus accumulating within the cell. In theory, glucose-6-phosphatase can dephosphorylate FDG-6-phosphate, but this enzyme is not greatly expressed outside the liver and skeletal muscle cells, and so this effect is considered negligible in atherosclerosis. FDG reflect glucose usage of the cell studied, since the rates at which glucose and FDG are phosphorylated are proportional to each other²⁶⁴. Macrophages play an active role in all stages of vascular inflammation and atherosclerotic plaque formation. Macrophages use exogenous glucose for energy. Increased radioactivity using ^{18}F -FDG-PET can be used to investigate macrophage activity because macrophages express a high basal metabolic rate that is GLUT-dependent²⁰⁹⁻²¹¹. Histological evidence suggesting a correlation between CD68 as marker of macrophage activity and FDG uptake^{220, 265} further validates this hypothesis. Activated macrophages have an enhanced metabolic rate that requires additional uptake of glucose. Increased oxidative metabolism with immune cell activation (the 'respiratory burst' - phenomenon) is associated with a 20-fold increase in the rate of glucose metabolism. Glucose uptake of macrophages is significantly higher than that of neighbouring cell types²⁶⁶. Compared with quiescent cells, activated macrophages show an increased expression of GLUT type 1 and type 3 receptors, along with hexokinase²⁶⁷⁻²⁶⁹. FDG uptake is therefore a function of macrophage density and activation, GLUT

transporter expression, hexokinase activity and dephosphorylation, but may also reflect hypoxia-stimulated macrophages rather than mere vascular inflammation²²⁶.

In vitro studies reported that moderate hyperglycaemia does not affect uptake into macrophages^{270, 271} but that, in humans, reproducibility in those with elevated blood glucose levels at the time of FDG imaging is likely to be reduced²⁷². Furthermore, *in vitro* FDG can be taken up into adjacent cell types including endothelial cells and lymphocytes²⁷³. Further studies are required to demonstrate the relationship between ¹⁸F-FDG vascular uptake and long-term clinical outcomes.

2.3.2. ¹¹C or ¹⁸F-choline

¹¹C- or ¹⁸F-choline tracer is metabolized and incorporated into cell membranes in tumour cells and macrophages. DeGrado *et al*²⁷⁴ and Hara²⁷⁵ first developed and described fluoromethyl-dimethyl-2-hydroxyethyl-ammonium or ¹⁸F- choline (¹⁸F-FCH) chemistry by the synthesis of no-carrier added ¹⁸F-FCH through the intermediate ¹⁸F-fluorobromo-methane (¹⁸F-FBM)^{276, 277}. Similarly to ¹⁸F-FDG, this choline derivative is absorbed into cells by specific transporter molecules, then phosphorylated by choline kinase, metabolized to phosphatidylcholine, and later incorporated into the cell membrane^{276, 277}. ¹¹C has a short half-life (20.4 mins), which researchers view as a logistical limiting imaging factor. An apolipoprotein E -deficient murine study reported supremacy of ¹⁸F-FCH over ¹⁸F-FDG with stronger correlation of fat staining and macrophage-positive areas (84% vs. 64%)²⁷⁸. Preliminary data in five patients with a total of 31 vessel wall alterations demonstrate the feasibility of ¹⁸F-FMCH for *in vivo* imaging of structural vessel wall alteration in humans. Furthermore, in a cohort of male cancer patients, a retrospective analysis observed that labelled choline was not taken up into normal vascular wall, or purely calcified lesions²⁷⁹.

2.3.3. Radiogallium-labelled compounds

Generator-produced short-lived radionuclide ⁶⁸Ga has a half-life of 68 mins and decays at 89% by β^+ -emission (with maximum energy of 1.92 MeV) and 11 % by electron capture to stable zinc (⁶⁸Zn), and for that reason it can be used for PET imaging²⁸⁰. It is an excellent probe for high specific activity labelling of small peptides with fast blood

clearance and target localization. The half-life is suitable for labelling many ligands for PET imaging and it is short enough to cause minimal radioactive burden for a patient²⁸¹. Six ligands are currently studied in predominantly tumour clinical trials. [⁶⁸Ga-DOTA, Tyr3]octreotide (⁶⁸Ga-DOTA-TOC), [⁶⁸Ga-DOTA, 1-Nal3]-octreotide (⁶⁸Ga-DOTA-NOC), [⁶⁸Ga-DOTA-2-Nal, Tyr3, ThrNH28]octreotide (⁶⁸Ga-DOTA-Lanreotide) and [⁶⁸Ga-DOTA, Tyr3, Thr8]octreotide (⁶⁸Ga-DOTATATE) bind differently to subtypes of somatostatin receptors (eg somatostatin, vasointestinal peptide receptors, bombesin, cholecystokinin, gastrin, and/or substance P), and are studied especially for the imaging of neuroendocrine tumours (NETs) and well-differentiated thyroid tumours²⁸²⁻²⁸⁶. ⁶⁸Ga-DOTATOC is the most widely used ⁶⁸Ga-based PET radiopharmaceutical. DOTATOC ([D]-Phe1-Thy3-octreotide) uptake is observed in lesions with up-regulated somatostatin (SMS) receptors. In a recent preliminary clinical study concerning ⁶⁸Ga-citrate PET, good visualization of inflammation was obtained at 1.5h after injection²⁸⁷.

2.3.4. Tracers in experimental phase

Other novel nuclear probes in experimental phase have been suggested for the study of vascular inflammation. A promising agent is the translocator protein/peripheral benzodiazepine receptor (TSPO) ligand. TSPO is expressed on macrophages at 20 times greater density than VSMCs and TSPO ligands PK11195 and DAA1106 have been shown to bind to macrophage-rich regions in human carotid plaque²⁸⁸. However, TBR ratio for TSPO tracers remains unsatisfactory for vascular imaging purposes and a recent 4D-PET study concluded that chronic inflammation found in AAA walls was not detectable with [¹¹C]-PK11195 and [¹¹C]-d-deprenyl²⁸⁹. Nevertheless, there have been recent promising studies in vasculitis²⁹⁰.

A recent rat study suggested an isomer of glucose, ¹⁸F-labelled mannose, as an additional avenue for atherosclerotic molecular imaging. In this study ¹⁸F-labelled mannose and ¹⁸F-FDG had comparable uptake. Similar to glucose, mannose is taken up by macrophages through glucose transporters, and mannose receptors are expressed on a subset of macrophages in high-risk plaques^{291, 292}.

Chemotaxis

Attempts have been made to image the chemokine activity within the vessel wall, since chemokines recruit inflammatory cells to the atherosclerotic plaque. Endothelial dysfunction and atherosclerotic progression have successfully been visualized using ^{99m}Tc -labelled monocyte chemoattractant protein 1 (MCP-1)²⁹³.

Adhesion molecules on endothelial cells or leucocytes

Both vascular cell adhesion molecules (VCAM-1) and leucocytes antigen-4 have been utilized in atherosclerotic plaque imaging studies^{294, 295}. Kelly *et al* successfully imaged atherosclerotic vessel wall with a conjugated magnetofluorescent nanoparticle VCAM-1 MRI ligand, since the agent was incorporated by cells expressing VCAM-1²⁹⁴. Clinical translation is awaited for (^{99m}Tc) -labelled, anti-VCAM-1 nanobody cAbVCAM1-5 which allowed visualization of VCAM-1 expression and displayed mouse and human cross-reactivity²⁹⁶.

Lipoproteins

It is suggested that low-density lipoproteins (LDLs) play a role in early atherosclerosis formation and are essential for foam cell generation. Overcoming earlier plaque-to-background ratio challenges in studying non-oxidized LDL, Ishino *et al* developed a radio-labelled monoclonal antibody targeting LDL receptor 1, to evaluate oxidized lipoproteins in the vessel walls²⁹⁷. Other research groups have identified radioiodinated AHP7 for selective vascular imaging of oxidized LDL²⁹⁸.

Proteolysis

ECM degradation by MMPs leads to progression and complications of atherosclerosis and aneurysms. MMPs produced by differentiated macrophages, endothelial cells and VSMCs help orchestrate an increased turnover of the ECM, thought to be the reason for destabilization of the vulnerable fibrous cap. MMP inhibitors conjugated to ^{123}I , ^{125}I or ^{99m}Tc , has been used for *in vivo* quantification of proteases in vascular inflammation²⁹⁹. In a murine study, TAA was successfully imaged using a protease-activated fluorescent imaging agent, MMPsense 680. Several MMPs can somewhat selectively cleave the peptide substrate contained in MMPsense 680³⁰⁰. A gadolinium-based MR contrast agent with affinities to MMPs (P947) has also been suggested as a molecular imaging tool in elastase-induced AAA³⁰¹.

In a SPECT study, RP782, an ^{111}In -labelled probe targeted to activated MMP, demonstrated focal tracer uptake that paralleled CD68 expression in iatrogenic induced carotid aneurysms in mice³⁰². Researchers also explored imaging multiple aspects of atherosclerosis formation and found a significant correlation between radiolabelled MMP and the annexin ligand AA5 (used in apoptosis evaluation) and significantly more uptake for both tracers in a high lipid diet rabbit group compared to controls³⁰³.

MR detected CAN-35, a collagen-binding protein that preferentially binds to less well-ordered collagen, has also been utilized in vascular imaging of animal AAA³⁰⁴.

Apoptosis

Atherosclerosis is characterized to some extent by apoptosis. ^{99}Tc -annexin V has been described for quantifying apoptosis³⁰⁵. This tracer targets phosphatidylserine exposed by apoptotic and necrotic cells which occurs in SMCs and macrophages in advanced lesions as a result of lesion inflammation. Aortic atherosclerosis was imaged by ^{99}Tc -mannexin A5 with micro SPECT. The quantitative uptake of this tracer correlated with histological plaque extent and macrophage content³⁰⁵. Nevertheless, the work of Isobe *et al* and other groups developing apoptosis targets with phosphatidylserine-targeted MRI-contrast agents remains experimental with clinical translation lacking³⁰⁶.

Angiogenesis

Evidence suggests neovascularization relates to the inflammatory reaction and infiltration of macrophages / foam cells within atherosclerotic plaques³⁰⁷. $\alpha\text{v}\beta\text{3}$ integrin is a cell/matrix mediator which also allows for cell signal transduction from low affinity to high affinity states. This glycoprotein is abundantly expressed in activated endothelial cells. Radiolabelled $\alpha\text{v}\beta\text{3}$ integrin antagonist for plaque activity characterization has been reported. Haubner *et al* reported ^{18}F galacto-RGD (arginine-glycine-aspartic), an $\alpha\text{v}\beta\text{3}$ integrin, a promising potential ligand for plaque inflammation visualization³⁰⁸. A recent murine study concluded that since ^{18}F galacto-RGD uptake was reduced by a lipid-lowering diet intervention, $\alpha\text{v}\beta\text{3}$ integrin expression is a potential for pharmacological therapy response evaluation of plaque³⁰⁹.

Although vascular endothelial growth factor (VEGF) receptors have a broad expression pattern, researchers have attempted molecular imaging with Cy 5.5-labelled single chain VEGF in angiotensin II-induced AAAs with some success³¹⁰.

Thrombogenicity

Thrombogenicity is a central feature of plaque vulnerability. Radio-labelled soluble glycoprotein VI (a platelet collagen receptor) for assessing thrombogenicity has been used to successfully visualize induced thrombogenic carotid vascular lesions in an experimental murine study³¹¹.

Calcification

Calcification is believed to represent final stages of the pathobiological process of atherosclerosis. ¹⁸F-NaF is suggested to detect lesions with active vascular calcification and therefore is advocated by Dweck *et al* as promising for coronary plaque imaging³¹².

Further work should be undertaken to establish the role of nuclear imaging of various pathogenic inflammation factors for non-invasive detection of the vulnerable atherosclerotic plaque, diseased or aneurysmal vessels. Time-consuming preparation, slow plasma clearance and high cost constraints are barriers for clinical use.

2.4. STANDARDIZED UPTAKE VALUE (SUV)

Several classes of the analysis suitable for PET imaging analysis have been described. Nevertheless, the semiquantitative analysis of uptake normalization as a ratio of the dose injected per unit weight (SUV) has grown in popularity due to its simplicity and convenience of method compared with others. In PET the SUV came to be used as an adjunct tool to visual analysis. The SUV is the average activity per unit volume in the region of interest³¹³. To obtain a dimensioned (in mg/mL or m²/mL) result, weight or body surface area is used as the time-invariant denominator³¹³. SUV calculation has the advantage that dynamic imaging and or blood sampling is not necessary. However, imaging must take place at a late time-point, and at the same time-point in sequential studies, to meaningfully compare results³¹⁴.

2.5. SUV_{MAX} , SUV_{MEAN} AND TARGET-TO-BACKGROUND RATIO

Calculating the SUV on the highest image pixel in the region of interest is referred to as the SUV_{max}. Cancer treatment response assessed with FDG PET is often reported using SUV_{max}. Alternatively, region volume can be calculated making use of threshold or region growing techniques, and average SUV within the region is presented and referred to as SUV_{mean} or multiplied by tumour volume to calculate the total glycolytic volume (TGV)³¹⁵. In order to correct for background activity and false high uptake values a target-to-background ratio (TBR) is calculated, by dividing the measured SUV by background tissue SUV³¹⁶.

SUV_{max} is more widely used than SUV_{mean} since it is more reproducible and to a lesser extent observer dependent³¹⁷. Furthermore, Rudd *et al* suggest that for pharmacological therapy trials looking at reducing systemic arterial inflammation, eg statins use, the mean TBR_{max} measurement across a substantial portion of the artery be used, since the drug effect is likely to be spread across the arterial bed. However, for evaluating locally affecting atherosclerotic plaque therapies (eg vulnerable plaque stent implantation or gene therapy), serial TBR_{max} measurement within the localized disease segment may be more accurate²²³.

2.6. WHOLE-VESSEL SUV

To maximize reproducibility, and as recently described, to assess systemic and homogenic inflammatory effect, a whole-vessel analysis of the imaged vessel is suggested^{223, 318, 319}. In these studies arterial ¹⁸F-FDG uptake in the vessel was quantified by drawing a ROI around the artery to include the vessel wall and content. The average and maximum ¹⁸F-FDG SUV_{max} and/or SUV_{mean} was calculated, for each axial level of the coregistered transaxial PET/CT images, by adding the values and then dividing by the total number of axial images to obtain an average SUV_{max} and/or SUV_{mean} for the whole vessel. TBR was obtained by division of average SUV by an average background blood ROI (a minimum of 8 ROI large vein measurements), estimated from the inferior or superior vena cava^{219, 223}. Influencing factors on SUV measurement should be

considered and appropriate measures taken into account when performing SUV analysis. This will be explored in the PET/CT limitations section of this chapter.

2.7. PET/CT LIMITATIONS

In the past, availability of hybrid PET/CT has been reported as a limitation of this molecular imaging technique; however, it has become much more widely accessible.

FDG PET/CT has technical limitations. It is suggested there may be a possible confounding effect of hyperglycaemia in ^{18}F -FDG vascular uptake, limiting its use in diabetics. The clinical significance of this theory has been confirmed by a recent vascular PET study showing pre-PET blood glucose levels affect FDG uptake in both aortic and carotid walls³²⁰. It is thought that competition for cellular transport exit glucose, and therefore FDG uptake, may be affected in these patients.

Furthermore, false positive results and reduced specificity is possible given that glucose uptake is a non-specific biomarker of inflammatory activity. Tissues surrounding the arteries such as fat and skeletal muscle may display high ^{18}F -FDG metabolic accumulation and results could be interpreted erroneously (spillover effects). This could be avoided by meticulous measurements of regions of interest, appreciating criteria defining precedents such as visual judgment, noise-affected maximum pixel, the character of heterogeneity and others³²¹.

The dose of radiation exposure using co-registration imaging modalities is another technical limitation to consider. Serial PET imaging may be useful but would be highly constrained by radiation dose. The combined radiation exposure from the injected radiopharmaceutical and the CT scan during a single PET/CT examination is significantly higher than other clinical studies or radiation from natural sources. A single ^{18}F -FDG injection can be the source of 7 millisievert (mSv) effective radiation and the dose of a limited CTA or CT could range from 3 to 15mSv depending on the acquisition protocol, which is comparable to approximately 3y of natural background radiation exposure. The cumulative and long-term effects of such levels of radiation are

unknown, with more definitive safety information required to consider serial use in younger populations.

Measuring vessel wall uptake ^{18}F -FDG is difficult, because of the dimensions involved, and the limited spatial resolution of PET. However, the loss of apparent activity (partial volume effect) can be overcome to some extent by measuring larger targets more than twice the full width at half maximum resolution³²². For example, measuring the increased diameter of the aorta rather than other studied vessels, eg carotid and coronary vessels, reduce partial volume effects. Also the aortic wall expands with aneurysm formation³²³, thus reducing partial volume effects. Accuracy can be improved by performing attenuation correction, standardizing reconstruction methods and by partial volume correction.

The time of image acquisition also is an important determining factor in SUV measurement. The acquisition interval is normally chosen at a time that $(\text{dSUV}/\text{dt})/\text{SUV}$ is not excessive and may vary between research groups. Furthermore it is suggested that lean body mass and body surface area rather than weight depict a body volume more accurately as denominator for SUV calculation³²¹.

2.8. ETHICAL APPROVAL

Ethical approval was obtained from the University College London Research Alpha Ethics committee and regional site specific approval was obtained from the Brighton & Mid Sussex Research Ethics committee. All subjects provided written informed consent.

SECTION II ORIGINAL WORK

CHAPTER 3. ABDOMINAL AORTIC ANEURYSM METABOLIC ACTIVITY DETECTED BY ¹⁸F-FLUORODEOXYGLUCOSE (¹⁸F-FDG) POSITRON EMISSION TOMOGRAPHY/COMPUTED TOMOGRAPHY (PET/CT)

3.1. INTRODUCTION

Abdominal aortic aneurysm (AAA) diameter is an important predictor of risk of aneurysm rupture^{23, 24}. However, some aneurysms rupture at a small size^{23, 324, 325}, and many large aneurysms grow to a considerable size without rupture. Size therefore is not the only determinant for the risk of rupture. Investigators have shown that anatomical and dynamic features such as aneurysm shape, aneurysm wall calcification and computed wall stress, are also associated with the risk of AAA rupture^{16, 326}.

AAAs are associated with an inflammatory cell infiltrate and enzymatic degradation of the vessel wall^{10, 34, 66}. Correlation between risk of rupture and biological markers of inflammation has been demonstrated³²⁷. Furthermore, immune-mediated processes play a role in initiation of AAA disease and rupture^{22, 106, 328}. ¹⁸F-FDG accumulates in macrophage-rich atherosclerotic plaques and demonstrates that vascular macrophage activity can be quantified non-invasively³²⁹. Investigators have shown that ¹⁸F-FDG positron emission tomography (PET) can reliably detect signals in atherosclerosis²¹⁴. Recently, more researchers showed compelling evidence that this PET signal may be related to vascular inflammation, using PET/CT to demonstrate correlation between histologically assessed macrophage-dense and/or lymphocyte infiltrate regions and FDG uptake^{221, 222}.

An early PET study has been reported to show an increased FDG uptake in only 39% of aneurysms^{34, 222}. However, this study assessed larger-size AAAs (mean AAA diameter 6.3±0.95) with a PET only scanner without the use of CT to correct for density or show anatomical detail. The hybrid PET/64-detector CT scanner allows a more reliable assessment of increased ¹⁸F-FDG uptake in areas of interest on a high resolution CT.

The associations between prognosis and the degree of FDG uptake in the wall of small AAAs and as assessed by hybrid PET/CT may become increasingly relevant with the implementation of aneurysm screening. Preliminary data show that there is increased focal uptake of ^{18}F -FDG within the aneurysm wall in patients with large, rapidly expanding or symptomatic aneurysms that are prone to rupture³³⁰. However, the role of hybrid PET/CT, especially in quantifying the degree of inflammation in patients with small AAAs under surveillance, remains to be defined.

Furthermore, the optimum circulation time of ^{18}F -FDG for vascular imaging is unknown. In oncology PET studies the 1h time-points are often used³³¹, whereas some researchers in cardiovascular imaging advocated performing imaging at 3h after the injection of ^{18}F -FDG to maximize the contrast between vascular ROI and background²¹⁰.

The aim of the research in this chapter was to assess the degree of metabolic activity in AAAs of patients undergoing surveillance, with ^{18}F -FDG -PET/CT. Assessment is also made of possible association between aneurysm tortuosity, calcification, intra-luminal thrombus (ILT), expansion rate, and ^{18}F -FDG Uptake. It was hypothesized that the detection of inflammation with hybrid PET/CT in the aneurysm walls may help predict growth rate and allow evaluation of pharmacological interventions for suppression of inflammation in small aneurysms. Further assessment was made of whether there were ^{18}F -FDG uptake differences in the aortic wall and lumen of the aneurysms at various PET imaging times (at 45, 60, 120, and 180min) after an injection of ^{18}F -FDG to determine the optimal time to image vascular metabolism using ^{18}F -FDG PET/CT.

3.2. MATERIALS AND METHODS

3.2.1. Patients

Seventeen patients (sixteen male and one female) with a mean age of 74 ± 5 y were prospectively studied. All patients had infra-renal AAAs. One of the seventeen patients also had common iliac aneurysms. One patient was symptomatic and underwent an EVAR (endovascular aneurysm repair). This patient had a large (6.7cm) AAA and

presented with associated back pain. Each patient underwent an ultrasound scan followed by PET/CT within approximately two weeks of the ultrasound scan. Exclusion criteria were the presence of congestive heart failure and/or impaired renal function (serum creatinine >1.8mg/dL. The patient characteristics for co-morbidities and oral medications are documented in Table 3.1. Study population data for patients with AAAs undergoing surveillance, is summarized in Table 3.2.

Table 3.1 Patient demographic data

Characteristics	Surveillance AAAs (n=17)
Age (mean \pm SD y)	74 (\pm 5)
Male M/F	16/1
Max diameter (mean \pm SD cm)	5.3 (\pm 0.9)
Asymptomatic	16
Symptomatic	1
Associated back pain	1
Auto-immune disease	1
Family history of AAA	0
Previous major surgery	4
Risk factors, yes/no	
Smoking (previous or current)	9/8
Hypertension	8/9
Hyperlipidaemia	9/8
Diabetes Mellitus	2/15
CAD	2/15
Prior CVA	0/17
Prior CABG	1/16
Malignancy	1/16
Medications, yes/no	
Anti-platelet therapy	6/11
B-blockers	3/14
ACE-inhibitors	6/11
Statin	10/7
Laboratory data,	
Elevated CRP	1
Elevated ESR	3

Abbreviations: CAD, coronary heart disease; PVD, peripheral vascular disease; CVA, cerebral vascular accident; CABG, coronary artery bypass grafting; ACE, angiotensin converting enzyme; CRP, C-reactive protein; ESR, erythrocyte sedimentation rate

Table 3.2 Patient characteristics with non-specific AAAs undergoing surveillance

ID			Diameter	Diameter	Increased	Remarks
No	Sex	Age	of AAA on U/S	of AAA on CT	FDG Uptake (SUV _{max} >2.5)	
1	M	77	5.3	5.6	YES	
2	M	77	5.7	5.8	YES	Prostate cancer
3	M	74	3.9	4.5	YES	
4	M	75	5.3	5.7	NO	Auto-immune disease, previous major surgery
5	M	79	5.1	5.6	YES	
6	M	73	4.5	4.5	YES	
7	M	74	4.4	5.3	NO	Previous major surgery
8	M	65	-	6.8	YES	
9	M	77	4.7	5.5	YES	
10	M	82	5.4	6.0	YES	Previous major surgery
11	M	80	3.1	3.4	NO	
12	M	68	4.3	4.7	YES	Back pain
13	M	68	4.3	4.7	YES	
14	M	64	4.3	4.9	YES	
15	M	70	6.4	6.7	YES	
16	M	76	4.5	4.4	YES	
17	F	71	4.3	4.7	NO	Previous major surgery

3.2.2. Protocol for ultrasound surveillance

All patients underwent ultrasound scans to measure the size of the aneurysm at intervals of 3, 6 or 12 months. All scans were performed in the same unit by experienced vascular scientists using standard protocol and equipment.

3.2.3. Protocol for FDG-PET/CT

Patients were instructed to fast for at least 6h prior to the FDG-PET/CT. Images were acquired from a single bed position at 45, 60, 120 and 180 minutes after injecting 200MBq of ^{18}F -FDG using a dedicated combined PET/64-detector CT instrument (GE Healthcare Technology, Waukesha, WI). Firstly, an attenuation correction CT was performed using $64 \times 3.75\text{mm}$ detectors, a pitch of 1.5 and a 5mm collimation (140kVp and 80mA in 0.8s) over the patient's abdominal aorta. Maintaining the patient position, an ^{18}F -FDG PET emission scan was performed and covered an area identical to that covered by CT. All acquisitions were carried out in 2D mode (8 min/bed position). Transaxial emission images of 3.27mm thickness (pixel size 3.9mm) were reconstructed using ordered subsets expectation maximization³³² with two iterations and 28 subsets. The axial field of view was 148.75mm, resulting in 47 slices per bed position.

3.2.4. Image analysis

PET/CT images of the infrarenal aorta were reviewed by two combined radiologist/nuclear medicine physicians in consensus. One of these readers had a specialist interest in cardiothoracic PET/CT (more than 5y). PET/CT images were loaded onto a Xeleris workstation (GE Healthcare Technology, Waukesha, WI). The maximum AP aneurysm diameter, tortuosity, symmetry, ILT presence and aneurysmal calcification score were determined on the attenuation correction CT. Tortuosity was determined through visual assessment. Asymmetry was defined as $>1\text{ cm}$ discrepancy in major and minor axial diameters. Substantial ILT of the aneurysmal segment was defined as ILT with a diameter $>10\text{mm}$ on axial plane¹⁹⁴. Through visual assessment of axial and coronal images, the area of most intense focal AAA wall ^{18}F -FDG uptake was identified. Image analysis of AAAs extending into the bifurcation and beyond was limited to the aorta. Regions of interest (ROIs) were then drawn over the AAA wall and lumen, and the maximum standardized uptake value (SUV_{max}) and target-to-background (TBR_{max}) blood pool metabolic activity were measured (Figure 3.1). Increased ^{18}F -FDG tracer uptake in AAA was defined as a $\text{SUV}_{\text{max}} > 2.5$ ³³³.

3.2.5. Calcification quantification

Calcium scores were calculated for the whole AAA using OsiriX software (Pixmeo, Geneva, Switzerland). Arterial calcification was measured from the CT images using a threshold for calcium ≥ 130 Hounsfield units³¹⁶.

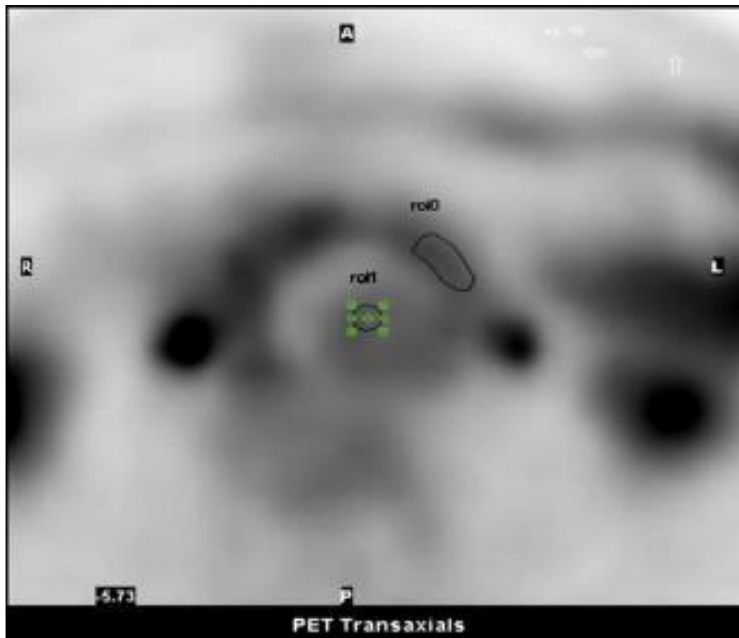


Figure 3.1 Axial PET image of an abdominal aortic aneurysm with regions of interest (ROI) placed on the lumen (roi1) and the wall of the aorta (roi0)

3.2.6. Statistical analysis

Data analysis was carried out using the statistical package SPSS® version 15.0 for Windows. Data were examined for normality using Kolmogorov-Smirnov testing. In a sub-group of fourteen subjects unpaired t-test was used for comparison of FDG uptake and the following groups: tortuous and non-tortuous aortas; heavily calcified AAAs and non-heavily calcified AAAs, ILT present and ILT absent. The relationship between increased FDG uptake and annual expansion was analyzed with Spearman rank correlation. The comparison of ^{18}F -FDG measurements across the 4 time-points was performed using ANOVA of repeated measures in all 17 participants. A paired 2-tailed t-test was used to compare differences between variables obtained at 1h and 3h. A p-value of less than 0.05 was considered statistically significant and SUV values were calculated as mean \pm standard deviation.

3.3. RESULTS

The mean maximum aneurysm diameter in the population studied was 5.3cm (SD±0.9cm). Recent AAA expansion within the last year as measured by ultrasound was seen in seven patients. Recent annual expansion ≤ 3 mm was observed in three patients and four patients had a recent annual growth rate >3 mm and <6 mm. Two patients presented with an expansion >6 mm in the last year. There were no asymmetrical aneurysms. Five aneurysms were tortuous. The mean aneurysmal calcification score was 7973 (SD±6980). Heavily calcified AAA was defined as AAA with a calcification score > 10000 . This threshold was at approximately the 75th percentile. Four aneurysms were heavily calcified with scores $>10\ 000$. Intra-luminal thrombus $>10\text{mm}^{194}$ in diameter was seen in the aneurysmal sac of six patients.

3.3.1. Relationship between clinical characteristics and ^{18}F -FDG Uptake

Thirteen aneurysms showed an increased FDG uptake ($\text{SUV}_{\text{max}} > 2.5$). No significant correlation was found between the degree of FDG uptake and recent AAA growth rate (Spearman's correlation coefficient; $r=0.18$; $p=0.60$). Furthermore no association was observed between cross-sectional infra-renal AAA diameter and SUV_{max} (Spearman's correlation coefficient; $r= -0.006$; $p=0.96$) (Figure 3.2). PET/CT revealed no other clinical findings. Furthermore, only four patients in our study revealed a $\text{SUV}_{\text{max}} \leq 2.5$.

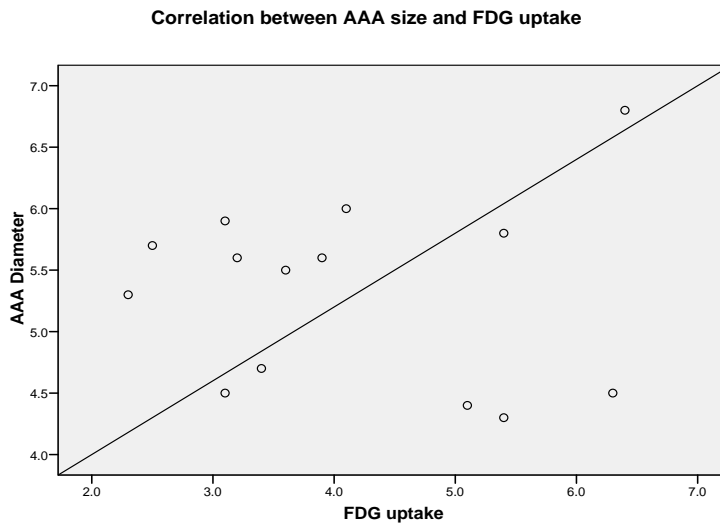


Figure 3.2 Scatter plot of maximum standard uptake values (SUV_{max}) of ^{18}F -fluorodeoxyglucose (^{18}F -FDG) illustrating no association between AAA size and FDG uptake ($r_s=-0.006$; $p=0.96$)

3.3.2. Relationship between anatomical characteristics and ^{18}F -FDG Uptake

There was no significant difference in FDG uptake between tortuous and non-tortuous aortas (unpaired t test; $t(12)=0.72$, $CI=-1.19-2.37$, $p=0.48$), or between heavily calcified aneurysms and non-heavily calcified aneurysms; (unpaired t test; $t(12)=-1.48$, $CI=-2.65-0.51$, $p=0.17$). This investigation failed to demonstrate a significant difference in SUV_{max} between AAAs with or without the presence of ILT (unpaired t test; $t(12)=0.51$, $CI=-1.26-2.03$, $p=0.62$).

3.3.3. Optimum circulation time for ^{18}F -FDG

Findings of the assessment of optimum circulation time for ^{18}F -FDG uptake are summarized in Table 3.3.

Table 3.3 Data for SUV_{max} of aortic wall, aortic lumen, and TBR_{max} at each time-point after injection of ^{18}F -FDG

<i>Area</i>	<i>Time (min)</i>			
Wall SUV_{max}	45	60	120	180
Mean	2.08	2.15	1.62	1.99
% change	0	+3%	-22%	-4%
SD	0.44	0.46	0.26	0.745
SE	0.11	0.11	0.62	0.18
Lumen SUV_{max}				
Mean	2.3	2.4*	1.74	1.7*
% change	0	+4%	-24%	-26%
SD	0.4	0.44	0.41	0.4
SE	0.1	0.11	0.1	0.1
TBR_{max}				
Mean	0.91	0.91	0.96	1.01
% change	0	0	+6%	+11%

SD – Standard deviation; SE – Standard error; TBR_{max} – Maximum target-to-background ratio

*Significant difference in SUV_{max} in lumen at 60 and 180 min (paired t test, $p < 0.001$) was observed

Aortic wall SUV_{max} and lumen SUV_{max} were significantly different with time (repeated measures ANOVA, $p=0.02$ and $p=0.001$, respectively). There was no significant difference in TBR_{max} with time (repeated measures ANOVA, $p=0.206$). Furthermore, no significant difference between SUV_{max} at 60 and 180 min in the aortic wall was observed (paired t test, $p=0.367$); however, there was a significant difference in SUV_{max} in the lumen at 60 and 180min (paired t test, $p=0.001$). There was no significant difference in TBR_{max} between 60 and 180min (paired t test, $p=0.131$).

3.4. DISCUSSION

The use of FDG-PET/CT *in vivo* has previously been described in patients with symptomatic and/or larger-sized AAAs³³⁰. In this chapter we evaluate for the first time the role of hybrid FDG-PET/CT to detect increased inhomogeneous metabolic activity

and its association with anatomical features, in predominantly small AAAs, in patients undergoing routine surveillance.

This study shows that the majority (n=13) of patients demonstrated an increased FDG uptake ($SUV_{max} > 2.5$) in the aneurysm wall. Inflammatory processes may, therefore, be present to some extent in most aneurysms. In contrast, a PET study by Sakalihan *N et al* reported increased FDG uptake in only 39% of their study population³⁴. However, in Van Damme and Sakalihan's study, their definition of PET positivity was not clearly defined, and positive PET findings may have been judged solely on appearance of 'hot spots'. Also patients with larger-size aneurysms were studied (mean AAA diameter 6.3 ± 0.95) as compared to our investigation of smaller aneurysms (mean AAA diameter 5.3 ± 0.9 cm). Furthermore, the study performed PET independent from CT scan, whereas in our study hybrid PET/CT was used. The benefit of hybrid PET/CT over independent imaging modalities is described in the literature³³⁴. Combined PET/CT, as used in our study, eliminates the positional discrepancies and some of the challenges brought on by different test timings when interpreting investigation findings. Improved test sensitivity due to technology and technique advances may partly explain the global higher SUV_{max} in our study. Factors influencing AAA wall inflammatory processes require further investigation and prospective studies are necessary to establish the role of PET/CT in quantitative assessment of inflammation in AAAs and the clinical significance thereof.

Rapid expansion in large aneurysms and its association with increased FDG uptake was reported in a preliminary study³³⁰. In comparison, our study revealed a weak correlation between recent AAA expansion (within the last year) and FDG uptake, which was not statistically significant ($p = 0.16$). Irregular and unpredictable progression of small AAAs³⁹ and small patient numbers (n=14) could explain our results. The relationship between FDG uptake and AAA growth rate and risk of rupture in AAA under surveillance remains unanswered. Furthermore, correlating focal increase in FDG uptake with histological findings from the rupture site may prove to be impossible.

Maximal AAA diameter measured with CT is significantly and consistently larger than maximal AAA diameter measured with ultrasound^{88, 336}. This explains the discrepancy seen in some of the maximal AAA measurements between ultrasound and CT displayed

in our study. Our work confirmed similar findings by Reeps *et al* in that no relationship was found between cross-sectional infra-renal AAA diameter and increased aortic wall glucose metabolism²²² (Figure 3.2). A recent study suggests aneurysm wall stress to be more predictive of rupture risk than AAA diameter³²⁶. Further research is required to assess the relationship between increased glucose metabolism and increased AAA wall stress.

Ruptured AAAs tend to be less tortuous, yet have greater cross-sectional diameter asymmetry¹⁶. Interestingly, our patient population showed anatomical characteristics of aneurysms associated with less risk of rupture. Tortuosity was demonstrated in five patients and no asymmetry detected, yet most study patients had an increased FDG uptake. PET/CT did not reveal a significant difference in FDG uptake between tortuous and non-tortuous AAAs ($p=0.48$). It is reported that the presence of calcification increases AAA peak wall stress, suggesting that calcification decreases the biomechanical stability of AAAs⁴⁰. Another study showed that the ¹⁸F-FDG uptake sites were mostly distinct from the calcification sites²¹⁵. There was no correlation detected between increased FDG uptake and degree of calcification found ($p=0.17$). We and others²¹⁹ suggest that the clinical significance of the relationship between vascular-wall ¹⁸F-FDG uptake and CT calcifications needs to be assessed by further prospective studies with long-term follow up. The role of intra-luminal thrombus and its influence on the AAA wall remains to be established. Although, studies suggest ILT reduces aneurysmal wall pressures^{40, 102}, pathological studies show formation and accumulation of inflammatory cells in thrombus-lined vessels that may perturb the structural integrity and stability of the vessel wall, and thereby increase the risk for aneurysm rupture¹⁹¹. No significant difference in increased FDG uptake between AAAs associated with or without ILT was observed ($p=0.62$). Nevertheless, these results should be interpreted with caution in a small preliminary study population in which type II statistical errors cannot be excluded.

There is a need for uniformity of vascular PET/CT imaging methodology to enable comparison and collaboration between institutions. The significant difference observed between ¹⁸F-FDG uptake at 1 and 3h post tracer injection has implications for patient throughput and to allow for a more acceptable patient journey. However, a recent vascular PET study has suggested an optimum FDG circulation time for vascular

PET/CT of about 2.5h, after tertile analyses revealed this ^{18}F -FDG circulation time has a favourable association between arterial and blood-pool FDG uptake³²⁰. At the time of the current study there was no uniformity in vascular PET/CT imaging time. Therefore, in this study ^{18}F -FDG uptake on PET/CT was measured at 3h to improve the reproducibility of the technique.

Despite the improved reliability of integrated 64 slice PET/CT there are some limitations that need to be addressed. The partial volume effect observed in small thin targets such as the AAA wall may affect the accuracy of FDG PET/CT. Results could be more accurate with the implementation of volume effect correction. Furthermore, differences in activity or volume could influence the accuracy of signal interpretation.

In an immunohistochemical study, Mochizuki *et al* reported that the expression of glucose transporter protein (GLUTs) was detected in inflammatory tissue, which showed ^{14}C -FDG uptake higher than that of normal control muscle³³⁷. Therefore, the presence of inflammation was suggested by FDG accumulation. The findings in this study offer *in vivo* evidence that AAA show increased glucose metabolism, mediated by the Glut-1 transporter. ^{18}F -FDG PET/CT identifies metabolic activity in abdominal aortic aneurysms, whether they have or have not the anatomical characteristics of aneurysms at risk of rupture. Increased glucose metabolic activity in the aneurysmal wall as detected by PET/CT may be present in most AAAs. Although preliminary data showed PET/CT to be promising in identification of a varying degree of glucose metabolic activity in AAAs, its clinical role in predicting growth rate and rupture risk in patients with small AAAs undergoing surveillance remains to be defined by larger studies. The possible benefit of anti-inflammatory therapeutic approaches in patients with AAA under surveillance is a prospect that remains to be demonstrated. Hybrid PET/CT may be a valuable assessment technique in identifying the role that inflammation or metabolism plays in AAA disease.

Summary of findings:

- Increased ^{18}F -FDG uptake ($\text{SUV}_{\text{max}} > 2.5$) was observed in 13/17 AAAs.
- Recent AAA expansion did not correlate with ^{18}F -FDG uptake.

- There was no significant difference in ^{18}F -FDG uptake between tortuous compared to non-tortuous aortas; heavily calcified *versus* non-heavily calcified; and AAAs with or without ILT.
- There was no significant advantage in imaging at 3h over 1h after ^{18}F -FDG injection.

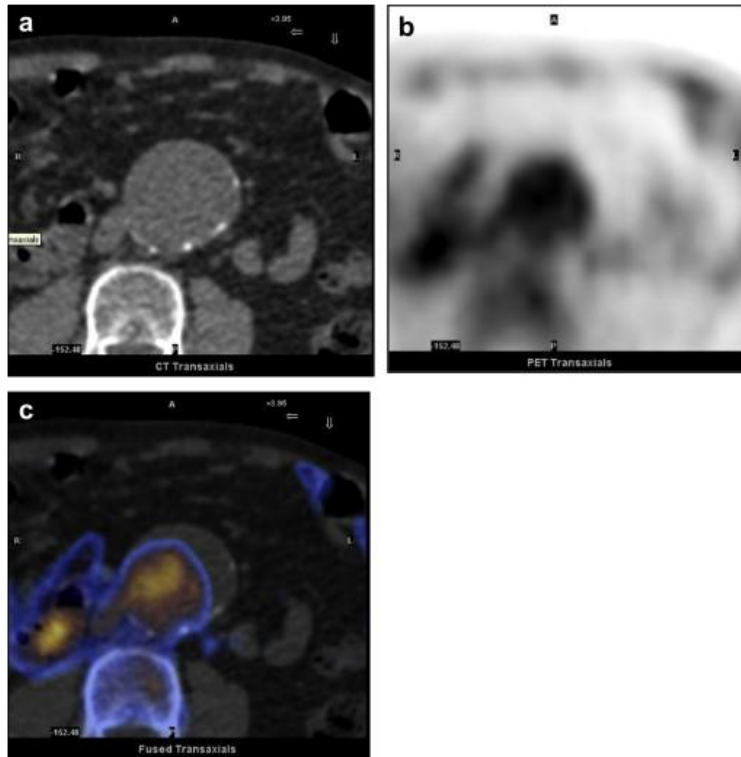


Figure 3.3 Axial (a) Unenhanced CT, (b) PET, and (c) PET/CT fusion of an AAA demonstrating ^{18}F -FDG circulating in the arterial and venous lumens and no uptake in the wall of the aorta

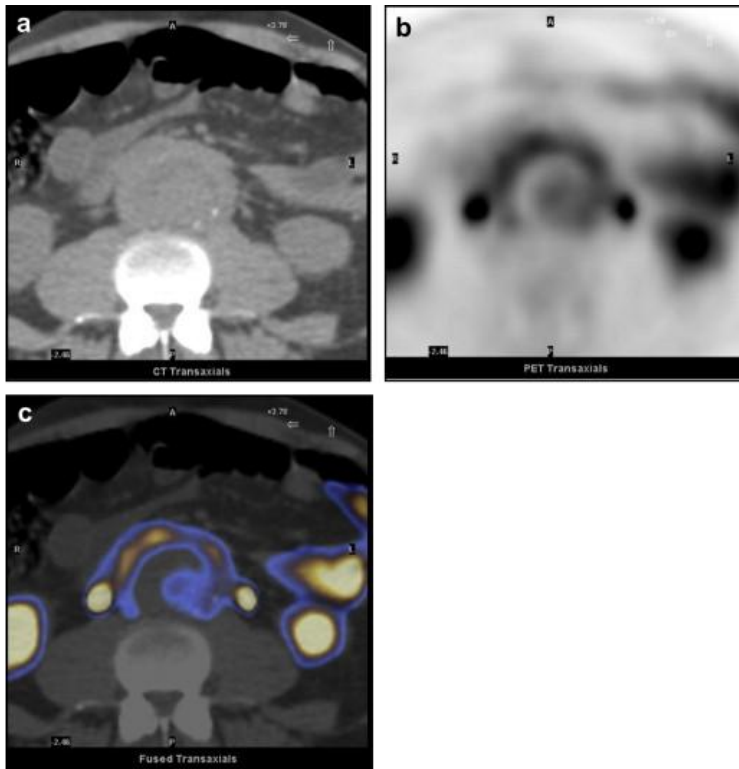


Figure 3.4 Axial (a) Unenhanced CT, (b) PET, and (c) PET/CT fusion of an AAA showing uptake in the lumen and increased uptake in the wall of the aorta

The relationship between ^{18}F -FDG PET and AAA expansion could be further investigated to provide insight into AAA biology. The next chapter in this thesis investigates the potential correlation between AAA wall inflammation and future aneurysm growth to gain insight in FDG PET/CT as a potential risk stratification method for small AAA.

CHAPTER 4. RELATIONSHIP BETWEEN ^{18}F -FDG AORTIC ANEURYSM UPTAKE ON PET/CT AND ANEURYSM GROWTH RATE

4.1. INTRODUCTION

Screening programmes for aortic aneurysms are being introduced in North America and Europe. The increase in surveillance is creating demand for further risk stratification whilst intensifying the need to develop strategies for retarding growth rate in small aneurysms (maximum diameter between 3.0 and 5.5cm)³³⁸. Investigators advocate a bi-modal growth pattern for AAA, with a recent finding of a significant association between annual AAA growth rate of at least 2mm and AAA-related events²¹. A watchful waiting approach is suggested for AAAs with lower growth rates as a result of lipid-lowering drug treatment or as determined by initial AAA diameter measurements³³. It would be important to detect sub-groups at risk of aortic expansion and to identify methods of measuring response to therapy in these patients^{73, 339-341}. It would also be attractive to develop non-invasive *in vivo* imaging techniques to detect and quantify aneurysm inflammation and thereby possibly growth rate.

The use of fluorodeoxyglucose positron emission tomography (^{18}F -FDG PET) as a potential biomarker in vascular disease is becoming more widespread^{73, 111, 210, 215, 217, 219, 339-344}. Although prospective ^{18}F -FDG PET data have demonstrated instability of plaque in the carotid arteries^{210, 219} and in the assessment of arteritis^{318, 345}, it has not been applied to risk- stratification in AAA expansion. A small study with standalone ^{18}F -FDG PET showed equivocal findings³⁴. ^{18}F -FDG hybrid PET/CT had not been used until recently, but recent histologically validated studies showed that increased aortic ^{18}F -FDG uptake on PET/CT predicts the degree of wall inflammation^{221, 222}.

Currently there are clinical management dilemmas in the treatment of patients with small aneurysms and patients with large aneurysms with co-morbidity rendering them at high surgical risk. Both these types of patients are increasingly being identified with newly implemented AA screening programmes³⁴⁶, thus exacerbating the dilemma. There is need to risk-stratify these patients and thus it is important to explore possible

roles of non-invasive imaging techniques such as ^{18}F -FDG PET/CT. We therefore prospectively studied the relationship between aortic wall ^{18}F -FDG uptake and expansion rate, in patients with AAA, undergoing routine surveillance with ultrasound size measurements.

4.2. MATERIAL AND METHODS

4.2.1. Patients

During a 12-month period, patients presenting to University College Hospital, London or Royal Sussex County Hospital, Brighton, with AAA undergoing surveillance were invited to participate in this prospective ^{18}F -FDG-PET/CT study. In that year, 34 consecutive patients [31 men, 3 women, median age 75y (IQR 71 - 78)] were recruited for ^{18}F -FDG-PET/CT. The patient clinical profile is presented in Table 4.1. Nine patients were lost to follow up at 12 months (deceased n=2, withdrew from study n=1, failed to attend ultrasound scan n=5, emergency AAA repair n=1), leaving 25 patients for analysis.

Table 4.1 Summary of the medical details of the patient population

History or Symptoms	Number of patients (n=25)
Back or abdominal pain present	3
Ischaemic heart disease	7
Raised lipids	19
Diabetes	3
Hypertension	19
Current or previous smoker	16

4.2.2. Duplex ultrasound image acquisition

Study patients underwent abdominal ultrasound at the time of PET/CT examination and subsequently routine ultrasound scan measurements at 6 and 12 months post PET/CT. Specialist vascular scientists, with greater than three years' experience, performed the

surveillance ultrasound scans (Philips, HDI 5000, C5-2, Curved Linear Probe). In keeping with other researchers³⁴⁷, maximal anteroposterior (AP) external aortic wall diameter was recorded on each occasion. To correct for baseline aneurysm size the authors calculated expansion at 12 months divided by aneurysm size at time of PET/CT scan.

4.2.3. PET/CT image acquisition

All patients were fasted for 6h prior to scans, and images were acquired 3h^{217, 219, 223, 348} after injecting 200MBq of ¹⁸F-FDG using a dedicated combined PET/64-detector CT instrument (GE Healthcare Technology, Waukesha, WI). CT was performed using 64×3.75 mm detectors, a pitch of 1.5 and 5mm collimation (140kVp and 80mA in 0.8s) over the patient's abdominal aorta. Maintaining the patient position, an ¹⁸F-FDG PET emission scan was performed and covered an area identical to that covered by CT. All acquisitions were in 2D mode (8 min/bed position). Transaxial emission images of 3.27mm thickness (pixel size 3.9mm) were reconstructed using ordered subsets expectation maximization³³² with 2 iterations and 28 subsets. The z-axial field of view was 148.75mm, resulting in 47 slices per bed position. Axial fused PET/CT (a) and PET (b) images of an AAA showing ¹⁸F-FDG uptake and minimal ¹⁸F-FDG uptake in the wall of the aorta are shown in Figure 4.1 and Figure 4.2, respectively.

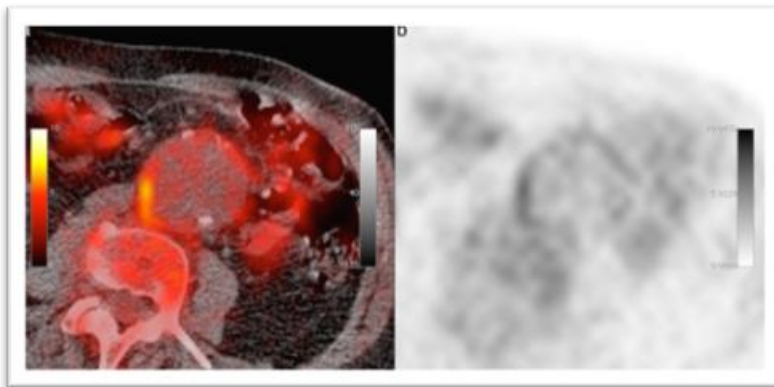


Figure 4.1 Axial fused PET/CT (a) and PET (b) images of an AAA showing ¹⁸F-FDG uptake in the wall of the aorta (whole vessel $SUV_{max}=3.35$; whole vessel $TBR_{max}=1.60$)

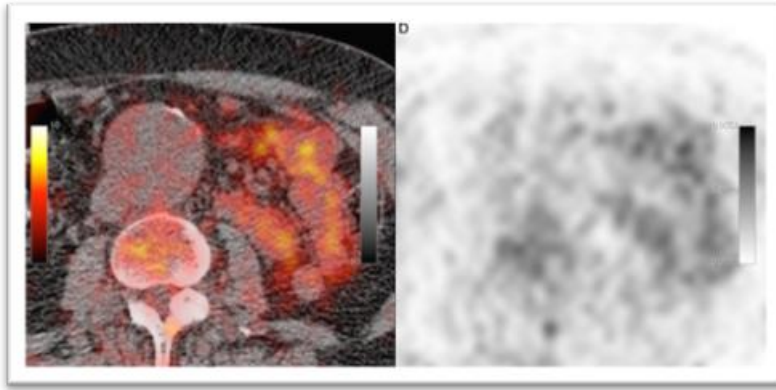


Figure 4.2 Axial fused PET/CT (a) and PET (b) images of an AAA showing minimal ^{18}F -FDG uptake in the wall of the aorta

4.2.4. Image analysis

PET/CT images were reviewed both by a dual accredited radiologist/nuclear medicine physician with a special interest in cardiovascular imaging and with greater than three years' experience of measuring vascular ^{18}F -FDG uptake, and by a surgeon with a special interest in vascular imaging, supervised by a dual accredited radiologist/nuclear medicine physician. (PET/CT images were loaded onto a Xeleris workstation (GE Healthcare Technology, Waukesha, WI). To maximize reproducibility and as recently described^{223, 318, 343}, we performed a whole vessel analysis of the imaged abdominal aorta³⁴⁹. Through visual assessment of axial and coronal planes of the imaged aorta, measurements were commenced on axial images from distal to the neck of the AAA and proximal to distal descending aorta where vessel diameter normalizes to include the whole volume of the aneurysm. AAAs extending into the bifurcation were measured up to the level of the bifurcation of the aorta. A region of interest (ROI) was placed to include the aneurysm wall and content. The maximum ^{18}F -FDG uptake (SUV_{max}) of the whole AAA was calculated subsequently for each axial level and the values were then summed and divided by the total number of axial images to obtain an average SUV_{max} for the whole AAA. TBR_{max} was calculated by division of average SUV_{max} by an average blood ROI (at least 8 venous ROI measurements), estimated from the inferior vena cava³¹⁶. In addition, for each individual AAA we identified the site of maximum aortic wall ^{18}F -FDG uptake. At this site we measured the SUV, yielding in each patient a

single site SUV_{max} , as previously described^{222, 348}. The SUV is the decay-corrected tissue concentration of ^{18}F -FDG (in kBq/g), adjusted for injected ^{18}F -FDG dose and body weight (in kBq/g)³⁵⁰. The interobserver agreement between the two readers was recorded.

4.2.5. Statistical analysis

Following tests for normality, non-parametric statistical tests were performed and median values thus presented. Mann-Whitney U tests were used to compare aortic wall ^{18}F -FDG uptake values and clinical factors. Correlations were performed using Spearman Rank Correlation. Statistical tests were performed with SPSS (Version 16.0). Statistical significance was set at 5%.

4.3. RESULTS

4.3.1. Aortic ^{18}F -FDG uptake and ultrasound measurements

The median maximal whole abdominal aortic wall ^{18}F -FDG uptake (SUV_{max}) was 1.70 (IQR 1.45-2.08). The median single site SUV_{max} was 2.17 (IQR 1.89-2.73). The median whole vessel TBR_{max} was 1.15 (IQR 1.00-1.40). The median maximal aortic AP diameter was 50.0 (IQR 40.4-53.5)mm. The median maximal aortic AP diameter 12 months following the PET/CT imaging was 53.0 (IQR 46.0-58.5)mm. The median aneurysm expansion at 12 months was 2.0 (IQR 0.05-5.0)mm (range 0-9)mm (Figure 4.3).

The correlation (r) between whole-vessel ^{18}F -FDG SUV_{max} and ultrasound expansion at one year was - 0.501 ($p=0.011$), (Figure 4.4). The correlation between the single site SUV_{max} and aneurysm growth after 12 months ($r = - 0.279$ $p=0.176$). No significant relationship between whole vessel TBR_{max} and annual expansion was found ($r=0.031$, $p=0.882$). Male patients had a median whole abdominal aortic wall SUV_{max} of 1.70 (IQR 1.45-1.95) whilst female patients had a median whole vessel SUV_{max} of 1.47 (IQR 1.45-1.50) ($p=0.267$). There was no correlation between patient age and whole abdominal aortic wall SUV_{max} or TBR_{max} observed ($r = - 0.031$; $p=0.882$; 0.02 , $p=0.925$). There was no association between whole abdominal aortic wall SUV_{max} and

initial aneurysm size ($r=0.032$, $p=0.878$). There was no significant difference between whole vessel TBR_{max} in aneurysms with greater or less than 5mm expansion at 12 months ($p=0.852$).

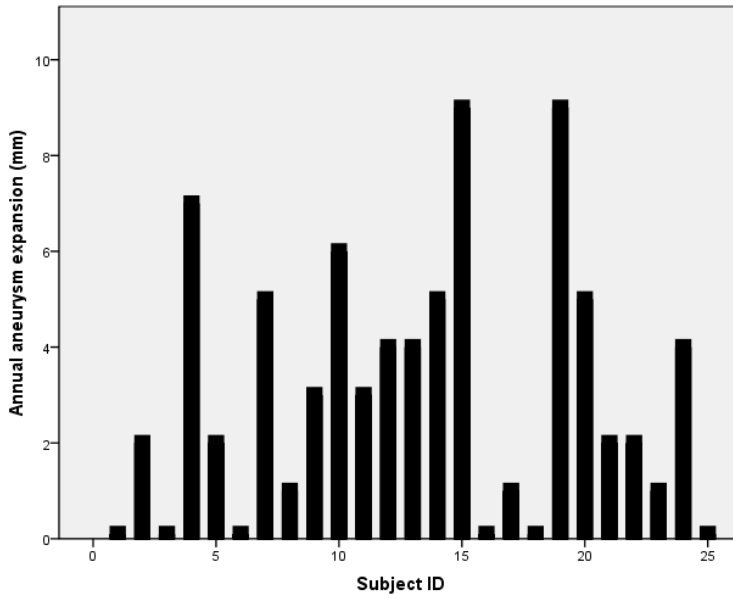


Figure 4.3 Bar chart showing the consecutive series of individual subject's AA expansion over 12 months

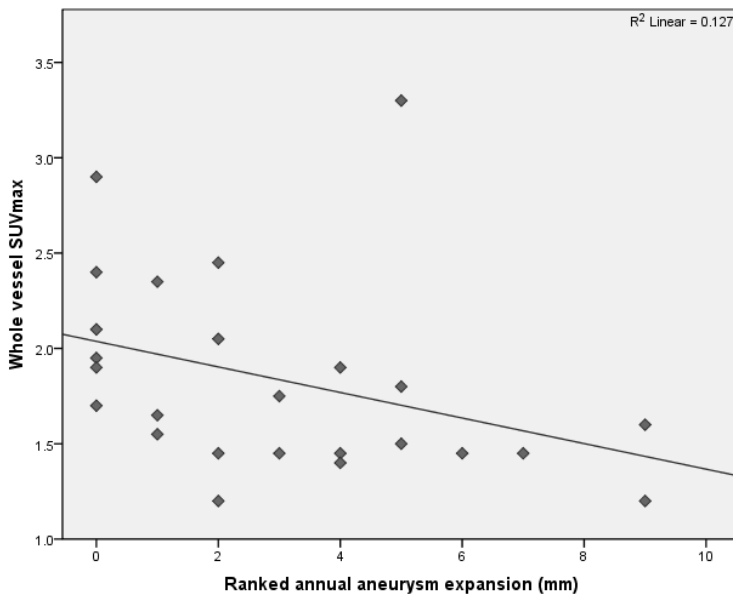


Figure 4.4 Scatter plot showing ranked correlation between ^{18}F -FDG uptake on baseline study against expansion at 12 months ($r_s = -0.501$; $p = 0.011$)

4.3.2. PET interobserver agreement

The mean difference between the two observers' measurements was 0.187 [95% CI: 1.608 – 1.792].

4.4. DISCUSSION

The findings from this chapter on 25 AAA patients suggest an inverse trend between ^{18}F -FDG uptake on PET and future AAA expansion.

There are multiple possible risk factors that have been identified for ruptured AA including age, gender, smoking and genetic factors^{73, 339-341}. Other than aneurysm size, other anatomical risk factors on imaging have been suggested to play a role in aneurysm growth and potential rupture, for example aortic calcification, aneurysm shape and computed wall stress¹⁶. Despite the recognition of many risk factors, their utility on risk-stratification or current screening programmes remains uncertain. Nonetheless there are now increasingly refined guidelines on screening aortic aneurysms³⁵¹. These recognize roles for ultrasound in screening. The findings in this chapter suggest that there could be a possible role for PET/CT in risk-stratification of patients with aneurysms detected during screening, since aortic ^{18}F -FDG uptake was inversely related to future aneurysm expansion.

There are reports that increased metabolic activity as detected by FDG-PET/CT may be present in asymptomatic AAAs^{352, 353}. However, there is difficulty when interpreting such studies as the data is derived solely at one time-point and therefore reflects aneurysm wall metabolism at a single moment in time. In contrast, the biology of AA formation is assumed to evolve over many years. ^{18}F -FDG PET studies showing longitudinal data are limited. In one AA study a follow-up component was provided³⁴ but the findings were difficult to interpret because follow-up was provided in only 6/26

patients and the follow-up period non-uniformly. In our study with homogenous longitudinal data in 25 patients over 12 months, we show that whole AAA ^{18}F -FDG uptake is less in aneurysms that expand more with time. These findings should be seen in the light of histologically validated evidence that ^{18}F -FDG uptake in humans is related to the degree of inflammatory markers and infiltrate in AAs²²² and in other arteries³²⁹. It could be argued that an initial inflammatory phase is followed by a dilatation phase. Such a hypothesis and our findings are consistent with emerging cellular evidence that aneurysm dilatation develops after initial inflammatory processes^{168, 169, 354} and calcification possibly represents a late burn-out stage of atherosclerosis³¹⁶. Interestingly, some PET imaging studies have confirmed that increased FDG uptake in arteries may not persist with time³⁵⁴.

Current medical therapies (statins, ACE inhibitors and beta blockers) for patients with aortic aneurysms have not been proven to be effective in influencing outcome³⁴⁰ and new targeted therapies are required. The potential role of ^{18}F -FDG -PET/CT in developing targeted metabolic treatment should be considered. There are many examples of monitoring cancer metabolic response to therapy with ^{18}F -FDG-PET/CT^{355, 356}. However, such models are not confined to oncology and there is increasing evidence that PET/CT can be used successfully to monitor treatment in atheroma^{217, 219, 342}. Since these early studies have shown promise, larger scale clinical trials are being performed and some of these have now been completed²²⁵.

There are study limitations and technical considerations when interpreting our findings. Our population size is larger than most arterial PET studies performed at the time of the current investigation. Our population size was similar to 2 recent longitudinal PET arterial dissection studies^{357, 358} and benefited from a longer follow-up period. Nonetheless more data would be needed to confirm our findings. Serial PET imaging may be useful but would be constrained by radiation exposure. This is reflected in the literature with only one case study reporting a correlation between aneurysm wall glucose metabolism and mechanical instability and inflammatory changes with increase in aneurysm size over time¹⁰⁷.

We performed whole vessel SUV and TBR analysis in keeping with current recommendations^{223, 319, 359}. Whole vessel SUV and TBR has been shown to maximize

reproducibility and has been advocated for plaque treatment response studies^{223, 359, 360}. Furthermore, by averaging SUV measurements to obtain a whole volume tracer uptake value, erroneous outlier measurements are to some extent being corrected for. In keeping with current concepts describing AAA as a systemic disease of the vasculature⁹, whole vessel SUV and TBR measurements may more accurately reflect AAA metabolic activity and should be considered in AAA risk stratification and treatment response studies. A limitation of this approach is that the site of maximal dilatation on ultrasound or site of aneurysm development may not be specifically evaluated on PET. However, we also observed a negative trend between single site SUV_{max} and annual AAA expansion, albeit not reaching statistical significance. We did not present mean SUV measurements since we were measuring large dilated vessels in which the PET signal will be diluted by a large blood pool component. For this reason also, it may not be appropriate to make target-to-background activity measurements. Other forms of AA have been studied including inflammatory³⁶¹ and acute aortic syndromes³³³. These forms so far are generally believed to be a separate pathology and were excluded from this investigation, although there may be an overlap in disease pathogenesis. Furthermore, since the magnitude of wall stress is related to AAA diameter³⁶² and possibly metabolic activity¹⁹⁶, the role of inflammation may be less in smaller aneurysms.

Mechanisms resulting in weakening of media layers of the aorta ultimately cause higher wall stress, which can induce aortic dilatation and lead to intramural haemorrhage, aortic dissection, or rupture³⁶³. This thesis investigated the relationship between FDG uptake in AAA and growth rate. Previous studies have documented FDG uptake in AAA at single time- points^{34, 222, 330, 352}. Sakalihasan *et al* reported increase FDG uptake in a proportion of AAA patients (10/26)³⁴; Truijers *et al* in comparison to non-aneurysmal aortas³⁵³; and Reeps *et al* in comparison to asymptomatic AAA²²². In one series of 5 patients, sites of focal FDG uptake led to focal expansion or dissection in time in 3 patients³⁵¹. Whether FDG uptake persists in AAA is unknown, but is unlikely given the waxing and waning uptake demonstrated by Menezes *et al*³⁴⁸, which is consistent with periods of rapid growth and quiescence in the natural history of AAA³⁶⁴. In common with other studies of the expansion of AAAs, there are methodological challenges: the change in aortic diameter over time is small and the measurement of aortic diameter using ultrasound (and to a lesser extent CT) has an error margin of 2 to

3mm which is larger than the annual expansion of many small AAAs³⁶⁴. Therefore larger longitudinal studies with longer follow-up are needed to clarify the role in risk prediction with FDG-PET in the surveillance of AAA.

In conclusion, the findings in this chapter suggest that there is an inverse trend between FDG uptake on PET and future AAA expansion. Aortic aneurysms with lower metabolic activity may therefore be more likely to expand.

Summary of findings:

- ^{18}F -FDG SUV_{max} correlated inversely with future AAA expansion at one year.

Combining imaging techniques with ^{18}F -FDG PET/CT may prove more effective in identifying patients at risk of significant expansion and therefore AAA-related events. The following chapter investigates AAA CT signal heterogeneity and its relationship with ^{18}F -FDG uptake on PET/CT and prospective aneurysm expansion in patients with small AAA to explore risk-stratification in AAA progression.

CHAPTER 5. INVESTIGATING AA CT TEXTURAL ANALYSIS AND ^{18}F -FDG UPTAKE ON PET/CT AND FUTURE GROWTH RATE

5.1. INTRODUCTION

Other than measuring AAA anteroposterior (AP) diameter on CT or ultrasound, other imaging methods have been used to improve risk-stratification in AAA. An area of interest has been the use of ^{18}F -FDG PET/CT, which has shown promise in semi-quantitative assessment of metabolic activity in AAA walls²²², the extent of which might predict future expansion³⁶⁵. Macrophages play an active role in all stages of vascular inflammation and atherosclerotic plaque formation. Increased radioactivity using ^{18}F -FDG-PET can be used to assess macrophage activity because these cells have a high basal metabolic rate that is GLUT (glucose transporter) dependent²⁰⁹⁻²¹¹.

Up until now the CT component of the PET/CT scan has been used mainly for PET co-registration. CT can be exploited to quantify signal heterogeneity of tissues via textural analysis by assessing image grey-level distribution and degree of coarseness. In vascular disease, CT textural analysis (CTTA) has been used to investigate intraluminal thrombus in AAA after intervention³⁶⁶ and carotid atherosclerosis³⁶⁷. An approach to quantify CT signal heterogeneity via CTTA is to use the filtration-histogram method to enhance features at fine, medium and coarse texture-scales. Histogram characteristics such as the standard deviation (SD) that relates the degree of variation from the mean pixel value, and kurtosis (K) that reflects the pointedness of the histogram, could then be quantified.

Furthermore, in oncology, CTTA parameters (SD and K) have been used to evaluate heterogeneity of various tumour types, with histological validation of the signals (representing hypoxia and neovascularization)^{368, 369}, that have been associated with overall and progression-free survival in lymphoma, oesophageal and colorectal cancers³⁶⁹⁻³⁷¹. The biological basis for such findings is unclear, but may reflect areas of hypoxia/metabolic mismatch. AAA is associated with atherosclerosis¹⁸⁶ and is characterized by structural enzymatic degradation of elastic media, inflammatory

infiltrate and neovascularisation⁵⁸. Increased CT signal heterogeneity of vasculature may suggest structural changes with increased vascularity³⁷²⁻³⁷⁴.

In this chapter we investigate small AAA using CTTA that attempts to link these parameters with prospective aneurysm growth. For these reasons we assessed the potential role of CTTA as a risk-stratification tool for expansion in patients with small AAAs under surveillance. We also assessed correlation of CT features of heterogeneity with the FDG signal derived from PET.

5.2. MATERIALS AND METHODS

5.2.1. Patients

During the period from February 2008 to June 2011, patients enrolled under AAA surveillance at one of our institutions (University College Hospital, London or Royal Sussex County Hospital, Brighton) were invited to participate in this prospective CTTA and ¹⁸F-FDG-PET/CT study. Fifty consecutive patients (44 men, 6 women, median age 75y, range 56-85y) with small aortic aneurysms (median diameter 48.5mm, IQR 43.0-53.0) under routine surveillance were recruited for CTTA and ¹⁸F-FDG-PET/CT. All patients had an asymptomatic infrarenal AAA. One patient also had an iliac aneurysm. Patients with thoracic, inflammatory and or symptomatic AAA were excluded. The baseline demographics are presented in Table 5.1. Institutional Review Board permission and informed patient consent were obtained.

5.2.2. PET/CT image acquisition

We used a combined PET/64-detector CT instrument (GE Healthcare Technology, Waukesha, WI) to obtain images. Patients fasted for 6h prior to scans. PET/CT images were acquired 3h after injecting 200MBq of ¹⁸F-FDG, according to recognized protocol^{219, 223, 344, 348}. CT was performed using 64 × 3.75mm detectors, a pitch of 1.5 and 5mm collimation (140kVp and 80mA in 0.8s) over the patient's abdominal aorta. The pixel size for the unenhanced CT images used in this study was 0.98mm x 0.98mm. Maintaining the patient position, an ¹⁸F-FDG PET emission scan was performed and covered an area identical to that covered by CT. All acquisitions were in 2D mode

(8min/bed position). Transaxial emission images of 3.27mm thickness (pixel size 3.9mm) were reconstructed using ordered subsets expectation maximization³³² with 2 iterations and 28 subsets. The z-axial field of view was 148.75mm, resulting in 47 slices per bed position.

5.2.3. CT texture analysis

Image heterogeneity of the AAA via CTTA using a filtration-histogram technique was assessed using TexRAD (TexRAD Ltd, Somerset, UK), a proprietary software algorithm developed by Ganeshan *et al*³⁷⁵. CTTA of AAA was derived by filtering each CT image to obtain: fine texture scale, ie filter value 1.0, approximately 2mm in width (radius) ; medium texture scale, ie filter value 1.5-2.0, approximately 3-5mm in width (radius); and coarse texture scale, ie filter value 2.5, approximately 6mm in width (radius). The filtered images were quantified using histogram-based parameters. These texture parameters include standard-deviation (SD) that relates the degree of variation from the mean pixel value (SD, width of the histogram) and kurtosis (K) that reflects pointedness of the histogram. SD increases approximately in proportion to the square-root of the number of features highlighted and their mean intensity difference compared to background (ie dark and bright features are both positive). Kurtosis is related inversely to the number of features highlighted (whether bright or dark) and increases by intensity variations in highlighted features. By quantifying these different image features (size, concentration and density-variation of the features highlighted by the filter) within a tissue (representing the different aspects of tissue heterogeneity), computed image texture analysis algorithms have the potential to provide additional morphological information relating to tissue heterogeneity³⁷⁶. A detailed description of the above image filtration and quantification is described in the appendix. CTTA was performed by an experienced reader (CW) under supervision from a researcher (BG) with 7 years' experience in texture analysis of radiographic images, who aided in inter-observer variability measurements. Both were blinded to the results of FDG-PET analysis and aneurysm growth rates. Interclass correlation coefficient (ICC) to assess inter-observer variability was performed by CW and BG. For each patient, a whole vessel analysis of the imaged AAA was performed. CTTA was measured over the whole volume of each AAA considering all the individual axial slices. A region of interest (ROI) was placed to include the aneurysm wall and content (Figure 5.1). To

adjust for textural features of background blood pool or luminal contents heterogeneity measurements were adjusted by dividing AAA heterogeneity measurements by the corresponding blood pool heterogeneity measurements for each aneurysm. The methodology to measure the CTTA for the blood pool was similar to the way CT signal heterogeneity for AAA was measured. The CTTA for blood pool was measured by placing a ROI to include AAA luminal contents (including intra-luminal thrombus and excluding AAA wall) on each of the axial CT slices comprising the whole volume (Figure 5.2)³⁴⁸, thereby, aiming to exclude heterogeneity changes derived from intra-luminal thrombus. The CT slices for analysis were comparable in terms of anatomical location to the PET image employed for measuring ¹⁸F-FDG uptake. The ROI enclosing the AAA on CT was drawn using the same guidelines as for PET image analysis. However, for PET measurements of blood pool activity, average ¹⁸F-FDG uptake of inferior vena cava (at least 8 measurements) was used. The CT ROI were further refined by excluding areas of air with a thresholding procedure which removed from analysis any pixels with attenuation values below -50 HU.

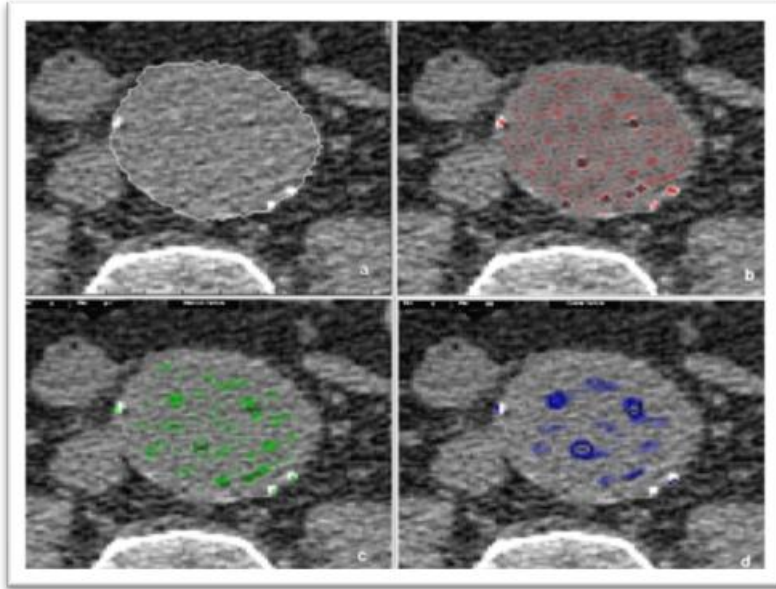


Figure 5.1 Computer tomography texture analysis of AAA wall and content - (a) Conventional infra renal AAA CT image. (b–d) Corresponding images selectively displaying filtration of the histogram at (b) fine (2mm in width), (c) medium (3-5mm in width), and (d) coarse (6mm in width) texture.

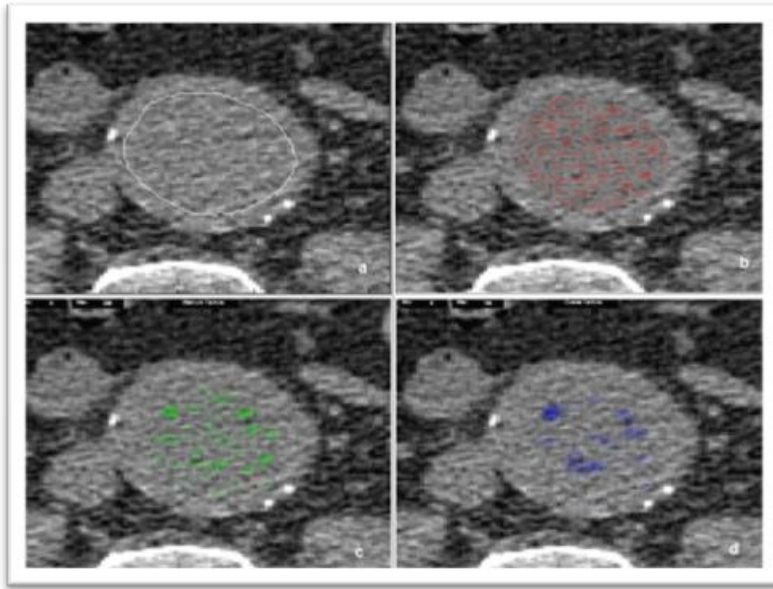


Figure 5.2 Computer tomography texture analysis of AAA luminal content including the blood pool and intraluminal thrombus (AAA wall excluded). (a) Conventional infra renal AAA CT image. (b–d) Corresponding images selectively displaying filtration of the histogram at (b) fine (2mm in width), (c) medium (3-5mm in width), and (d) coarse (6mm in width) texture.

5.2.4. PET/CT image analysis

PET/CT images were reviewed both by a dual accredited radiologist/nuclear medicine physician with a special interest in cardiovascular imaging and with greater than four years' experience of measuring vascular ^{18}F -FDG uptake who was blinded to clinical data, and by a surgeon with a special interest in vascular imaging, supervised by a dual accredited radiologist/nuclear medicine physician. PET/CT images were loaded onto a Xeleris workstation (GE Healthcare Technology, Waukesha, WI). Similar to CTTA, we also performed a whole vessel analysis of the imaged AAA³¹⁶.

Through visual assessment of axial and coronal planes of the imaged aorta, measurements were commenced on axial images from distal to the neck of the AAA and proximal to distal descending aorta where vessel diameter normalizes to include the whole volume AAA. AAAs extending into the bifurcation were measured up to the

level of the bifurcation of the aorta. A region of interest (ROI) was placed to include the aneurysm wall and content. The maximum standardized uptake value (SUV_{max}) of the AAA was calculated subsequently for each axial level and the values were then summed and divided by the total number of axial images to obtain an average SUV_{max} for the whole AAA. In order to adjust for back ground metabolic activity and potential false high uptake values a target-to-back ground ratio (TBR_{max}) was calculated by dividing the average AAA SUV_{max} by an average blood ROI (at least 8 venous ROI measurements), estimated from the inferior vena cava²²³. In addition, for each individual aortic aneurysm we identified the site of maximum aortic wall ^{18}F - FDG uptake. At this site we measured the SUV, yielding in each patient, a single site SUV_{max} and TBR value, as previously described^{222, 348}. The SUV is the decay-corrected tissue concentration of ^{18}F -FDG (in kBq/g), adjusted for injected ^{18}F -FDG dose and body weight (in kBq/g).

5.2.5. Duplex ultrasound image acquisition

Study patients underwent abdominal ultrasound at the time of PET/CT examination and subsequently routine ultrasound scan measurements at 6 and 12 months post PET/CT. In keeping with Thapar *et al*³⁴⁷, maximal anteroposterior (AP) external aortic wall diameter was recorded on each occasion. To adjust for baseline aneurysm size we calculated expansion at 12 months divided by aneurysm size at time of PET/CT scan (adjusted for baseline size longitudinal AAA expansion). Specialist vascular scientists (with greater than three years' experience), who were blinded to CTTA, FDG uptake results and expansion results, performed the surveillance ultrasound scans (Philips, HDI 5000, C5-2, Curved Linear Probe).

5.2.6. Statistical analysis

Statistical analyses were performed using SPSS for Windows version 18.0. After data were examined for normality, non-parametric statistical tests were performed, and median values and interquartile range (IQR) presented. Spearman's rank correlation was used to assess the association between AAA CTTA, aortic wall ^{18}F -FDG uptake values and corrected for baseline longitudinal AAA growth. Univariate analysis of clinical factors was performed and where appropriate adjustments were made to account for

confounding clinical factors. Intra-class correlation coefficient was used to assess inter-observer test/re-test results. Sensitivity, specificity and the area under the receiver-operating-characteristics (ROC) curve were established for significant parameters that identified annual AAA expansion ≥ 2 mm. The point on the ROC curve furthest from the line of no discrimination was considered the optimum (diagnostic) threshold for predicting a significant AAA expansion. Statistical significance was set at 5%.

5.3. RESULTS

Ten patients were lost to follow-up at 12 months (non-aneurysmal deaths n=2, withdrew from study n=2, failed to attend ultrasound scan n=5, emergency AAA repair n=1), leaving 40 patients (36 men, 4 women, median age 74y (range 60-85y) for analysis (Table 5.1). The patient who underwent an emergency AAA had a symptomatic rapid expanding AAA (expansion of >10mm per annum).

Table 5.1 Summary of the medical details of the patient population

History or Symptoms	N = 40
Age (median, range)	74 (60-85) y
Male	36
Female	4
Ischaemic heart disease	13
Raised lipids	30
Statin use	28
Diabetes	4
Hypertension	31
Current or previous smoker	22
Median maximal AAA diameter	49.5 (IQR 43.0-53.0)mm *
	51.0 (IQR 41.0-55.8)mm †

* Baseline median maximal AAA diameter as measured on duplex ultrasound

† Baseline median maximal AAA diameter as measured on CT

The baseline median maximal aortic AP diameter on ultrasound was 49.5 (IQR 43.0-53.0)mm *versus* 51.0 (IQR 41.0-55.8)mm on CT ($r=0.945$; $p< 0.0001$) (paired t-test;

$t(39) = -2.29, p=0.027$). The median maximal aortic AP diameter 12 months following the PET/CT imaging was 53.0 (IQR 44.3-57.5)mm. The median aneurysm expansion at 12 months was 2.0 (IQR 0.0-4.0)mm (range 0-9mm). The median annual growth adjusted for baseline size was 4.4% (IQR 0.0-9.2). The median corrected whole aneurysm texture parameters are summarized in Table 5.2. The median maximal whole abdominal aortic wall ^{18}F FDG uptake (SUV_{max}) was 1.798 (IQR 1.463-2.256). The median whole AAA TBR_{max} was 1.200 (IQR 1.100-1.506). The median single site SUV_{max} was 1.796 (IQR 1.500-2.402).

Table 5.2 The median whole AAA texture parameters at fine, medium and coarse filter levels for standard deviation (SD) and kurtosis (K)

Filter	Standard deviation*	Range (min-max)	Kurtosis †	Range (min-max)
Fine	2.66	1.20-7.54	28.06	-1113.12-502.07
Medium	4.94	1.45-10.51	7.22	-322.09-370.07
Coarse	3.57	1.59-11.56	4.71	-56.89-220.70

†Texture parameter kurtosis (K), which is quantified from filtered images, does not have units. This parameter describes the shape of the histogram: positive kurtosis suggests the histogram is pointed, negative kurtosis suggests the histogram is flatter, 0 kurtosis suggest the histogram is Gaussian.

*SD takes on the unit of the original data. In this instance it is the filtered image which is an intensity image with positive and negative values representing features of a particular size based on the filter. Unlike the conventional image units that are reported in Hounsfield units (HU), the filtered image does not have any units and therefore SD too is without units.

5.3.1. Texture-metabolic association for AAA

Whole AAA coarse texture SD showed an inverse association with AAA SUV_{max} ($r_s = -0.456, p=0.003$) (Figure 5.3). Furthermore, we observed a trend between fine texture K and AAA TBR_{max} ($r_s = 0.324, p=0.041$). Correlations between texture parameters and AAA metabolic activity, before and after adjusting for confounding clinical factors (back pain), are summarized in Table 5.3.

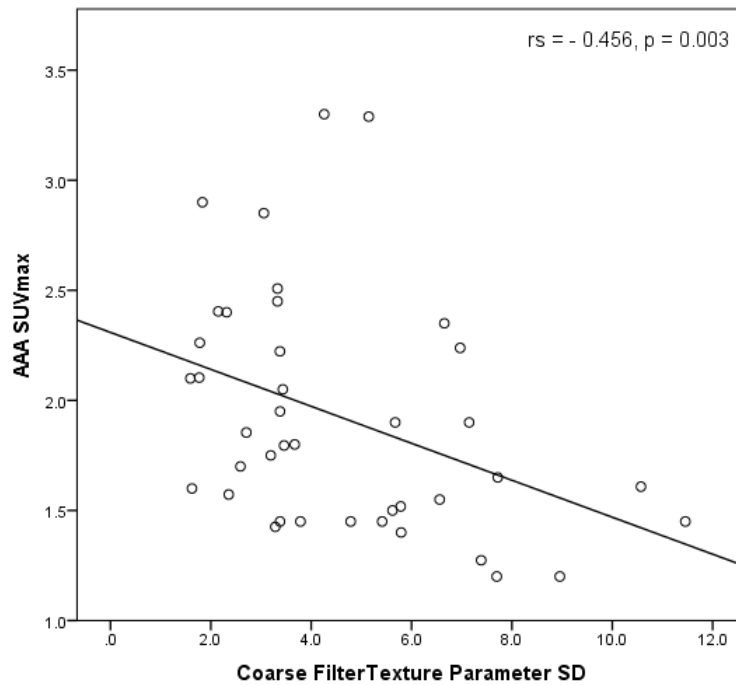


Figure 5.3 Scatter plot of whole AAA metabolic activity measured as SUV_{max} and coarse texture parameter standard deviation (SD) ($n=40$).

Spearman correlation coefficient r_s (with p -value) between the two variables is presented at top right.

Table 5.3 The correlation of texture parameters kurtosis (K) and standard deviation (SD) with metabolic activity measured as FDG uptake before and after adjusting for confounding clinical factors (back pain)

Texture parameter filter	SUV _{max} (Spearman r_s = ; p=)	TBR _{max} (Spearman r_s = ; p=)
Fine		
K	0.165; 0.310	0.324; 0.041*
	0.173; 0.291†	0.330; 0.043*†
SD	-0.419; 0.007*	-0.186; 0.251
	-0.449; 0.004*†	-0.200; 0.222†
Medium		
K	0.187; 0.248	0.212; 0.188
	0.204; 0.213†	0.224; 0.170†
SD	-0.435; 0.005*	-0.136; 0.402
	-0.463; 0.003*†	-0.148; 0.370†
Coarse		
K	0.045; 0.782	0.073; 0.656
	0.066; 0.691†	0.086; 0.602†
SD	-0.456; 0.003*	-0.095; 0.560
	-0.473; 0.002*†	-0.101; 0.541†

*Indicates significance set at ≤ 0.05

† Correlation after adjusting for clinical factors (back pain)

5.3.2. Aortic CTTA and future AAA expansion

There was no significant difference in AAA expansion for any of the clinical variables (Table 5.4). In 2/40 (5%) patients who suffered from back pain, the AAA growth rate at one year was borderline significantly larger than those who did not suffer back pain (minimum adjusted growth: 0 vs 9.3%; maximum adjusted growth: 16.7% vs 15.5%; $p=0.069$).

Table 5.4 Univariate analysis of clinical factors to identify confounding factors for AAA expansion adjusted for baseline AAA size and annual expansion > 2mm

Clinical factors	AAA expansion adjusted for baseline		(p=)	Annual expansion $\geq 2mm$		OR (p=)
	AAA size Median (IQR)			No expansion N (%)	Expansion	
Sex (F M) 4:36	0.47 (0.06; 1.04)	0.44 (0.00; 0.92)	0.964	13/15 (86.7% ♂)	23/25 (92% ♂)	1.8 (0.622)
Hypertension (N Y) 8:32	0.64 (0.10 ; 0.94)	0.41 (0.00; 0.86)	0.550	13/15 (86.7)	19/25 (76)	0.5 (0.686)
Beta-blocker use (N Y) 24:16	0.55 (0.19; 0.94)	0.38 (0.00; 0.85)	0.167	7/15 (46.7)	9/25 (36)	0.6 (0.527)
ACE-inhibitor use (N Y) 25:13	0.42 (0.00; 0.94)	0.45 (0.10; 0.72)	0.963	5/14 (35.7)	8/24 (33.3)	0.9 (1.000)
Ischaemic heart disease 27:13	0.53 (0.00; 0.93)	0.42 (0.00; 0.91)	0.630	5/15 (33.3)	8/25 (32)	0.9 (1.000)
Raised lipids (N Y) 11:29	0.71 (0.38; 0.93)	0.39 (0.00; 0.91)	0.257	13/15 (86.7)	16/25 (64)	0.3 (0.158)
Statin use (N Y) 9:31	0.73 (0.19; 1.23)	0.42 (0.00; 0.87)	0.359	13/15 (86.7)	18/25 (72)	0.4 (0.440)
Smoking (N Y) 35:5	0.45 (0.19; 0.87)	0.00 (0.00; 0.94)	0.385	3/15 (20)	2/25 (8)	0.3 (0.345)
Diabetes (N Y) 35:4	0.45 (0.19; 0.93)	0.00 (0.00; 1.00)	0.223	3/14 (21.4)	1/25 (4)	0.2 (0.123)
Back pain (N Y) 38:2	0.42 (0.00; 0.83)	0.93 - 1.24	0.069	0/15 (0)	2/25 (8)	0.6 (0.519)

*Indicates significance set at ≤ 0.05

Medium texture K positively correlated with absolute future AAA expansion ($r_s=0.470$, $p=0.002$, Figure 5.4). Medium texture K also positively correlated with future AAA expansion adjusted for baseline AP AAA diameter ($r_s=0.343$, $p=0.030$). Coarse texture SD positively correlated with future AAA expansion adjusted for baseline AP AAA diameter ($r_s=0.325$, $p=0.041$). Correlations between AAA texture parameters and future expansion, before and after adjusting for confounding clinical factors (back pain), are summarized in Table 5.5.

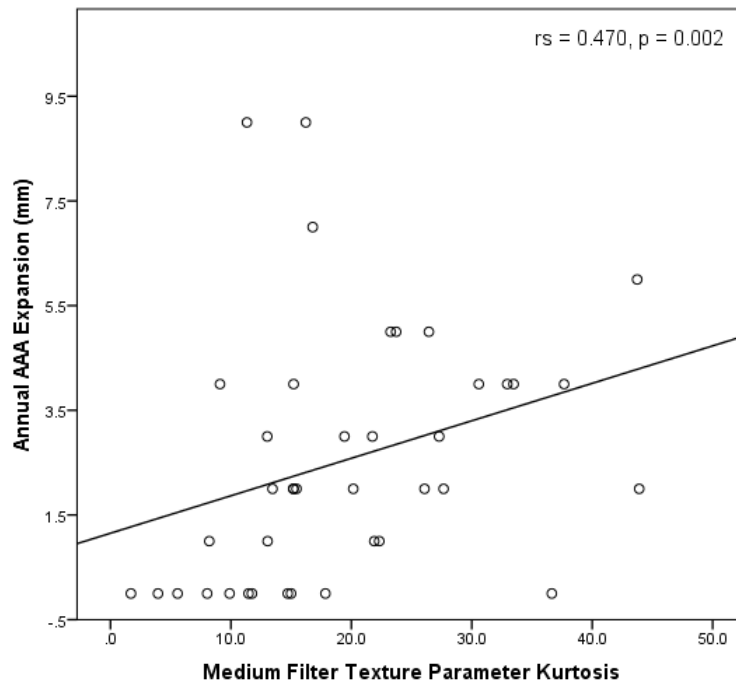


Figure 5.4 Scatter plot of AAA expansion at 1y and medium coarseness texture parameter kurtosis (K) (n=40). Spearman correlation coefficient r_s (with p -value) between the two variables is presented at top right

Table 5.5 The correlation of texture parameters kurtosis (K) and standard deviation (SD) with future growth before and after adjusting for confounding clinical factors

Texture parameter filter	Absolute AAA expansion at 1 year	AAA expansion adjusted for baseline AAA Size
	(Spearman r_s ; p=)	(Spearman r_s ; p=)
Fine		
K	0.422; 0.007*	0.119, 0.465
	0.454; 0.004*†	0.083; 0.617†
SD	-0.208; 0.198	0.212; 0.189
	-0.129; 0.433†	0.315; 0.051†
Medium		
K	0.470; 0.002*	0.343; 0.030*
	0.456; 0.004*†	0.274; 0.091†
SD	-0.184; 0.256	0.325; 0.041*
	-0.970; 0.557†	0.421; 0.008*†
Coarse		
K	0.401; 0.010*	0.226; 0.161
	0.436; 0.025*†	0.142; 0.389†
SD	-0.139; 0.392	0.312; 0.050*
	-0.051; 0.760†	0.386; 0.015*†

*Indicates significance set at ≤ 0.05

† Adjusted for clinical factors

5.3.3. Texture analysis comparison between aneurysmal and normal aorta

Whole vessel CTTA of aneurysmal compared to normal aorta was significantly different for coarse SD (Wilcoxon signed rank test, $p=0.001$, Figure 5.5).

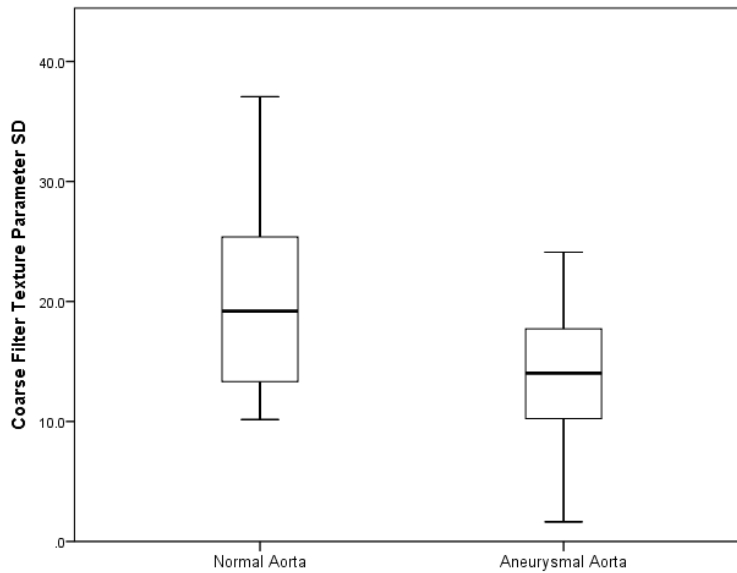


Figure 5.5 Box plot showing a significant difference between coarse texture parameter SD of aneurysmal compared to normal aorta (Wilcoxon signed rank test, $p=0.001$)

5.3.4. Inter-observer variability for whole aneurysm CTTA

Intra-class correlation coefficient (ICC) between observers were as follows: fine (K, $r=0.987$, 95% CI 0.948-0.997, $p<0.0001$ and SD, $r=0.993$, 95% CI 0.975-0.998, $p<0.0001$), medium (K, $r=0.954$, 95% CI 0.797-0.989, $p<0.0001$ and SD, $r=0.978$, 95% CI 0.916- 0.994, $p=0.001$) and coarse texture (K, $r=0.963$, 95% CI 0.841- 0.990, $p<0.001$ and SD, $r=0.995$, 95% CI 0.980- 0.999, $p<0.001$).

5.3.5. Aortic ^{18}F -FDG uptake and future AAA expansion

In addition, we observed that SUV_{max} correlated inversely with future expansion at one year ($r_s = -0.383$, $p = 0.015$, Figure 5.6). A borderline significant inverse trend was observed between highest single site TBR_{max} and annual expansion ($r_s = -0.304$, $p = 0.057$). No significant association between average AAA TBR_{max} and annual expansion was found ($r_s = -0.021$, $p = 0.889$).

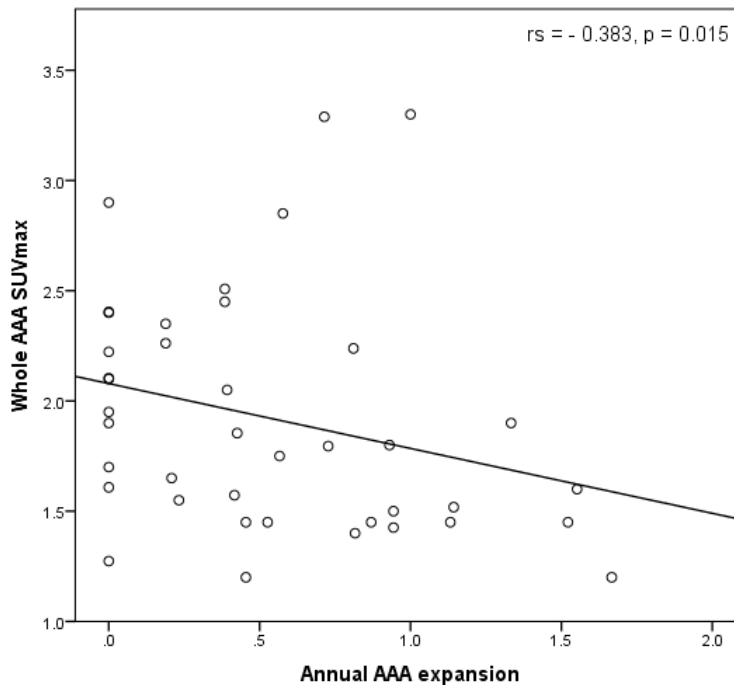


Figure 5.6 Scatter plot of AAA expansion at 1y adjusted for baseline aneurysm size and whole AAA metabolic activity measured as SUV_{max} ($n=40$). Spearman correlation coefficient r_s (with p -value) between the two variables is presented at top right.

5.3.6. Diagnostic criteria for imaging parameters to identify significant AAA expansion

We observed no statistically significant association between clinical variables and annual AAA expansion $\geq 2\text{mm}$ (Table 5.4). AAA medium texture K identified patients with significant annual AAA expansion ($\geq 2\text{mm}$). In particular, a kurtosis value > 15

identified patients with AAA expansion (≥ 2 mm) with a sensitivity of 80% and a specificity of 73% (AUC= 0.813, $p= 0.001$, 95% CI 0.672-0.955). In a multiple logistic regression, the relationship between medium texture K and AAA expansion persisted after adjusting for clinical variables of ischaemic heart disease, hypertension, beta blocker use, ACE-inhibitor use, raised lipids, statin use, diabetes and back pain (OR=1.348, 95% CI 1.072 - 1.695 , $p=0.011$, $c=0.917$). Medium texture K (adjusted for back ground blood pool activity) also identified patients with significant AAA expansion (≥ 2 mm). A kurtosis value > 3 identified patients with AAA expansion (≥ 2 mm) with a sensitivity of 68% and a specificity of 60% (AUC=0.725, $p=0.018$, 95% CI 0.569; 0.881). The relationship between medium texture K (adjusted for back ground blood pool activity) and AAA expansion remained statistically significant after adjusting for clinical variables in a logistic regression model (OR=1.036, 95% CI 1.002 - 1.072, $p=0.038$). Coarse texture SD did not identify patients with significant annual AAA expansion (AUC=0.373, 95% CI 0.171 - 0.575, $p=0.103$). There was no relationship between SD (adjusted for back ground blood pool texture) and AAA expansion (AUC=0.629, 95% CI 0.422 - 0.836, $p=0.106$). There was no correlation between texture K and SD values (Spearman $r_s=-.214$, 95% CI (-0.164; 0.154)) or texture K and SD adjusted for back ground blood pool texture (Spearman $r_s=-0.077$, 95% CI (-0.391; 0.254)).

5.4. DISCUSSION

This project represents the first use of CT signal heterogeneity to investigate the relationship between AAA heterogeneity and future AAA growth. The results suggest CTTA assessment in small aortic aneurysms may be considered as a risk-stratification tool for validation in future prospective studies to identify aneurysms at risk of significant expansion. In addition CT textural data may reflect AAA metabolism as measured by ^{18}F -FDG PET.

Studies have explored risk-stratification properties of texture analysis in symptomatic atherosclerotic carotid plaque that correlated with ipsilateral stroke³⁷⁷ and ability to predict incidence of silent infarcts in patients who underwent carotid endarterectomy³⁷⁸. Furthermore, CT-measured arterial wall thickness and volume in conjunction with

functional PET signal has been utilized in assessment of atherosclerosis extent³⁷⁹; however, our work is the first application of CTTA as measure of aneurysmal atherosclerotic plaque texture in relation to future expansion. Our findings suggest aortic aneurysms with greater medium CT signal heterogeneity K may be more likely to exhibit greater expansion. In addition, increased coarse AAA heterogeneity SD and decreased AAA medium heterogeneity K may be present in aneurysms that exhibit lower metabolic activity. On a histogram, increased K and SD values may suggest surface anatomical textural changes in AAA, possibly reflecting underlying pathobiology and associated metabolic activity. These findings have to be rationalized in light of current histological validated evidence. This CTTA technique has identified possible biological correlates for CTTA parameters (SD at medium to coarse feature-scale) and histological markers of hypoxia (pimonidazole) and angiogenesis (CD34, VEGF) in non-small cell lung and colorectal cancers^{368, 380}. Furthermore, recent test/re-test data from clinical studies in rectal cancer and test-objects demonstrate reproducibility of CTTA results³⁸¹. Regions of hypoxia and angiogenesis have been implicated in both atherosclerosis^{382, 383} and development of AAA^{134, 190, 384}. In AAA, Vorp *et al* identified localized areas of hypoxia with possible localized mural neovascularization and inflammation in regions of thicker intraluminal thrombus¹⁹⁰. We and other researchers argue that increased CT signal heterogeneity K of vasculature may reflect tissue vascular density or increased angiogenesis³⁷²⁻³⁷⁴. It is hypothesized that normal vessel walls can be considered to have well organized long microvascular channels, which become disorganized with angiogenesis, resulting in a mix of long channels and short vascular hot spots, causing flow voids and hypoxia. The histogram quantification can reflect image signal heterogeneity which may constitute the size, concentration and density (in relation to the background) of textural features within the vessel wall enhanced by the filter and may be associated with adverse biology³⁷⁶.

In a large observational study, Thompson *et al* reported that an adjusted annual growth rate of ≥ 2 mm was significantly associated with clinical events such as intervention or rupture²¹. Since medium AAA heterogeneity parameter K was significantly different in aneurysms, growing at least 2mm in one year, it may be rationalized that AAAs expanding 2mm or more per annum might demonstrate increased aneurysm wall vascular density. This is in keeping with histological studies showing increased AAA wall angiogenesis and associated AAA adverse events^{169, 384}. Analogous findings have

already been shown in oncology, where coarse texture parameters on CT correlated with hepatic blood flow, glucose metabolism^{313, 373, 374}, disease extent³⁷⁴ and patient survival^{368, 369, 373, 385, 386}, establishing its role as a potential biomarker in cancer. However, CTTA may measure the complexity of the shape of the edge of the AAA thrombus wall rather than angiogenesis of AAA wall. Therefore, in our study we performed CTTA of AAA luminal contents, including intra-luminal thrombus and excluding AAA wall, to exclude heterogeneity signals derived from intra-luminal thrombus. Nevertheless, histological PET/CT heterogeneity studies are needed to underpin structural characteristics associated with significant disease progression to provide possible explanations for these study findings.

The additional finding of inverse correlation between ¹⁸F-FDG uptake and future expansion may be explained by current biological evidence suggesting that ¹⁸F-FDG uptake in humans is related to the degree of inflammatory markers and infiltrate in aortic aneurysms³¹⁶ and other arteries²¹⁹. We and other researchers^{168, 169, 354} suggest that an initial inflammatory phase followed by a dilatation phase with calcification possibly represents a late burn-out stage of atherosclerosis³¹⁶. Furthermore, the potential effects of statins in reducing or preventing AAA expansion³⁸⁷ needs consideration. In our study cohort 28 of 40 patients were receiving statins. This may explain the annual aneurysm expansion of 2.0mm, (IQR 0.0-4.0).

In tumour studies, both FDG PET and CTTA have been described in measuring response to therapy^{355, 388}. Our study identified that CT texture characteristics (and FDG PET uptake) derived from baseline PET/CT images are associated with prospective AAA growth rate, thus validating the role of these modalities in studying AAA and providing a foundation for further larger studies.

There are study limitations and technical considerations when interpreting our findings. In this preliminary analysis patients underwent non-enhanced PET/CT for aneurysm assessment. Nevertheless, CTTA without IV contrast has been shown to provide useful information on underlying tumour heterogeneity^{375, 386} and has the added benefit that potential effects of contrast administration are nullified. A 2mm AAA wall axial thickness³⁸⁹ was measured where accurate delineation of AAA wall could not be attained. In addition, in this study we performed a whole vessel type texture analysis to

avoid misleading findings on limited aneurysm area, thereby increasing validity and in keeping with recommended AAA PET/CT analysis. The study population size of 50 is commensurate with a proof of concept investigation and compares favourably with many initial functional arterial PET studies^{357, 358}. Nonetheless, larger and more extended studies are needed. Furthermore, we recognize the limitations associated with small participant numbers, the exclusion of age and baseline AAA diameter in the logistic regression analysis; and that information on time from AAA diagnosis to recruitment in this study is lacking. This may allow for the possibility of by-chance findings, potential selection bias and or lack of generalizability. Models used in finite element analysis and AAA wall stress studies may define different regions of interest as described in our study. It would, however, be interesting to assess if areas of high wall stress are more heterogeneous. More histological validated evidence linked with CTTA is needed. However, histology as ‘gold standard’ for tissue characterization may be limited since preparation removes calcium and lipid which may affect structural integrity of tissue³⁹⁰. In common with other expansion studies, there are methodological challenges, ie the change in aortic diameter over time is small and the measurement of aortic diameter using ultrasound (and to a lesser extent CT) has an error margin of 2 to 3mm, which is larger than the annual expansion of many small AAAs³⁶⁴.

In conclusion, in this chapter we present the first application of CT textural analysis to investigate the relationship between AAA heterogeneity and future AAA growth. Our results suggest that AAA CT heterogeneity may be considered as a risk stratification tool in future prospective studies to identify aneurysms at risk of significant expansion. In addition we observed a potentially interesting metabolic correlate between CT textural features and AAA metabolism on PET that could be further investigated to provide insight into AAA biology.

Summary of findings:

- Coarse texture SD showed an inverse association with SUV_{max} .
- Fine texture K correlated with TBR_{max} .
- Medium coarse texture K correlated with future AAA expansion.

- CTTA parameters were significantly different for coarse SD when aneurysmal and normal aorta were compared.
- SUV_{max} correlated inversely with future expansion.

The next chapter assess the relationship between serum biomarkers of vascular inflammation and ^{18}F -FDG uptake in small AAA to establish the role of PET/CT in quantitative assessment of metabolic activity in AAAs and the clinical significance thereof.

CHAPTER 6. RELATIONSHIP BETWEEN SERUM BIOMARKERS AND ¹⁸F-FDG AORTIC ANEURYSM UPTAKE ON PET/CT

6.1. INTRODUCTION

Inflammation involving infiltration of macrophages, lymphocytes, neutrophils and mast cells has been shown to be critical for the formation and progression of AAA; however, the molecular mechanisms of AAA pathogenesis are not fully understood³⁰⁴.

Inflammatory serum biomarkers have been reported to be associated with the presence of AAA^{111, 391, 392} and rupture^{327, 393}; the relationship between serum biomarkers and AAA progression is currently unclear, with studies reporting negative results³⁹⁴.

Up until now, PET/CT biomarker studies have focussed on different aspects of the atherothrombotic process. Wu *et al* reported a link between circulating matrix metalloproteinases (MMP-1) and ¹⁸F-FDG PET in symptomatic carotid disease subjects²¹⁶. Other vascular PET researchers observed associations between MMP-3 levels and inflammation in the aorta³¹⁶. Since inflammation is central in AAA pathobiology and progression, it is hypothesized that circulating inflammatory serum biomarker levels are associated with the AAA metabolic activity in the patient with small AAA. The relationship between AA wall metabolic activity as measured by ¹⁸F-FDG PET/CT and recognised circulating vascular serum biomarkers remains to be established.

For these reasons, we assessed correlations between serum biomarker levels of high sensitivity MMP-9 (hsMMP-9), high sensitivity MMP-2 (hsMMP-2), high sensitivity interferon-gamma (hsIFN- γ) and high sensitivity C-reactive protein (hsCRP) with the tracer signal derived from PET in patients with small AAA under routine surveillance.

6.2. MATERIALS AND METHODS

6.2.1. Patients and baseline characteristics

During a 12-month period, patients presenting to one of our institutions with AAA and deemed suitable for surveillance were invited to participate in this serological and PET/CT study. Twenty-four consecutive patients (20 men, 4 women, median age 74y (SD \pm 6.23) with small AA under routine surveillance were recruited. All patients had an infrarenal AAA. Patients with thoracic, inflammatory and or symptomatic AAA were excluded. Sixteen healthy control subjects were recruited from a social club for biomarker analysis. The baseline demographics for subjects and controls are presented in Table 6.1. Seven patients had at least 3 risk factors for atherosclerosis. An example of AAA wall ^{18}F -FDG uptake is shown in Figure 6.1.

Table 6.1 Summary of the medical details of the patient population and control group

<i>History or symptoms</i>	<i>Participants (n)</i>	<i>Control group (n)</i>
Age (mean, SD)	74 y (\pm 6.23)	65 y (\pm 3.68)
Male	20	11
Female	4	5
Back pain	1	-
Ischaemic heart disease	9	-
Raised lipids	10	3
Diabetes	2	-
Hypertension	19	-
Current or previous smoker	9	11
Statin use	20	-
ACE-inhibitor use	6	-
Beta-blocker use	12	-

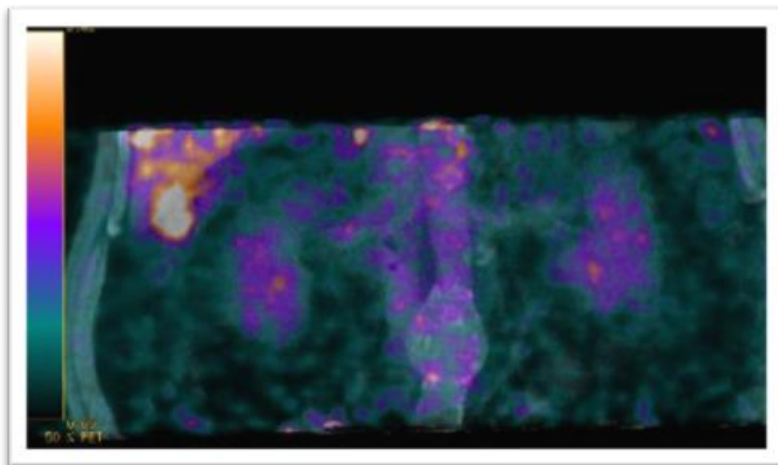


Figure 6.1 Sagittal fused PET/CT image of an AAA showing ^{18}F -FDG uptake in the aneurysm

6.2.2. PET/CT image acquisition

A combined PET/64-detector CT instrument (GE Healthcare Technology, Waukesha, WI) was used to obtain images. Patients fasted for 6h prior to scans. PET/CT images were acquired 3h after injecting 200MBq of ^{18}F -FDG, according to recognized protocol^{219, 223, 344, 348}. CT was performed using $64 \times 3.75\text{mm}$ detectors, a pitch of 1.5 and 5mm collimation (140kVp and 80mA in 0.8s) over the patient's abdominal aorta. Maintaining the patient position, an ^{18}F -FDG PET emission scan was performed and covered an area identical to that covered by CT. All acquisitions were in 2D mode (8min/bed position). Transaxial emission images of 3.27mm thickness (pixel size 3.9mm) were reconstructed using ordered subsets expectation maximization³³² with 2 iterations and 28 subsets. The axial field of view was 148.75mm, resulting in 47 slices per bed position.

6.2.3. PET/CT image analysis

PET/CT images were reviewed by an experienced reader (CW) with a special interest in vascular imaging, supervised by a dual accredited radiologist/nuclear medicine physician (LJ). PET/CT images were loaded onto a Xeleris workstation (GE Healthcare Technology, Waukesha, WI). We performed a whole vessel analysis of the imaged AAA²²³. A region of interest (ROI) was placed to include the aneurysm wall and content. The maximum tracer uptake (SUV_{max}) of the AAA was calculated subsequently

for each axial level and the values were then summed and divided by the total number of axial images to an average (SUV_{max}) for the whole AAA. Whole AAA target-to-background ratio (TBR_{max}) was calculated by dividing the average absolute SUV_{max} by an average blood ROI (at least 8 venous ROI measurements), estimated from the inferior vena cava³¹⁹. The SUV is the decay-corrected tissue concentration of ^{18}F -FDG (in kBq/g), adjusted for injected ^{18}F -FDG dose and body weight (in kBq/g).

6.2.4. Biomarker measurements

Biomarker analyses were carried out at the Adipokines and Metabolism Laboratory at UCL (London, UK). Biomarkers were chosen to cover different aspects of the AAA pathobiological inflammatory process. The levels of hsMMP-9, hsMMP-2, hsIFN- γ and hsCRP were analysed and compared to healthy control subjects. Peripheral venous blood samples were collected prior to the PET/CT, before tracer injection. In control subjects, venous blood samples were taken following consent. The samples were collected with potassium ethylenediaminetetraacetic acid tubes and were centrifuged to obtain serum aliquots (3500rpm for 15mins). Aliquots were stored at -80°C until assayed. High sensitivity IFN- γ and hs-CRP were measured by (enzyme-linked immunosorbent assay) ELISA (GenWay Biotech and Gen-Probe Diaclone SAS Inc.). The lowest detectable level of the hs-CRP assay was 0.005 mg/dL. High sensitivity MMP-9 and MMP-2 were determined by a commercially available ELISA, using the QuickZyme Biosciences Assay System (Netherlands). Circulating serum biomarker assays were performed twice and average biomarker levels are presented.

Manufacturers' protocols were meticulously followed. Serum samples were diluted in the appropriate calibrator diluent and added to wells with standards and appropriate controls, then left to incubate. Washed wells were further incubated with the diluted biotinylated detection antibody specific to the analytes of interest added. Stop solution was added to each well, following a further wash to expose unbound biotinylated antibody. The suspended biomarker levels were read using the Luminex analyzer (BioRad, Austin, Texas).

6.2.5. Statistical analysis

Each data set was analysed appropriately following tests for normality. Continuous variables are displayed by their mean and SD. For comparison of circulating serum biomarker levels between subjects and controls, and to explore the associations between tracer variables and biomarkers, linear regression analyses were performed. Average whole AAA tracer uptake values were used to compare aortic wall tracer uptake values with clinical factors and circulating biomarkers. Student's t-test was used to compare FDG tracer uptake and clinical factors. Mann-Whitney U test was used to compare biomarker measurements across clinical factor groups. To investigate associations we performed Pearson's correlation and Spearman's rank correlation coefficients as appropriate. Statistical tests were performed with SPSS (Version 18.0, SPSS Inc, Chicago, Ill). Statistical significance was set at 5%. Corrections were applied for differences in age, gender, statin use and smoking habits between subjects and controls.

6.3. RESULTS

The mean whole AAA SUV_{max} was 2.188 ($\text{SD}\pm 0.541$). The mean whole AAA TBR_{max} was 1.414 ($\text{SD}\pm 0.312$). The mean AAA size at the time of PET/CT was 4.31 cm ($\text{SD}\pm 1.03$).

Table 6.2 Summary of the mean levels of studied circulating biomarkers

<i>Circulating biomarker</i>	<i>Mean</i>	<i>SD</i>
hsMMP-9	5.692	± 5.83
hsMMP-2	2.256	± 1.35
hsIFN- γ	1.850	± 3.80
hsCRP	3.194	± 2.77

6.3.1. Clinical factors and associations with serum biomarkers

We observed a lower AAA SUV_{max} uptake in subjects with hypertension ($p=0.040$, CI = - 0.900 – - 0.022) (Figure 6.2). Subjects with raised lipids ($p=0.022$), hypertension

($p=0.005$) and ischemic heart disease ($p=0.004$) had significantly higher levels of hsMMP-9 (Figure 6.3). Subjects with raised lipids ($p=0.015$), ischaemic heart disease ($p=0.027$) and ex-smokers ($p=0.033$) had significantly higher levels of hsMMP-2. In subjects who gave up smoking, we observed higher levels of hsCRP ($p=0.047$). No other significant differences were found across clinical risk factors for FDG uptake and circulating biomarkers.

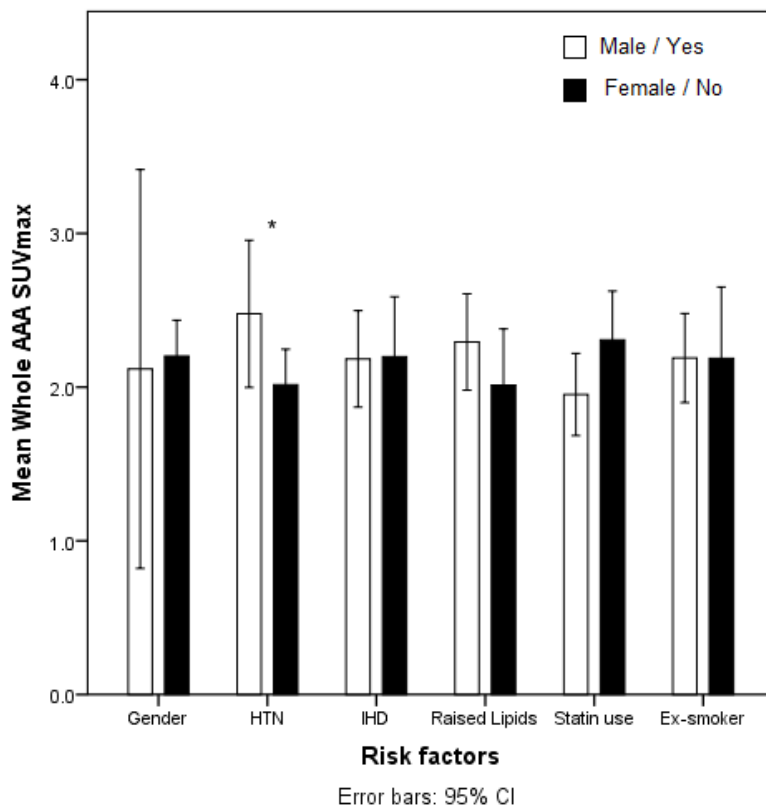


Figure 6.2 Aortic wall metabolic activity variations among different risk factor groups

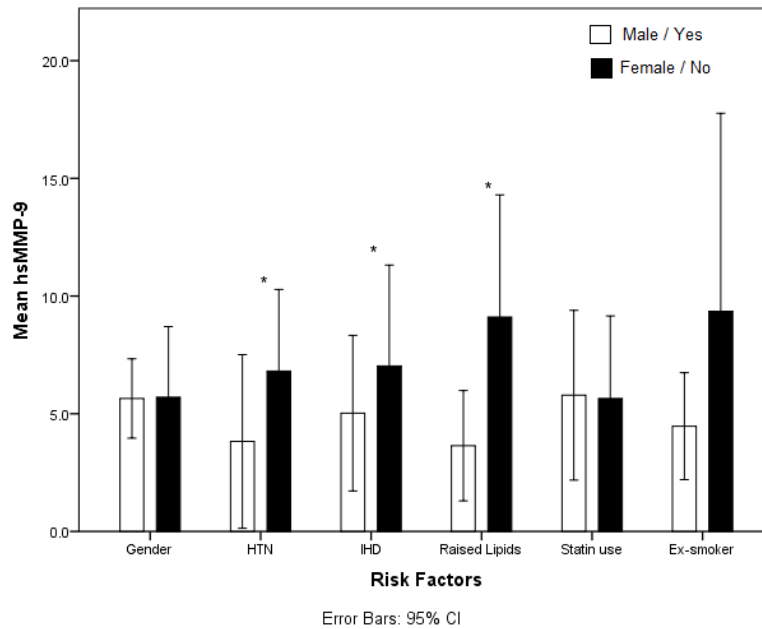


Figure 6.3 High sensitivity metalloproteinase-9 variations among different risk factor groups

Abbreviations: HTN, hypertension; IHD, ischaemic heart disease; * $p < 0.05$

6.3.2. Increased levels of hsMMP-9 & hsMMP-2 were observed in AAA subjects compared to controls.

hsMMP-9 and hsMMP-2 levels adjusted for age, gender, hypertension, ischaemic heart disease, raised lipids and statin use were significantly higher in subjects *versus* controls ($p \leq 0.001$). There was borderline significantly increased levels of hsCRP observed in subjects *versus* controls ($p = 0.057$). There was no significant difference found between subjects and controls for hsIFN- γ ($p = 0.501$).

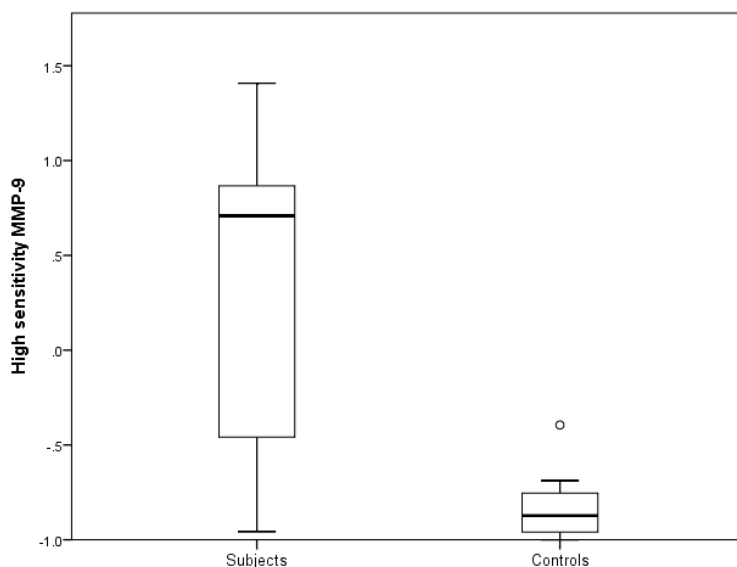


Figure 6.4 Box plot showing higher levels of circulating high sensitivity metalloproteinase-9 in subjects compared to controls ($p < 0.001$)

6.3.3. AAA wall FDG uptake does not correlate with levels of circulating inflammatory biomarkers

No correlations were found for whole AAA SUV_{max} and levels of hsMMP-9 ($r_s = -0.037$, $p = 0.865$), hsMMP-2 ($r_s = -0.226$, $p = 0.239$), hsINF- γ ($r = 0.210$, $p = 0.404$) and hsCRP ($r_s = -0.009$, $p = 0.966$). Furthermore, there were no correlations for whole AAA TBR_{max} and levels of hsMMP-9 ($r_s = 0.120$, $p = 0.576$), hsMMP-2 ($r_s = -0.059$, $p = 0.806$), hsINF- γ ($r_s = 0.029$, $p = 0.908$) and hsCRP ($r_s = 0.138$, $p = 0.521$).

6.4. DISCUSSION

This observational project investigates for the first time the relationship between circulating serum biomarkers and ^{18}F -FDG PET/CT in small AAA. The results suggest the degree of small AAA metabolism may not be reflected in the blood levels of serum biomarkers.

Prospective event-driven studies combining potential biomarkers and ^{18}F -FDG PET/CT in small AAA are needed to establish the role of these biomarkers in AAA risk-stratification and future clinical practice.

The role of ^{18}F -FDG PET/CT as surrogate marker of vascular inflammation is well established^{107, 209, 329, 395} and increased levels of circulating biomarkers compared to control subjects have been reported^{329, 391, 396-399}. Our study confirmed higher circulating levels of MMP-9 and MMP-2 compared to healthy control subjects, a finding previously observed by Hovsepian and colleagues³⁹¹. This finding affirms the role of MMP-9 and MMP-2 as potential biomarkers of connective tissue metabolism in patients with AAA. In a large prospective cohort study assessing CRP in patients with small aneurysms, followed up for a median of 4y, baseline CRP levels were higher in larger aneurysms, but CRP was not associated with expansion rate³⁹⁹. Similarly, our study showed increased levels of hsCRP in the AAA group, albeit of only borderline statistical significance. This affirms the non-specific characteristics of CRP found in other studies^{399, 400}. It may well be that higher levels of circulating CRP are symptom-driven, as suggested by Domanovits³⁹⁶. Although reports of serum hsCRP associated with aneurysmal size exist, thereby underscoring the inflammatory nature of AAA disease^{401, 402}, we have found no such relationship ($p=0.278$). Furthermore, it is unclear in our study why no significant difference was observed between circulating levels of hsIFN- γ in subjects and controls, whereas Juvonen *et al*³⁹² have reported such a difference; it is possible that small participant numbers may explain our results.

The specific regulatory traits of components of the inflammatory cascades and of proteases that cause aneurysmal progression remain largely unresolved. In particular the role of Th1 cytokine IFN- γ in AAA disease continues to be debated. In animal studies, Th1 cytokines together with leukocyte recruitment typically characterize early atherogenesis^{403, 404} and IFN- γ -depleted mice demonstrate markedly augmented inflammatory responses, suggesting Th1 cytokines might even protect against aneurysm development⁴⁰⁵. Other researchers have found that CD4-deficient mice do not develop experimental aneurysms, unless IFN- γ is administered¹³¹. However, this cytokine, depending on the experimental environment, may either induce or inhibit AAA formation. IFN- γ inhibits MMP-9 production^{406, 407} in murine and human macrophages and collagen production by VSMCs⁴⁰⁸. Furthermore, reports suggest a relationship between levels of circulating metalloproteinases (MMP-1, -3, and -9) and vessel wall ^{18}F -FDG uptake in patients with vascular disease^{216, 319}. In contrast, our study revealed no association between ^{18}F -FDG uptake in small aneurysm walls and circulating markers of vascular inflammation, thus suggesting the degree of small AAA wall metabolic activity may not be reflected in the blood levels of biomarkers. Although it is believed that macrophage metabolic activity is central to inflammatory cascades in AAA, our finding confirms reports that these inflammatory cascades are complex and poorly understood³⁰⁴. In this cohort, a low median ^{18}F -FDG TBR_{max} (median uptake 1.4 ± 0.3) and lack of association with circulating markers imply this association appears to be difficult to evaluate.

This also questions the ability of the studied circulating biomarkers to reflect or detect vascular inflammation, and therefore their diagnostic and risk-stratification potential in small AAA. Golledge *et al* in their extensive review on potential circulating markers of AAA diagnosis and progression, reported that biomarker sensitivity and specificity appear inadequate for the use of an individual circulating marker in AAA diagnosis and therefore called for combined biomarker diagnostic potential to be evaluated in large population-based studies³⁹⁴. Furthermore, Li *et al* questioned whether all accumulations of ^{18}F -FDG within the arteries are due to macrophage-mediated inflammatory activity, since high levels of ^{18}F -FDG were observed in patients with both high and low risk cardiovascular disease⁴⁰⁹. Nevertheless, reproducibility of results when large arteries were studied confirms the useful application of the ^{18}F -FDG tracer in vascular inflammation imaging³¹⁹.

Our study observed a lower AAA ^{18}F -FDG uptake in subjects with hypertension ($p=0.040$). This may be due to effective medical therapy in our study group (11 subjects were taking B-blockers and 4 subjects an ACE-inhibitor) at the time of the investigation. Both Beta-blocker and ACE-inhibitor use has been associated with a marked reduction in the increased circulating levels of cytokines^{410, 411}. Similar to Rudd^{316, 410, 411} and in contrast to Tahara^{217, 316, 410, 411} we have found no relationship between statin use and ^{18}F -FDG uptake. This is most likely due to the small sample size in our non-statin subgroup.

Multiple risk factors for atherosclerosis and AAA development and rupture including age, gender, hypertension, raised lipids and smoking have been identified^{182, 412}. It is reassuring in our study that subjects with risk factors for atherosclerosis (raised lipids, hypertension, ischaemic heart disease, ex-smokers) had significantly higher hsMMP-9, hsMMP-2 levels, given that the relationship between these biomarkers and AAA is well established^{327, 391, 398}. Similar to previous observational work^{413, 414} we observed higher levels of hsCRP ($p=0.047$) in subjects who had stopped smoking. Chronic low grade inflammation measured as a continuous high hsCRP is thought to be a consequence of smoking and a marker of tissue injury, suggesting continuous inflammation (ie high levels of hsCRP) can persist long after smoking cessation^{413, 414}. It is thought that metabolic factors (such as weight gain) contribute to such a persistent inflammatory state⁴¹³.

There are study limitations and technical considerations when interpreting our findings. In this study we have performed a whole vessel type texture analysis to avoid misleading findings on limited aneurysm area, thereby increasing the validity of our study findings and in keeping with recommended AAA PET/CT analysis²¹⁰. The study population size of 24 is small but compares favourably with many initial functional arterial PET studies^{357, 358}. Nonetheless, larger and more extended and perhaps combined studies of several vascular serum biomarkers and PET are needed.

In conclusion, this chapter has presented the first investigation of the possible association of AAA wall metabolic activity as measured by ^{18}F -FDG PET/CT and circulating serum biomarkers in small AAA. The results suggest the degree of AAA

wall inflammation is generally not reflected by levels of the circulating serum biomarkers studied. However, to demonstrate such a relationship may prove difficult due to the relatively low metabolic activity in the arterial walls of small AAA, and large participant numbers may be required to overcome inherent PET limitations.

Summary of findings:

- Cardiovascular risk factors were associated with higher serum levels of hsMMP-9 and hsMMP-2.
- Patients with AAA had significantly higher levels of hsMMP-9 and hsMMP-2 (adjusted for age, gender, hypertension, ischaemic heart disease, raised lipids and statin use) compared to healthy controls.
- No correlations were found for AAA ^{18}F -FDG uptake and circulating levels of hsMMP-9, hsMMP-2, hsINF- γ and hsCRP.

CHAPTER 7. DISCUSSION

7.1. VASCULAR METABOLISM - ^{18}F -FDG HYBRID PET/CT UPTAKE IN AAA

This project to detect increased metabolic activity with ^{18}F -FDG-PET/CT in predominantly small AAAs, in patients undergoing surveillance, demonstrated that the majority (n=13/17) of patients (with mean AP diameter 5.4+0.8cm) had an increased ^{18}F -FDG uptake ($\text{SUV}_{\text{max}} > 2.5$) when ROI was drawn to include hotspots in the aneurysm wall. From this data it is inferred that ^{18}F -FDG PET/CT offer *in vivo* evidence that small AAA show increased glucose metabolism. We reported higher SUV_{max} values in our hybrid PET/CT camera cohort compared to a stand-alone PET camera study (mean AAA diameter 6.3+0.95cm) reporting only 39% high FDG uptake³⁴. Size discrepancies and technology advances may in part explain our findings. It was also observed that aneurysm wall glucose uptake as measured by TBR_{max} remained relatively unchanged at various time points with PET imaging, even though a significant difference in blood-pool activity was observed between 1 and 3h. Wu *et al* noted in their dual time-point vascular ^{18}F -FDG PET carotid study that the delayed images allowed for better lesion-to-background contrast during visual assessment; however, both the pattern and location of ^{18}F -FDG uptake could be detected on both early and delayed images²¹⁶. It is suggested that the resulting decay of the tracer with subsequent increase in image noise may be implicated in delayed arterial ^{18}F -FDG PET imaging. Therefore, the possible benefits of delayed imaging are counterbalanced by the effects of image noise and more variable SUV_{max} measurements³⁴⁸. Performing vascular PET at 1h compared to 3h time-point has logistical benefits. Large multicentre PET trials to assess arterial inflammation and atheroma vulnerability and to monitor the effects of pharmacologic therapies could be made more feasible by improved workflow, and participation would be less onerous for patients. Since metabolic activity (to a lesser or greater degree) detected by ^{18}F -FDG PET/CT is present in small AAA, we explored the risk-stratification potential of ^{18}F -FDG PET in prospective aneurysm growth studies.

7.2. RELATIONSHIP BETWEEN ^{18}F -FDG AORTIC ANEURYSM UPTAKE ON PET/CT AND ANEURYSM GROWTH RATE

This chapter takes the view that ^{18}F -FDG PET has a potential role in risk-stratification of patients with aneurysms detected during screening, since aortic ^{18}F -FDG uptake was inversely related to future aneurysm expansion. This finding suggests that aortic aneurysms with lower ^{18}F -FDG metabolic activity seem more likely to expand. We and other researchers suggest aneurysm dilatation develops after initial inflammatory processes^{134, 168, 354} and calcification possibly represents a late burn-out stage of atherosclerosis^{316, 354}. However, these findings need to be rationalized in light of a single time-point investigation and that increased ^{18}F -FDG uptake in arteries may not persist with time³⁴⁸. Therefore, before general application of ^{18}F -FDG PET as a marker of significant aneurysm expansion in clinical practice, larger scale studies should be performed to confirm these study findings. Furthermore, identifying relationships when combining *in vivo* imaging techniques such as both ^{18}F -FDG PET/CT and CT heterogeneity may increase our understanding of the role vascular metabolism plays in AAA formation and progression.

7.3. INVESTIGATING AAA TEXTURE ANALYSIS AND ^{18}F -FDG UPTAKE ON PET/CT AND FUTURE GROWTH RATE

In this chapter a prospective longitudinal study was performed examining whether AAA heterogeneity using CT texture measurements were associated with future aneurysm expansion and also for associations between aneurysm glucose metabolism and CT texture. Increased coarse texture parameters (SD) were found in aneurysms that exhibit lower metabolic activity affirming that surface anatomical heterogeneity changes in AAA walls may reflect underlying inflammatory pathobiology. The medium texture parameters (K) correlated strongest with significant AAA expansion, suggesting that aneurysms with greater medium heterogeneity (K) may be more likely to exhibit greater AAA expansion. This part of the thesis therefore identified CT texture characteristics and ^{18}F -FDG PET uptake derived from baseline PET/CT images that are associated with prospective AAA growth rate, thus validating the role of these modalities in studying AAA and providing a foundation for further larger studies. Histological PET

heterogeneity studies are needed to underpin structural characteristics associated with significant disease progression to provide possible explanations for these study findings. Future studies assessing the relationship between calcium burden, AAA wall texture and inflammation may be useful. Furthermore, assessing the association between ^{18}F -FDG PET AAA uptake and circulating serum biomarkers of inflammation in patients with small AAA may broaden our insight into AAA pathobiology to identify serumbiomarkers with potential in AAA risk-stratification.

7.4. SERUM BIOMARKERS AND ^{18}F -FDG AAA UPTAKE ON PET/CT

This chapter evaluated the relationship between abdominal aneurysm wall ^{18}F -FDG uptake using PET/CT with recognized circulating serum biomarkers of inflammation. Although subjects with AAA had significantly higher levels of hsMMP-2 and -9 in our study and other studies³⁹¹, no link between AAA ^{18}F -FDG uptake and circulating levels of hsMMP-2, -9, hsINF- γ and or hsCRP were identified. Since ^{18}F -FDG PET uptake reflects metabolic activity^{221, 222}, this finding suggests the degree of AAA wall inflammation may not be reflected in the blood levels of the circulating serum biomarkers studied. The study findings need to be rationalized against study limitations including small participant numbers and reproducibility challenges of ELISA assay results along with inherent errors in AAA SUV measurements. Furthermore, ^{18}F -FDG is a non-specific PET tracer, albeit generally accumulated in greater amounts in macrophages in atherosclerosis.

CHAPTER 8. CONCLUSION AND FUTURE WORK

Screening programmes for aortic aneurysms are being introduced in North America and Europe. The increase in surveillance is creating demand for further risk-stratification whilst intensifying the need to develop strategies for managing the growth rate of small aneurysms. *In vivo* imaging of AAA using ^{18}F -FDG hybrid PET/CT shows potential to identify patients at risk of disease progression. FDG PET/CT could also be considered as an imaging modality for possibly assessing response to non-surgical treatment and the need for re-intervention following EVAR.

Contemporary data suggest a role for vascular PET/CT in evaluation of aortic dissection³⁵⁷ and aortitis⁴¹⁵. This thesis aimed to increase our understanding of the role for clinical PET/CT in patients with small AAA. Relationships between aortic aneurysm wall ^{18}F -FDG uptake and future AAA expansion were identified.

Based on positive outcome of results the following recommendations are made:

- a. The introduction of 4-D PET and appropriate gating may help overcome recognized technical constraints for PET/CT, however, the ideal vascular tracer remains unknown²⁸⁹. Histological correlation studies with ^{68}Ga -DOTATATE as vascular imaging tracer are needed.
- b. Further improvements in isolating the SUV measurement from the aneurysm wall might also improve accuracy²²³. We suggest further analysis using a ‘doughnut’ type ROI measurement of the aneurysmal wall where the ROI does not include the arterial lumen.
- c. PET/CT to investigate AAA pathobiology should be performed with intravenous contrast to aid more accurate identification of ILT and to facilitate further work on the influence of ILT in AAA pathobiology with PET/CT.
- d. CT texture analysis with particular emphasis on medium and coarse texture parameters could be further explored in AAA risk stratification.
- e. Furthermore, future prospective studies could also focus on large AAA and rupture risk stratification with PET/CT.

APPENDIX

CT Textural analysis

Brief description:

The CTTA technique comprised an initial band-pass image filtration using a Laplacian of Gaussian (LoG) filter (Figure A1) to produce a series of derived images of the AAA, displaying features at different anatomical scales from fine to coarse texture (Figures A1 and A2 and Table A1). AAA heterogeneity within each filtered image was quantified using histogram-based parameters, including standard deviation (SD) (degree of variation from the mean pixel value or scale of the distribution) and kurtosis (K) (pointedness of the distribution may reflect structures such as vessels). SD and K then describe the gray-level variation and pointiness respectively of the histograms representing structures within the AAA.

Technical description:

CTTA comprised of two main stages, image filtration and quantification of texture.

Image filtration

A LoG band-pass filter was chosen, and modulated to highlight different spatial scales between fine texture (filter value = 1.0) and coarse texture (filter value = 2.5). This scale can be considered as the width at which structures in the image will be highlighted and enhanced, while structures less than this width will become blurred.

The two-dimensional (2D) Gaussian distribution G is given by

$$G(x, y) = e^{-\frac{x^2 + y^2}{2\sigma^2}} \quad \text{Equation 1}$$

where x, y are the spatial coordinates of the image matrix and σ is the standard deviation of the Gaussian distribution. The 2D Gaussian distribution effectively blurs the image, wiping out all structures at scales much smaller than the sigma of the Gaussian. This distribution has the desirable characteristics of being smooth and localized in both the spatial and frequency domains, and is therefore less likely to introduce any changes to the original image. Thus, the Gaussian distribution corresponding to a particular σ value allows the highlighting in CT images of texture features of a particular scale. We have

used this filtration technique to filter out textural features of varying scale, from; fine to medium to coarse.

The reason for using the Laplacian (∇^2) is that it is the lowest-order orientation-independent (isotropic) differential operator and inherently has less computational burden and can be used to detect intensity changes in an image that correspond to the zero crossings of the filter. $\nabla^2 G$ is the LoG filter, a circularly symmetric, Mexican-hat-shaped filter (see Figure A1 for spatial and frequency domain representations of the filter) whose distribution in the 2D spatial domain is given by

$$\nabla^2 G(x, y) = \frac{-1}{\pi\sigma^4} \left(1 - \frac{x^2 + y^2}{2\sigma^2} \right) e^{-\left(\frac{x^2 + y^2}{2\sigma^2}\right)} . \quad \text{Equation 2}$$

From the mathematical expression of this circularly symmetric filter at different σ values, the number of pixels representing the width between the diametrically opposite zero-crossing points in this filter can be calculated. The width of the filter at different σ values is obtained by evaluating the LoG spatial distribution along the x and y directions. The lower the σ value, the smaller is the width of the filter in the spatial domain and the larger is the band-pass region of the filter in the frequency domain, highlighting fine details or features in the filtered image in the spatial domain. Similarly in the spatial domain, a higher σ value allows coarse features to be highlighted in the filtered image.

Filtration can be done in the spatial or frequency domain. In the spatial domain, the filter mask is convolved with the image, which involves intensive computation. It is more efficient to use the filter in the frequency domain, as convolution of the filter mask and the image in the spatial domain is equivalent to multiplication of the Fourier transforms of the filter mask and image in the frequency domain. The inverse Fourier transform of the filtered spectrum gives the resultant filtered image in the spatial domain. Also, the accuracy of this filtering operation is improved when used in the frequency domain, as the quantization errors arising from the convolution of the filter, especially for small σ values in the spatial domain, would distort the image. In our study, the filter was applied in the frequency domain.

Quantification of texture

A region of interest (ROI) was placed to include the aneurysm wall and content as well as to include only the luminal content on each individual axial slice comprising the whole vessel AAA. The ROI was further refined by the exclusion of areas of air with a thresholding procedure that removed from analysis any pixels with attenuation values below -50 HU. Median ROI size (from the whole vessel AAA) was 20919 pixels (range, 4084-123572 pixels). The ROIs for texture analysis were stored as a binary mask and assigned to the corresponding individual patient lesion. This ensured that the same patient-specific ROI was used for the texture analyses of different σ values. The resulting images underwent 2D band-pass filtering with the LoG filter using each of the following filter values: (fine, filter width: 2mm radius); (medium, filter width: 3-5mm radius); (coarse, filter width: 6mm radius) (Table A1). Heterogeneity within this ROI was quantified with image filtration. The histogram of AAA pixel values with image filtration was characterized by SD (degree of variation from the mean pixel value or scale of the distribution) and K (pointedness of the distribution may reflect structures such as vessels) using the equations below:

$$SD = \left(\frac{1}{n-1} \sum_{(x,y) \in R} [a(x,y) - \bar{a}]^2 \right)^{\frac{1}{2}} \quad \text{Equation 3}$$

$$K = \frac{n(n+1)}{(n-1)(n-2)(n-3)} \frac{\sum_{(x,y) \in R} [a(x,y) - \bar{a}]^4}{[sd(a)]^4} - 3 \frac{(n-1)^2}{(n-2)(n-3)} \quad \text{Equation 4}$$

where R is the ROI within the image $a(x,y)$, n is the total number of pixels in R , \bar{a} is the mean value within R .

Table A1 Filter values and the corresponding widths of the filter in mm

Filter value	Filter width (radius) in mm
Fine	2
Medium	3-5
Coarse	6

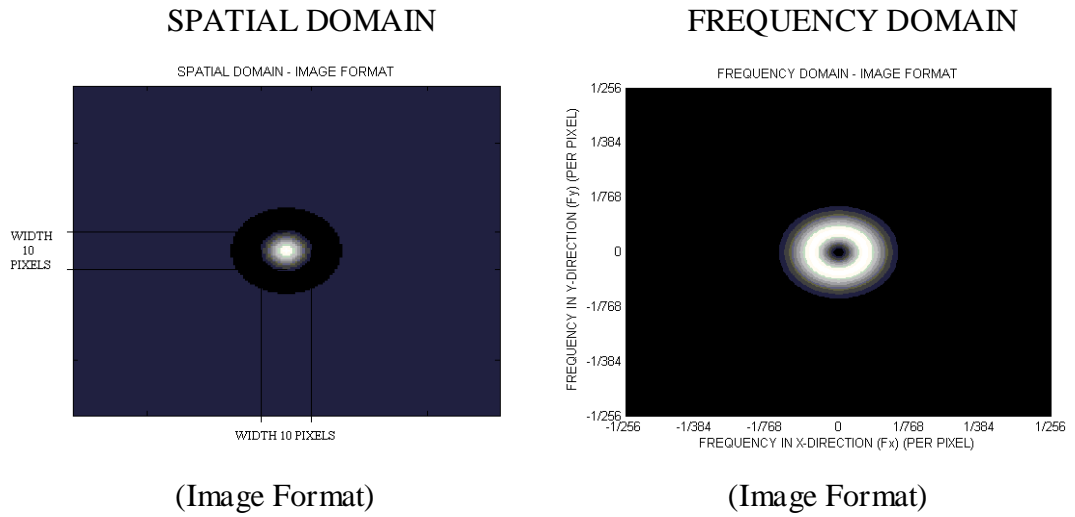


Figure A1 The 2-D forms of the LoG filter in the spatial and frequency domain at extract medium texture

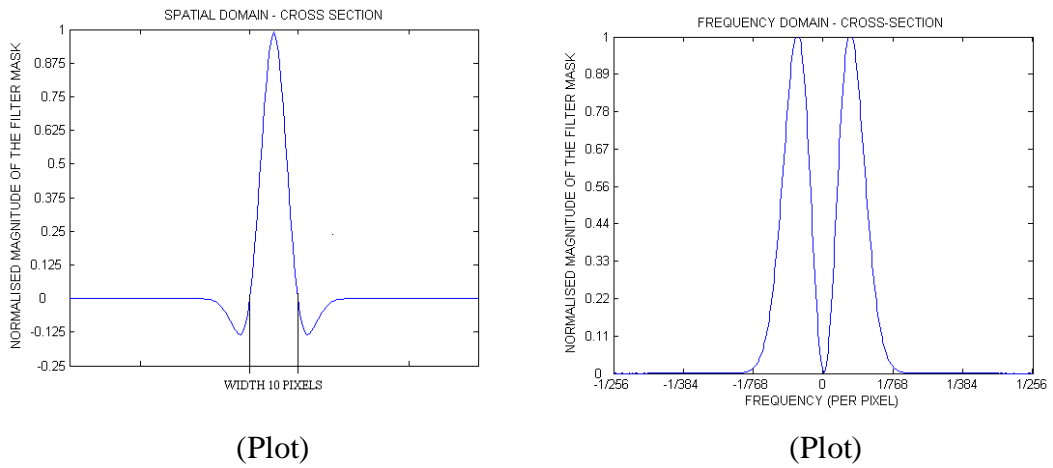


Figure A2 The 2-D forms of the LoG filter in the spatial and frequency domain at filter value of 2.0 (extract medium texture)

REFERENCES

1. Cosford PA, Leng GC. Screening for abdominal aortic aneurysm. *Cochrane database of systematic reviews* 2007(2): CD002945.
2. Hoornweg LL, Storm-Versloot MN, Ubbink DT, Koelemay MJ, Legemate DA, Balm R. Meta analysis on mortality of ruptured abdominal aortic aneurysms. *European journal of vascular and endovascular surgery : the official journal of the European Society for Vascular Surgery* 2008;**35**(5): 558-570.
3. Johnston KW, Rutherford RB, Tilson MD, Shah DM, Hollier L, Stanley JC. Suggested standards for reporting on arterial aneurysms. Subcommittee on Reporting Standards for Arterial Aneurysms, Ad Hoc Committee on Reporting Standards, Society for Vascular Surgery and North American Chapter, International Society for Cardiovascular Surgery. *Journal of vascular surgery* 1991;**13**(3): 452-458.
4. Scott RAP. The Multicentre Aneurysm Screening Study (MASS) into the effect of abdominal aortic aneurysm screening on mortality in men: a randomised controlled trial. *The Lancet* 2002;**360**(9345): 1531-1539.
5. Liakischev AA. [Comparison of Endovascular Aneurysm Repair With Open Repair in Patients With Abdominal Aortic Aneurysm, 30-day Operative Mortality RESULTS: Randomised Controlled Trial. Results of the EVAR 1 Trial.]. *Kardiologija* 2004;**44**(11): 90.
6. Framework for improving the results of AAA repair. <http://www.vascularsociety.org.uk/vascular/wp-content/uploads/2012/11/VSGBI-AAA-QIF-2011-v4.pdf> [October 1 2013].
7. Screening for Abdominal Aortic Aneurysm. <http://www.uspreventiveservicestaskforce.org/uspstf/uspsaneu.htm> [July 1 2012].
8. Wassef M, Baxter BT, Chisholm RL, Dalman RL, Fillinger MF, Heinecke J, Humphrey JD, Kuivaniemi H, Parks WC, Pearce WH, Platsoucas CD, Sukhova GK, Thompson RW, Tilson MD, Zarins CK. Pathogenesis of abdominal aortic aneurysms: a multidisciplinary research program supported by the National Heart, Lung, and Blood Institute. *Journal of vascular surgery* 2001;**34**(4): 730-738.
9. Nordon IM, Hinchliffe RJ, Loftus IM, Thompson MM. Pathophysiology and epidemiology of abdominal aortic aneurysms. *Nature reviews Cardiology* 2011;**8**(2): 92-102.
10. Lindholt JS, Shi GP. Chronic inflammation, immune response, and infection in abdominal aortic aneurysms. *European journal of vascular and endovascular surgery : the official journal of the European Society for Vascular Surgery* 2006;**31**(5): 453-463.
11. Kirsch EW, Radu NC, Allaire E, Loisanche DY. Pathobiology of idiopathic ascending aortic aneurysms. *Asian cardiovascular & thoracic annals* 2006;**14**(3): 254-260.
12. Michel JB, Martin-Ventura JL, Egado J, Sakalihasan N, Treska V, Lindholt J, Allaire E, Thorsteinsdottir U, Cockerill G, Swedenborg J, consortium FE. Novel aspects of the pathogenesis of aneurysms of the abdominal aorta in humans. *Cardiovascular research* 2011;**90**(1): 18-27.
13. Shum J, Martufi G, Di Martino E, Washington CB, Grisafi J, Muluk SC, Finol EA. Quantitative assessment of abdominal aortic aneurysm geometry. *Annals of biomedical engineering* 2011;**39**(1): 277-286.

14. Elger DF, Blackketter DM, Budwig RS, Johansen KH. The influence of shape on the stresses in model abdominal aortic aneurysms. *Journal of biomechanical engineering* 1996;**118**(3): 326-332.
15. Vorp DA, Raghavan ML, Webster MW. Mechanical wall stress in abdominal aortic aneurysm: influence of diameter and asymmetry. *Journal of vascular surgery* 1998;**27**(4): 632-639.
16. Fillinger MF, Racusin J, Baker RK, Cronenwett JL, Teutelink A, Schermerhorn ML, Zwolak RM, Powell RJ, Walsh DB, Ruzicidlo EM. Anatomic characteristics of ruptured abdominal aortic aneurysm on conventional CT scans: Implications for rupture risk. *J Vasc Surg* 2004;**39**(6): 1243-1252.
17. Maier A, Gee MW, Reeps C, Eckstein HH, Wall WA. Impact of calcifications on patient-specific wall stress analysis of abdominal aortic aneurysms. *Biomechanics and modeling in mechanobiology* 2010;**9**(5): 511-521.
18. Lederle FA, Johnson GR, Wilson SE, Ballard DJ, Jordan WD, Jr., Blebea J, Littooy FN, Freischlag JA, Bandyk D, Rapp JH, Salam AA. Rupture rate of large abdominal aortic aneurysms in patients refusing or unfit for elective repair. *JAMA* 2002;**287**(22): 2968-2972.
19. Brewster DC, Cronenwett JL, Hallett JW, Jr., Johnston KW, Krupski WC, Matsumura JS, Joint Council of the American Association for Vascular S, Society for Vascular S. Guidelines for the treatment of abdominal aortic aneurysms. Report of a subcommittee of the Joint Council of the American Association for Vascular Surgery and Society for Vascular Surgery. *Journal of vascular surgery* 2003;**37**(5): 1106-1117.
20. Powell JT, Sweeting MJ, Brown LC, Gotensparre SM, Fowkes FG, Thompson SG. Systematic review and meta-analysis of growth rates of small abdominal aortic aneurysms. *The British journal of surgery* 2011;**98**(5): 609-618.
21. Thompson AR, Cooper JA, Ashton HA, Hafez H. Growth rates of small abdominal aortic aneurysms correlate with clinical events. *The British journal of surgery* 2010;**97**(1): 37-44.
22. Choke E, Cockerill G, Wilson WR, Sayed S, Dawson J, Loftus I, Thompson MM. A review of biological factors implicated in abdominal aortic aneurysm rupture. *European journal of vascular and endovascular surgery : the official journal of the European Society for Vascular Surgery* 2005;**30**(3): 227-244.
23. Limet R, Sakalihassan N, Albert A. Determination of the expansion rate and incidence of rupture of abdominal aortic aneurysms. *J Vasc Surg* 1991;**14**(4): 540-548.
24. Brown PM, Zelt DT, Sobolev B. The risk of rupture in untreated aneurysms: the impact of size, gender, and expansion rate. *J Vasc Surg* 2003;**37**(2): 280-284.
25. Cronenwett JL, Sargent SK, Wall MH, Hawkes ML, Freeman DH, Dain BJ, Cure JK, Walsh DB, Zwolak RM, McDaniel MD, et al. Variables that affect the expansion rate and outcome of small abdominal aortic aneurysms. *Journal of vascular surgery* 1990;**11**(2): 260-268; discussion 268-269.
26. Bengtsson H, Bergqvist D, Ekberg O, Ranstam J. Expansion pattern and risk of rupture of abdominal aortic aneurysms that were not operated on. *The European journal of surgery = Acta chirurgica* 1993;**159**(9): 461-467.
27. Grimshaw GM, Thompson JM. Changes in diameter of the abdominal aorta with age: an epidemiological study. *Journal of clinical ultrasound : JCU* 1997;**25**(1): 7-13.
28. Hirose Y, Hamada S, Takamiya M. Predicting the growth of aortic aneurysms: a comparison of linear vs exponential models. *Angiology* 1995;**46**(5): 413-419.
29. Santilli SM, Littooy FN, Cambria RA, Rapp JH, Tretinyak AS, d'Audiffret AC, Kuskowski MA, Roethle ST, Tomczak CM, Krupski WC. Expansion rates and

- outcomes for the 3.0-cm to the 3.9-cm infrarenal abdominal aortic aneurysm. *Journal of vascular surgery* 2002;**35**(4): 666-671.
30. Choyke PL, Gomes MN. Surgery for "small" abdominal aortic aneurysm. *Lancet* 1993;**342**(8884): 1377.
31. Schewe CK, Schweikart HP, Hammel G, Spengel FA, Zollner N, Zoller WG. Influence of selective management on the prognosis and the risk of rupture of abdominal aortic aneurysms. *The Clinical investigator* 1994;**72**(8): 585-591.
32. MacSweeney ST, Ellis M, Worrell PC, Greenhalgh RM, Powell JT. Smoking and growth rate of small abdominal aortic aneurysms. *Lancet* 1994;**344**(8923): 651-652.
33. Schlosser FJ, Tangelder MJ, Verhagen HJ, van der Heijden GJ, Muhs BE, van der Graaf Y, Moll FL, group Ss. Growth predictors and prognosis of small abdominal aortic aneurysms. *J Vasc Surg* 2008;**47**(6): 1127-1133.
34. Sakalihasan N, Van Damme H, Gomez P, Rigo P, Lapiere CM, Nusgens B, Limet R. Positron emission tomography (PET) evaluation of abdominal aortic aneurysm (AAA). *European journal of vascular and endovascular surgery : the official journal of the European Society for Vascular Surgery* 2002;**23**(5): 431-436.
35. Matsushita M, Nishikimi N, Sakurai T, Nimura Y. Relationship between aortic calcification and atherosclerotic disease in patients with abdominal aortic aneurysm. *International angiology : a journal of the International Union of Angiology* 2000;**19**(3): 276-279.
36. Meirelles GS, Gonen M, Strauss HW. 18F-FDG uptake and calcifications in the thoracic aorta on positron emission tomography/computed tomography examinations: frequency and stability on serial scans. *Journal of thoracic imaging* 2011;**26**(1): 54-62.
37. Lindholt JS, Norman P. Screening for abdominal aortic aneurysm reduces overall mortality in men. A meta-analysis of the mid- and long-term effects of screening for abdominal aortic aneurysms. *European journal of vascular and endovascular surgery : the official journal of the European Society for Vascular Surgery* 2008;**36**(2): 167-171.
38. Lindholt JS. Aneurysmal wall calcification predicts natural history of small abdominal aortic aneurysms. *Atherosclerosis* 2008;**197**(2): 673-678.
39. Vega de Ceniga M, Gomez R, Estallo L, de la Fuente N, Vivien B, Barba A. Analysis of expansion patterns in 4-4.9 cm abdominal aortic aneurysms. *Ann Vasc Surg* 2008;**22**(1): 37-44.
40. Li ZY, J UK-I, Tang TY, Soh E, See TC, Gillard JH. Impact of calcification and intraluminal thrombus on the computed wall stresses of abdominal aortic aneurysm. *Journal of vascular surgery* 2008;**47**(5): 928-935.
41. Speelman L, Bohra A, Bosboom EM, Schurink GW, van de Vosse FN, Makaorun MS, Vorp DA. Effects of wall calcifications in patient-specific wall stress analyses of abdominal aortic aneurysms. *Journal of biomechanical engineering* 2007;**129**(1): 105-109.
42. Matsushita M, Ikezawa T. Factors affecting the regression of surgically replaced abdominal aortic aneurysms. *Surgery today* 2006;**36**(2): 147-150.
43. Basalyga DM, Simionescu DT, Xiong W, Baxter BT, Starcher BC, Vyavahare NR. Elastin degradation and calcification in an abdominal aorta injury model: role of matrix metalloproteinases. *Circulation* 2004;**110**(22): 3480-3487.
44. Dobrin PB, Mrkvicka R. Failure of elastin or collagen as possible critical connective tissue alterations underlying aneurysmal dilatation. *Cardiovascular surgery* 1994;**2**(4): 484-488.
45. Tilson MD. Histochemistry of aortic elastin in patients with nonspecific abdominal aortic aneurysmal disease. *Archives of surgery* 1988;**123**(4): 503-505.

46. Alexander JJ. The pathobiology of aortic aneurysms. *The Journal of surgical research* 2004;**117**(1): 163-175.
47. Rucker RB, Tinker D. Structure and metabolism of arterial elastin. *International review of experimental pathology* 1977;**17**: 1-47.
48. Stromberg DD, Wiederhielm CA. Viscoelastic description of a collagenous tissue in simple elongation. *Journal of applied physiology* 1969;**26**(6): 857-862.
49. Dobrin PB. Distribution of lamellar deformations: implications for properties of the arterial media. *Hypertension* 1999;**33**(3): 806-810.
50. Prockop DJ. Mutations that alter the primary structure of type I collagen. The perils of a system for generating large structures by the principle of nucleated growth. *The Journal of biological chemistry* 1990;**265**(26): 15349-15352.
51. Satta J, Haukipuro K, Kairaluoma MI, Juvonen T. Aminoterminal propeptide of type III procollagen in the follow-up of patients with abdominal aortic aneurysms. *Journal of vascular surgery* 1997;**25**(5): 909-915.
52. Menashi S, Campa JS, Greenhalgh RM, Powell JT. Collagen in abdominal aortic aneurysm: typing, content, and degradation. *Journal of vascular surgery* 1987;**6**(6): 578-582.
53. Dobrin PB. Mechanical properties of arteries. *Physiological reviews* 1978;**58**(2): 397-460.
54. Dobrin PB. Mechanics of normal and diseased blood vessels. *Ann Vasc Surg* 1988;**2**(3): 283-294.
55. Lesauskaite V, Ivanoviene L, Valanciute A. [Programmed cellular death and atherogenesis: from molecular mechanisms to clinical aspects]. *Medicina* 2003;**39**(6): 529-534.
56. O'Callaghan CJ, Williams B. Mechanical strain-induced extracellular matrix production by human vascular smooth muscle cells: role of TGF-beta(1). *Hypertension* 2000;**36**(3): 319-324.
57. Patel MI, Melrose J, Ghosh P, Appleberg M. Increased synthesis of matrix metalloproteinases by aortic smooth muscle cells is implicated in the etiopathogenesis of abdominal aortic aneurysms. *Journal of vascular surgery* 1996;**24**(1): 82-92.
58. Sakalihasan N, Limet R, Defawe OD. Abdominal aortic aneurysm. *Lancet* 2005;**365**(9470): 1577-1589.
59. Clarke MC, Littlewood TD, Figg N, Maguire JJ, Davenport AP, Goddard M, Bennett MR. Chronic apoptosis of vascular smooth muscle cells accelerates atherosclerosis and promotes calcification and medial degeneration. *Circulation research* 2008;**102**(12): 1529-1538.
60. Campa JS, Greenhalgh RM, Powell JT. Elastin degradation in abdominal aortic aneurysms. *Atherosclerosis* 1987;**65**(1-2): 13-21.
61. White JV, Haas K, Phillips S, Comerota AJ. Adventitial elastolysis is a primary event in aneurysm formation. *Journal of vascular surgery* 1993;**17**(2): 371-380; discussion 380-371.
62. Economou SG, Taylor CB, Beattie EJ, Jr., Davis CB, Jr. Persistent experimental aortic aneurysms in dogs. *Surgery* 1960;**47**: 21-28.
63. Carmo M, Colombo L, Bruno A, Corsi FR, Roncoroni L, Cuttin MS, Radice F, Mussini E, Settembrini PG. Alteration of elastin, collagen and their cross-links in abdominal aortic aneurysms. *European journal of vascular and endovascular surgery : the official journal of the European Society for Vascular Surgery* 2002;**23**(6): 543-549.
64. Cohen JR, Mandell C, Chang JB, Wise L. Elastin metabolism of the infrarenal aorta. *Journal of vascular surgery* 1988;**7**(2): 210-214.

65. Halloran BG, Baxter BT. Pathogenesis of aneurysms. *Semin Vasc Surg* 1995;**8**(2): 85-92.
66. Shimizu K, Mitchell RN, Libby P. Inflammation and cellular immune responses in abdominal aortic aneurysms. *Arteriosclerosis, thrombosis, and vascular biology* 2006;**26**(5): 987-994.
67. Goodall S, Porter KE, Bell PR, Thompson MM. Enhanced invasive properties exhibited by smooth muscle cells are associated with elevated production of MMP-2 in patients with aortic aneurysms. *European journal of vascular and endovascular surgery : the official journal of the European Society for Vascular Surgery* 2002;**24**(1): 72-80.
68. He CM, Roach MR. The composition and mechanical properties of abdominal aortic aneurysms. *Journal of vascular surgery* 1994;**20**(1): 6-13.
69. Raghavan ML, Webster MW, Vorp DA. Ex vivo biomechanical behavior of abdominal aortic aneurysm: assessment using a new mathematical model. *Annals of biomedical engineering* 1996;**24**(5): 573-582.
70. Sakalihasan N, Heyeres A, Nusgens BV, Limet R, Lapiere CM. Modifications of the extracellular matrix of aneurysmal abdominal aortas as a function of their size. *European journal of vascular surgery* 1993;**7**(6): 633-637.
71. Webster MW, McAuley CE, Steed DL, Miller DD, Evans CH. Collagen stability and collagenolytic activity in the normal and aneurysmal human abdominal aorta. *American journal of surgery* 1991;**161**(6): 635-638.
72. Allaire E, Muscatelli-Groux B, Mandet C, Guinault AM, Bruneval P, Desgranges P, Clowes A, Melliere D, Becquemin JP. Paracrine effect of vascular smooth muscle cells in the prevention of aortic aneurysm formation. *Journal of vascular surgery* 2002;**36**(5): 1018-1026.
73. Kuivaniemi H, Platsoucas CD, Tilson MD, 3rd. Aortic aneurysms: an immune disease with a strong genetic component. *Circulation* 2008;**117**(2): 242-252.
74. Kuivaniemi H, Tromp G, Prockop DJ. Genetic causes of aortic aneurysms. Unlearning at least part of what the textbooks say. *J Clin Invest* 1991;**88**(5): 1441-1444.
75. Verloes A, Sakalihasan N, Koulischer L, Limet R. Aneurysms of the abdominal aorta: familial and genetic aspects in three hundred thirteen pedigrees. *Journal of vascular surgery* 1995;**21**(4): 646-655.
76. Coady MA, Davies RR, Roberts M, Goldstein LJ, Rogalski MJ, Rizzo JA, Hammond GL, Kopf GS, Elefteriades JA. Familial patterns of thoracic aortic aneurysms. *Archives of surgery* 1999;**134**(4): 361-367.
77. Clifton MA. Familial abdominal aortic aneurysms. *The British journal of surgery* 1977;**64**(11): 765-766.
78. Tilson MD, Seashore MR. Human genetics of the abdominal aortic aneurysm. *Surgery, gynecology & obstetrics* 1984;**158**(2): 129-132.
79. Bowers D, Cave WS. Aneurysms of the abdominal aorta: a 20-year study. *Journal of the Royal Society of Medicine* 1985;**78**(10): 812-820.
80. Powell JT, Greenhalgh RM. Multifactorial inheritance of abdominal aortic aneurysm. *European journal of vascular surgery* 1987;**1**(1): 29-31.
81. Majumder PP, St Jean PL, Ferrell RE, Webster MW, Steed DL. On the inheritance of abdominal aortic aneurysm. *American journal of human genetics* 1991;**48**(1): 164-170.
82. Johansen K, Koepsell T. Familial tendency for abdominal aortic aneurysms. *JAMA* 1986;**256**(14): 1934-1936.
83. Coady MA, Rizzo JA, Elefteriades JA. Pathologic variants of thoracic aortic dissections. Penetrating atherosclerotic ulcers and intramural hematomas. *Cardiology clinics* 1999;**17**(4): 637-657.

84. Rizzo RJ, McCarthy WJ, Dixit SN, Lilly MP, Shively VP, Flinn WR, Yao JS. Collagen types and matrix protein content in human abdominal aortic aneurysms. *Journal of vascular surgery* 1989;**10**(4): 365-373.
85. Oleszak EL, Chang JR, Friedman H, Katsetos CD, Platsoucas CD. Theiler's virus infection: a model for multiple sclerosis. *Clinical microbiology reviews* 2004;**17**(1): 174-207.
86. Platsoucas CD, Lu S, Nwaneshiudu I, Solomides C, Agelan A, Ntaoula N, Purev E, Li LP, Kratsios P, Mylonas E, Jung WJ, Evans K, Roberts S, Lu Y, Layvi R, Lin WL, Zhang X, Gaughan J, Monos DS, Oleszak EL, White JV. Abdominal aortic aneurysm is a specific antigen-driven T cell disease. *Annals of the New York Academy of Sciences* 2006;**1085**: 224-235.
87. Li ZY, Sadat U, J UK-I, Tang TY, Bowden DJ, Hayes PD, Gillard JH. Association between aneurysm shoulder stress and abdominal aortic aneurysm expansion: a longitudinal follow-up study. *Circulation* 2010;**122**(18): 1815-1822.
88. Sprouse LR, 2nd, Meier GH, 3rd, Lesar CJ, Demasi RJ, Sood J, Parent FN, Marcinyzyck MJ, Gayle RG. Comparison of abdominal aortic aneurysm diameter measurements obtained with ultrasound and computed tomography: Is there a difference? *Journal of vascular surgery* 2003;**38**(3): 466-471; discussion 471-462.
89. Ku DN, Giddens DP, Zarins CK, Glagov S. Pulsatile flow and atherosclerosis in the human carotid bifurcation. Positive correlation between plaque location and low oscillating shear stress. *Arteriosclerosis* 1985;**5**(3): 293-302.
90. Miller FJ, Jr. Aortic aneurysms: It's all about the stress. *Arteriosclerosis, thrombosis, and vascular biology* 2002;**22**(12): 1948-1949.
91. Zeng Z, Kallmes DF, Durka MJ, Ding Y, Lewis D, Kadirvel R, Robertson AM. Hemodynamics and anatomy of elastase-induced rabbit aneurysm models: similarity to human cerebral aneurysms? *AJNR American journal of neuroradiology* 2011;**32**(3): 595-601.
92. Zarins CK, Giddens DP, Bharadvaj BK, Sottiurai VS, Mabon RF, Glagov S. Carotid bifurcation atherosclerosis. Quantitative correlation of plaque localization with flow velocity profiles and wall shear stress. *Circulation research* 1983;**53**(4): 502-514.
93. Platt MO, Ankeny RF, Jo H. Laminar shear stress inhibits cathepsin L activity in endothelial cells. *Arteriosclerosis, thrombosis, and vascular biology* 2006;**26**(8): 1784-1790.
94. Carlier SG, van Damme LC, Blommerde CP, Wentzel JJ, van Langehove G, Verheye S, Kockx MM, Knaapen MW, Cheng C, Gijssen F, Duncker DJ, Stergiopoulos N, Slager CJ, Serruys PW, Krams R. Augmentation of wall shear stress inhibits neointimal hyperplasia after stent implantation: inhibition through reduction of inflammation? *Circulation* 2003;**107**(21): 2741-2746.
95. Langille BL, O'Donnell F. Reductions in arterial diameter produced by chronic decreases in blood flow are endothelium-dependent. *Science* 1986;**231**(4736): 405-407.
96. Sho E, Sho M, Singh TM, Nanjo H, Komatsu M, Xu C, Masuda H, Zarins CK. Arterial enlargement in response to high flow requires early expression of matrix metalloproteinases to degrade extracellular matrix. *Experimental and molecular pathology* 2002;**73**(2): 142-153.
97. Topper JN, Cai J, Falb D, Gimbrone MA, Jr. Identification of vascular endothelial genes differentially responsive to fluid mechanical stimuli: cyclooxygenase-2, manganese superoxide dismutase, and endothelial cell nitric oxide synthase are selectively up-regulated by steady laminar shear stress. *Proceedings of the National Academy of Sciences of the United States of America* 1996;**93**(19): 10417-10422.

98. Miller FJ. Oxidative Stress in Human Abdominal Aortic Aneurysms: A Potential Mediator of Aneurysmal Remodeling. *Arteriosclerosis, Thrombosis, and Vascular Biology* 2002;**22**(4): 560-565.
99. Immenschuh S, Ramadori G. Gene regulation of heme oxygenase-1 as a therapeutic target. *Biochemical pharmacology* 2000;**60**(8): 1121-1128.
100. Rajagopalan S, Meng XP, Ramasamy S, Harrison DG, Galis ZS. Reactive oxygen species produced by macrophage-derived foam cells regulate the activity of vascular matrix metalloproteinases in vitro. Implications for atherosclerotic plaque stability. *J Clin Invest* 1996;**98**(11): 2572-2579.
101. Inzoli F, Boschetti F, Zappa M, Longo T, Fumero R. Biomechanical factors in abdominal aortic aneurysm rupture. *European journal of vascular surgery* 1993;**7**(6): 667-674.
102. Mower WR, Quinones WJ, Gambhir SS. Effect of intraluminal thrombus on abdominal aortic aneurysm wall stress. *Journal of vascular surgery* 1997;**26**(4): 602-608.
103. Stringfellow MM, Lawrence PF, Stringfellow RG. The influence of aorta-aneurysm geometry upon stress in the aneurysm wall. *The Journal of surgical research* 1987;**42**(4): 425-433.
104. Allaire E, Schneider F, Saucy F, Dai J, Cochennec F, Michineau S, Zidi M, Becquemin JP, Kirsch M, Gervais M. New insight in aetiopathogenesis of aortic diseases. *European journal of vascular and endovascular surgery : the official journal of the European Society for Vascular Surgery* 2009;**37**(5): 531-537.
105. Yamawaki-Ogata A, Hashizume R, Satake M, Kaneko H, Mizutani S, Moritan T, Ueda Y, Narita Y. A doxycycline loaded, controlled-release, biodegradable fiber for the treatment of aortic aneurysms. *Biomaterials* 2010;**31**(36): 9554-9564.
106. Ailawadi G, Eliason JL, Upchurch GR, Jr. Current concepts in the pathogenesis of abdominal aortic aneurysm. *J Vasc Surg* 2003;**38**(3): 584-588.
107. Reeps C, Gee MW, Maier A, Pelisek J, Gurdan M, Wall W, Mariss J, Eckstein HH, Essler M. Glucose metabolism in the vessel wall correlates with mechanical instability and inflammatory changes in a patient with a growing aneurysm of the abdominal aorta. *Circulation Cardiovascular imaging* 2009;**2**(6): 507-509.
108. McMillan WD, Pearce WH. Increased plasma levels of metalloproteinase-9 are associated with abdominal aortic aneurysms. *Journal of vascular surgery* 1999;**29**(1): 122-127; discussion 127-129.
109. Mao D, Lee JK, VanVickle SJ, Thompson RW. Expression of collagenase-3 (MMP-13) in human abdominal aortic aneurysms and vascular smooth muscle cells in culture. *Biochemical and biophysical research communications* 1999;**261**(3): 904-910.
110. Abdul-Hussien H, Soekhoe RG, Weber E, von der Thusen JH, Kleemann R, Mulder A, van Bockel JH, Hanemaaijer R, Lindeman JH. Collagen degradation in the abdominal aneurysm: a conspiracy of matrix metalloproteinase and cysteine collagenases. *The American journal of pathology* 2007;**170**(3): 809-817.
111. Takagi H, Manabe H, Kawai N, Goto SN, Umemoto T. Circulating matrix metalloproteinase-9 concentrations and abdominal aortic aneurysm presence: a meta-analysis. *Interactive cardiovascular and thoracic surgery* 2009;**9**(3): 437-440.
112. Pyo R, Lee JK, Shipley JM, Curci JA, Mao D, Ziporin SJ, Ennis TL, Shapiro SD, Senior RM, Thompson RW. Targeted gene disruption of matrix metalloproteinase-9 (gelatinase B) suppresses development of experimental abdominal aortic aneurysms. *J Clin Invest* 2000;**105**(11): 1641-1649.
113. Wilson WR, Anderton M, Choke EC, Dawson J, Loftus IM, Thompson MM. Elevated plasma MMP1 and MMP9 are associated with abdominal aortic aneurysm

- rupture. *European journal of vascular and endovascular surgery : the official journal of the European Society for Vascular Surgery* 2008;**35**(5): 580-584.
114. Knox JB, Sukhova GK, Whittmore AD, Libby P. Evidence for altered balance between matrix metalloproteinases and their inhibitors in human aortic diseases. *Circulation* 1997;**95**(1): 205-212.
115. Allaire E, Forough R, Clowes M, Starcher B, Clowes AW. Local overexpression of TIMP-1 prevents aortic aneurysm degeneration and rupture in a rat model. *J Clin Invest* 1998;**102**(7): 1413-1420.
116. Wilton E, Bland M, Thompson M, Jahangiri M. Matrix metalloproteinase expression in the ascending aorta and aortic valve. *Interactive cardiovascular and thoracic surgery* 2008;**7**(1): 37-40.
117. Lesauskaite V, Sinkunaite G, Benetis R, Grabauskas V, Vaskelyte J, Smalinskiene A, Simonyte S, Jariene G, Tatarunas V, Klumbiene J, Petkeviciene J, Kinduris S, Giedraitis S, Sakalauskas J, Bolys R, Sirvinskas E, Lenkutis T, Pangonyte D. Matrix metalloproteinase-3 gene polymorphism and dilatative pathology of ascending thoracic aorta. *Medicina* 2008;**44**(5): 386-391.
118. Silence J, Lupu F, Collen D, Lijnen HR. Persistence of atherosclerotic plaque but reduced aneurysm formation in mice with stromelysin-1 (MMP-3) gene inactivation. *Arteriosclerosis, thrombosis, and vascular biology* 2001;**21**(9): 1440-1445.
119. Longo GM, Buda SJ, Fiotta N, Xiong W, Griener T, Shapiro S, Baxter BT. MMP-12 has a role in abdominal aortic aneurysms in mice. *Surgery* 2005;**137**(4): 457-462.
120. Luttun A, Lutgens E, Manderveld A, Maris K, Collen D, Carmeliet P, Moons L. Loss of matrix metalloproteinase-9 or matrix metalloproteinase-12 protects apolipoprotein E-deficient mice against atherosclerotic media destruction but differentially affects plaque growth. *Circulation* 2004;**109**(11): 1408-1414.
121. Busuttill RW, Abou-Zamzam AM, Machleder HI. Collagenase activity of the human aorta. A comparison of patients with and without abdominal aortic aneurysms. *Archives of surgery* 1980;**115**(11): 1373-1378.
122. Irizarry E, Newman KM, Gandhi RH, Nackman GB, Halpern V, Wishner S, Scholes JV, Tilson MD. Demonstration of interstitial collagenase in abdominal aortic aneurysm disease. *The Journal of surgical research* 1993;**54**(6): 571-574.
123. Li Y, Shao AZ, Jiang HT, Dong GH, Xu B, Yi J, Jing H. The prominent expression of plasma matrix metalloproteinase-8 in acute thoracic aortic dissection. *The Journal of surgical research* 2010;**163**(2): e99-104.
124. Cohen JR, Sarfati I, Ratner L, Tilson D. Alpha 1-antitrypsin phenotypes in patients with abdominal aortic aneurysms. *The Journal of surgical research* 1990;**49**(4): 319-321.
125. Schweitzer M, Mitmaker B, Obrand D, Sheiner N, Abraham C, Dostanic S, Meilleur M, Sugahara T, Chalifour LE. Atorvastatin modulates matrix metalloproteinase expression, activity, and signaling in abdominal aortic aneurysms. *Vascular and endovascular surgery* 2010;**44**(2): 116-122.
126. Dawson JA, Choke E, Loftus IM, Cockerill GW, Thompson MM. A randomised placebo-controlled double-blind trial to evaluate lipid-lowering pharmacotherapy on proteolysis and inflammation in abdominal aortic aneurysms. *European journal of vascular and endovascular surgery : the official journal of the European Society for Vascular Surgery* 2011;**41**(1): 28-35.
127. Shah PK. Inflammation, metalloproteinases, and increased proteolysis: an emerging pathophysiological paradigm in aortic aneurysm. *Circulation* 1997;**96**(7): 2115-2117.

128. Golledge AL, Walker P, Norman PE, Golledge J. A systematic review of studies examining inflammation associated cytokines in human abdominal aortic aneurysm samples. *Disease markers* 2009;**26**(4): 181-188.
129. Wills A, Thompson MM, Crowther M, Sayers RD, Bell PR. Pathogenesis of abdominal aortic aneurysms--cellular and biochemical mechanisms. *European journal of vascular and endovascular surgery : the official journal of the European Society for Vascular Surgery* 1996;**12**(4): 391-400.
130. Gertz SD, Kurgan A, Eisenberg D. Aneurysm of the rabbit common carotid artery induced by periarterial application of calcium chloride in vivo. *J Clin Invest* 1988;**81**(3): 649-656.
131. Xiong W, Zhao Y, Prall A, Greiner TC, Baxter BT. Key roles of CD4+ T cells and IFN-gamma in the development of abdominal aortic aneurysms in a murine model. *J Immunol* 2004;**172**(4): 2607-2612.
132. Anidjar S, Dobrin PB, Chejfec G, Michel JB. Experimental study of determinants of aneurysmal expansion of the abdominal aorta. *Ann Vasc Surg* 1994;**8**(2): 127-136.
133. Prall AK, Longo GM, Mayhan WG, Waltke EA, Fleckten B, Thompson RW, Baxter BT. Doxycycline in patients with abdominal aortic aneurysms and in mice: comparison of serum levels and effect on aneurysm growth in mice. *Journal of vascular surgery* 2002;**35**(5): 923-929.
134. Choke E, Cockerill GW, Dawson J, Wilson RW, Jones A, Loftus IM, Thompson MM. Increased angiogenesis at the site of abdominal aortic aneurysm rupture. *Annals of the New York Academy of Sciences* 2006;**1085**: 315-319.
135. Abdul-Hussien H, Hanemaaijer R, Kleemann R, Verhaaren BF, van Bockel JH, Lindeman JH. The pathophysiology of abdominal aortic aneurysm growth: corresponding and discordant inflammatory and proteolytic processes in abdominal aortic and popliteal artery aneurysms. *Journal of vascular surgery* 2010;**51**(6): 1479-1487.
136. Schonbeck U, Sukhova GK, Gerdes N, Libby P. T(H)2 predominant immune responses prevail in human abdominal aortic aneurysm. *The American journal of pathology* 2002;**161**(2): 499-506.
137. Shimizu K, Shichiri M, Libby P, Lee RT, Mitchell RN. Th2-predominant inflammation and blockade of IFN-gamma signaling induce aneurysms in allografted aortas. *J Clin Invest* 2004;**114**(2): 300-308.
138. Sho E, Sho M, Hoshina K, Kimura H, Nakahashi TK, Dalman RL. Hemodynamic forces regulate mural macrophage infiltration in experimental aortic aneurysms. *Experimental and molecular pathology* 2004;**76**(2): 108-116.
139. Xiong W, Knispel R, MacTaggart J, Greiner TC, Weiss SJ, Baxter BT. Membrane-type 1 matrix metalloproteinase regulates macrophage-dependent elastolytic activity and aneurysm formation in vivo. *The Journal of biological chemistry* 2009;**284**(3): 1765-1771.
140. Werb Z, Bainton DF, Jones PA. Degradation of connective tissue matrices by macrophages. III. Morphological and biochemical studies on extracellular, pericellular, and intracellular events in matrix proteolysis by macrophages in culture. *The Journal of experimental medicine* 1980;**152**(6): 1537-1553.
141. Hanemaaijer R, Visser H, Koolwijk P, Sorsa T, Salo T, Golub LM, Van Hinsbergh VWM. Inhibition of MMP Synthesis by Doxycycline and Chemically Modified Tetracyclines (CMTs) in Human Endothelial Cells. *Advances in Dental Research* 1998;**12**(1): 114-118.

142. Hellenthal FA, Buurman WA, Wodzig WK, Schurink GW. Biomarkers of abdominal aortic aneurysm progression. Part 2: inflammation. *Nature reviews Cardiology* 2009;**6**(8): 543-552.
143. Thompson RW, Parks WC. Role of matrix metalloproteinases in abdominal aortic aneurysms. *Annals of the New York Academy of Sciences* 1996;**800**: 157-174.
144. Lindholt JS, Fasting H, Henneberg EW, Ostergaard L. A review of Chlamydia pneumoniae and atherosclerosis. *European journal of vascular and endovascular surgery : the official journal of the European Society for Vascular Surgery* 1999;**17**(4): 283-289.
145. Cardy CMC, D. Large vessel vasculitides. *Elsevier Science* 2010;**38**(2): 97-100.
146. Caspary L. Vasculitides of large vessels. *VASA Zeitschrift fur Gefasskrankheiten* 2011;**40**(2): 89-98.
147. Vaglio A, Pipitone N, Salvarani C. Chronic periaortitis: a large-vessel vasculitis? *Current opinion in rheumatology* 2011;**23**(1): 1-6.
148. Kasashima S, Zen Y. IgG4-related inflammatory abdominal aortic aneurysm. *Current opinion in rheumatology* 2011;**23**(1): 18-23.
149. Walker DI, Bloor K, Williams G, Gillie I. Inflammatory aneurysms of the abdominal aorta. *The British journal of surgery* 1972;**59**(8): 609-614.
150. Goldstone J, Malone JM, Moore WS. Inflammatory aneurysms of the abdominal aorta. *Surgery* 1978;**83**(4): 425-430.
151. Paravastu SC, Murray D, Ghosh J, Serracino-Inglott F, Smyth JV, Walker MG. Inflammatory abdominal aortic aneurysms (IAAA): past and present. *Vascular and endovascular surgery* 2009;**43**(4): 360-363.
152. Sterpetti AV, Hunter WJ, Feldhaus RJ, Chasan P, McNamara M, Cisternino S, Schultz RD. Inflammatory aneurysms of the abdominal aorta: incidence, pathologic, and etiologic considerations. *Journal of vascular surgery* 1989;**9**(5): 643-649; discussion 649-650.
153. Koch AE, Haines GK, Rizzo RJ, Radosevich JA, Pope RM, Robinson PG, Pearce WH. Human abdominal aortic aneurysms. Immunophenotypic analysis suggesting an immune-mediated response. *The American journal of pathology* 1990;**137**(5): 1199-1213.
154. Leu HJ. Inflammatory abdominal aortic aneurysms: a disease entity? Histological analysis of 60 cases of inflammatory aortic aneurysms of unknown aetiology. *Virchows Archiv A, Pathological anatomy and histopathology* 1990;**417**(5): 427-433.
155. Rose AG, Dent DM. Inflammatory variant of abdominal atherosclerotic aneurysm. *Arch Pathol Lab Med* 1981;**105**(8): 409-413.
156. Nyberg A, Skagius E, Englund E, Nilsson I, Ljungh A, Henriksson AE. Abdominal aortic aneurysm and the impact of infectious burden. *European journal of vascular and endovascular surgery : the official journal of the European Society for Vascular Surgery* 2008;**36**(3): 292-296.
157. Parums DV, Dunn DC, Dixon AK, Mitchinson MJ. Characterization of inflammatory cells in a patient with chronic periaortitis. *The American journal of cardiovascular pathology* 1990;**3**(2): 121-129.
158. Sodeck G, Domanovits H, Khanakah G, Schillinger M, Thalmann M, Bayegan K, Schoder M, Grabenwoeger M, Hoelzenbein T, Boehmig G, Laggner AN, Stanek G. The role of Chlamydia pneumoniae in human aortic disease-a hypothesis revisited. *European journal of vascular and endovascular surgery : the official journal of the European Society for Vascular Surgery* 2004;**28**(5): 547-552.

159. Vaglio A, Corradi D, Manenti L, Ferretti S, Garini G, Buzio C. Evidence of autoimmunity in chronic periaortitis: a prospective study. *The American journal of medicine* 2003;**114**(6): 454-462.
160. Jagadesham VP, Scott DJ, Carding SR. Abdominal aortic aneurysms: an autoimmune disease? *Trends in molecular medicine* 2008;**14**(12): 522-529.
161. Tang T, Boyle JR, Dixon AK, Varty K. Inflammatory abdominal aortic aneurysms. *European journal of vascular and endovascular surgery : the official journal of the European Society for Vascular Surgery* 2005;**29**(4): 353-362.
162. Hill J, Charlesworth D. Inflammatory abdominal aortic aneurysms: a report of thirty-seven cases. *Ann Vasc Surg* 1988;**2**(4): 352-357.
163. Crawford JL, Stowe CL, Safi HJ, Hallman CH, Crawford ES. Inflammatory aneurysms of the aorta. *Journal of vascular surgery* 1985;**2**(1): 113-124.
164. Boontje AH, van den Dungen JJ, Blanksma C. Inflammatory abdominal aortic aneurysms. *The Journal of cardiovascular surgery* 1990;**31**(5): 611-616.
165. Fiorani P, Bondanini S, Faraglia V, Spartera C, Speziale F, Taurino M, Pistolesse GR. Clinical and therapeutical evaluation of inflammatory aneurysms of the abdominal aorta. *International angiology : a journal of the International Union of Angiology* 1986;**5**(1): 49-53.
166. Brophy CM, Reilly JM, Smith GJ, Tilson MD. The role of inflammation in nonspecific abdominal aortic aneurysm disease. *Ann Vasc Surg* 1991;**5**(3): 229-233.
167. Newman KM, Jean-Claude J, Li H, Ramey WG, Tilson MD. Cytokines that activate proteolysis are increased in abdominal aortic aneurysms. *Circulation* 1994;**90**(5 Pt 2): II224-227.
168. Wilson WR, Anderton M, Schwalbe EC, Jones JL, Furness PN, Bell PR, Thompson MM. Matrix metalloproteinase-8 and -9 are increased at the site of abdominal aortic aneurysm rupture. *Circulation* 2006;**113**(3): 438-445.
169. Choke E, Thompson MM, Dawson J, Wilson WR, Sayed S, Loftus IM, Cockerill GW. Abdominal aortic aneurysm rupture is associated with increased medial neovascularization and overexpression of proangiogenic cytokines. *Arterioscler Thromb Vasc Biol* 2006;**26**(9): 2077-2082.
170. Wilson WR, Wills J, Furness PN, Loftus IM, Thompson MM. Abdominal aortic aneurysm rupture is not associated with an up-regulation of inflammation within the aneurysm wall. *European journal of vascular and endovascular surgery : the official journal of the European Society for Vascular Surgery* 2010;**40**(2): 191-195.
171. Miller FJ, Jr., Sharp WJ, Fang X, Oberley LW, Oberley TD, Weintraub NL. Oxidative stress in human abdominal aortic aneurysms: a potential mediator of aneurysmal remodeling. *Arteriosclerosis, thrombosis, and vascular biology* 2002;**22**(4): 560-565.
172. Guo DC, Papke CL, He R, Milewicz DM. Pathogenesis of thoracic and abdominal aortic aneurysms. *Annals of the New York Academy of Sciences* 2006;**1085**: 339-352.
173. Virmani R, Avolio AP, Mergner WJ, Robinowitz M, Herderick EE, Cornhill JF, Guo SY, Liu TH, Ou DY, O'Rourke M. Effect of aging on aortic morphology in populations with high and low prevalence of hypertension and atherosclerosis. Comparison between occidental and Chinese communities. *The American journal of pathology* 1991;**139**(5): 1119-1129.
174. Vardulaki KA, Walker NM, Day NE, Duffy SW, Ashton HA, Scott RA. Quantifying the risks of hypertension, age, sex and smoking in patients with abdominal aortic aneurysm. *The British journal of surgery* 2000;**87**(2): 195-200.

175. Wu XF, Zhang J, Paskauskas S, Xin SJ, Duan ZQ. The role of estrogen in the formation of experimental abdominal aortic aneurysm. *American journal of surgery* 2009;**197**(1): 49-54.
176. Brown LC, Powell JT. Risk factors for aneurysm rupture in patients kept under ultrasound surveillance. UK Small Aneurysm Trial Participants. *Annals of surgery* 1999;**230**(3): 289-296; discussion 296-287.
177. McPhee JT, Hill JS, Eslami MH. The impact of gender on presentation, therapy, and mortality of abdominal aortic aneurysm in the United States, 2001-2004. *Journal of vascular surgery* 2007;**45**(5): 891-899.
178. Kanematsu Y, Kanematsu M, Kurihara C, Tsou TL, Nuki Y, Liang EI, Makino H, Hashimoto T. Pharmacologically induced thoracic and abdominal aortic aneurysms in mice. *Hypertension* 2010;**55**(5): 1267-1274.
179. Lederle FA, Johnson GR, Wilson SE, Chute EP, Littooy FN, Bandyk D, Krupski WC, Barone GW, Acher CW, Ballard DJ. Prevalence and associations of abdominal aortic aneurysm detected through screening. Aneurysm Detection and Management (ADAM) Veterans Affairs Cooperative Study Group. *Annals of internal medicine* 1997;**126**(6): 441-449.
180. Szilagyi DE, Elliott JP, Smith RF. Clinical fate of the patient with asymptomatic abdominal aortic aneurysm and unfit for surgical treatment. *Archives of surgery* 1972;**104**(4): 600-606.
181. Brady AR, Thompson SG, Fowkes FG, Greenhalgh RM, Powell JT, Participants UKSAT. Abdominal aortic aneurysm expansion: risk factors and time intervals for surveillance. *Circulation* 2004;**110**(1): 16-21.
182. Lederle FA, Johnson GR, Wilson SE, Chute EP, Hye RJ, Makaroun MS, Barone GW, Bandyk D, Moneta GL, Makhoul RG. The aneurysm detection and management study screening program: validation cohort and final results. Aneurysm Detection and Management Veterans Affairs Cooperative Study Investigators. *Arch Intern Med* 2000;**160**(10): 1425-1430.
183. Stolle K, Berges A, Lietz M, Lebrun S, Wallerath T. Cigarette smoke enhances abdominal aortic aneurysm formation in angiotensin II-treated apolipoprotein E-deficient mice. *Toxicology letters* 2010;**199**(3): 403-409.
184. Meszaros I, Morocz J, Szlavi J, Schmidt J, Tornoci L, Nagy L, Szep L. Epidemiology and clinicopathology of aortic dissection. *Chest* 2000;**117**(5): 1271-1278.
185. Isselbacher EM. Thoracic and abdominal aortic aneurysms. *Circulation* 2005;**111**(6): 816-828.
186. Tilson MD. Atherosclerosis and aneurysm disease. *J Vasc Surg* 1990;**12**(3): 371-372.
187. Golledge J, Norman PE. Atherosclerosis and abdominal aortic aneurysm: cause, response, or common risk factors? *Arteriosclerosis, thrombosis, and vascular biology* 2010;**30**(6): 1075-1077.
188. Johnsen SH, Forsdahl SH, Singh K, Jacobsen BK. Atherosclerosis in abdominal aortic aneurysms: a causal event or a process running in parallel? The Tromso study. *Arteriosclerosis, thrombosis, and vascular biology* 2010;**30**(6): 1263-1268.
189. Harter LP, Gross BH, Callen PW, Barth RA. Ultrasonic evaluation of abdominal aortic thrombus. *Journal of ultrasound in medicine : official journal of the American Institute of Ultrasound in Medicine* 1982;**1**(8): 315-318.
190. Vorp DA, Lee PC, Wang DH, Makaroun MS, Nemoto EM, Ogawa S, Webster MW. Association of intraluminal thrombus in abdominal aortic aneurysm with local hypoxia and wall weakening. *Journal of vascular surgery* 2001;**34**(2): 291-299.

191. Kazi M, Thyberg J, Religa P, Roy J, Eriksson P, Hedin U, Swedenborg J. Influence of intraluminal thrombus on structural and cellular composition of abdominal aortic aneurysm wall. *Journal of vascular surgery* 2003;**38**(6): 1283-1292.
192. Carrell TW, Burnand KG, Booth NA, Humphries J, Smith A. Intraluminal thrombus enhances proteolysis in abdominal aortic aneurysms. *Vascular* 2006;**14**(1): 9-16.
193. Folkesson M, Kazi M, Zhu C, Silveira A, Hemdahl AL, Hamsten A, Hedin U, Swedenborg J, Eriksson P. Presence of NGAL/MMP-9 complexes in human abdominal aortic aneurysms. *Thrombosis and haemostasis* 2007;**98**(2): 427-433.
194. Wiernicki I, Stachowska E, Safranow K, Cnotliwy M, Rybicka M, Kaczmarczyk M, Gutowski P. Enhanced matrix-degrading proteolytic activity within the thin thrombus-covered wall of human abdominal aortic aneurysms. *Atherosclerosis* 2010;**212**(1): 161-165.
195. Coutard M, Touat Z, Houard X, Leclercq A, Michel JB. Thrombus versus wall biological activities in experimental aortic aneurysms. *Journal of vascular research* 2010;**47**(4): 355-366.
196. Xu XY, Borghi A, Nchimi A, Leung J, Gomez P, Cheng Z, Defraigne JO, Sakalihasan N. High levels of 18F-FDG uptake in aortic aneurysm wall are associated with high wall stress. *Eur J Vasc Endovasc Surg* 2010;**39**(3): 295-301.
197. Roy J, Labruto F, Beckman MO, Danielson J, Johansson G, Swedenborg J. Bleeding into the intraluminal thrombus in abdominal aortic aneurysms is associated with rupture. *Journal of vascular surgery* 2008;**48**(5): 1108-1113.
198. Polzer S, Gasser TC, Swedenborg J, Bursa J. The impact of intraluminal thrombus failure on the mechanical stress in the wall of abdominal aortic aneurysms. *European journal of vascular and endovascular surgery : the official journal of the European Society for Vascular Surgery* 2011;**41**(4): 467-473.
199. Parr A, McCann M, Bradshaw B, Shahzad A, Buttner P, Golledge J. Thrombus volume is associated with cardiovascular events and aneurysm growth in patients who have abdominal aortic aneurysms. *Journal of vascular surgery* 2011;**53**(1): 28-35.
200. Speelman L, Hellenthal FA, Pulinx B, Bosboom EM, Breeuwer M, van Sambeek MR, van de Vosse FN, Jacobs MJ, Wodzig WK, Schurink GW. The influence of wall stress on AAA growth and biomarkers. *European journal of vascular and endovascular surgery : the official journal of the European Society for Vascular Surgery* 2010;**39**(4): 410-416.
201. Speelman L, Schurink GW, Bosboom EM, Buth J, Breeuwer M, van de Vosse FN, Jacobs MH. The mechanical role of thrombus on the growth rate of an abdominal aortic aneurysm. *Journal of vascular surgery* 2010;**51**(1): 19-26.
202. Georgakarakos E, Ioannou CV, Volanis S, Papaharilaou Y, Ekaterinaris J, Katsamouris AN. The influence of intraluminal thrombus on abdominal aortic aneurysm wall stress. *International angiology : a journal of the International Union of Angiology* 2009;**28**(4): 325-333.
203. Sanz J, Fayad ZA. Imaging of atherosclerotic cardiovascular disease. *Nature* 2008;**451**(7181): 953-957.
204. Sadeghi MM, Glover DK, Lanza GM, Fayad ZA, Johnson LL. Imaging atherosclerosis and vulnerable plaque. *Journal of nuclear medicine : official publication, Society of Nuclear Medicine* 2010;**51 Suppl 1**: 51S-65S.
205. Hashimoto T, Meng H, Young WL. Intracranial aneurysms: links among inflammation, hemodynamics and vascular remodeling. *Neurological research* 2006;**28**(4): 372-380.

206. Herschman HR. Molecular imaging: looking at problems, seeing solutions. *Science* 2003;**302**(5645): 605-608.
207. Eraso LH, Reilly MP, Sehgal C, Mohler ER, 3rd. Emerging diagnostic and therapeutic molecular imaging applications in vascular disease. *Vascular medicine* 2011;**16**(2): 145-156.
208. Newby AC. Dual role of matrix metalloproteinases (matrixins) in intimal thickening and atherosclerotic plaque rupture. *Physiological reviews* 2005;**85**(1): 1-31.
209. Ogawa M, Ishino S, Mukai T, Asano D, Teramoto N, Watabe H, Kudomi N, Shiomi M, Magata Y, Iida H, Saji H. (18)F-FDG accumulation in atherosclerotic plaques: immunohistochemical and PET imaging study. *J Nucl Med* 2004;**45**(7): 1245-1250.
210. Rudd JH, Warburton EA, Fryer TD, Jones HA, Clark JC, Antoun N, Johnstrom P, Davenport AP, Kirkpatrick PJ, Arch BN, Pickard JD, Weissberg PL. Imaging atherosclerotic plaque inflammation with [18F]-fluorodeoxyglucose positron emission tomography. *Circulation* 2002;**105**(23): 2708-2711.
211. Zhang Z, Machac J, Helft G, Worthley SG, Tang C, Zaman AG, Rodriguez OJ, Buchsbaum MS, Fuster V, Badimon JJ. Non-invasive imaging of atherosclerotic plaque macrophage in a rabbit model with F-18 FDG PET: a histopathological correlation. *BMC Nucl Med* 2006;**6**: 3.
212. Yun M, Jang S, Cucchiara A, Newberg AB, Alavi A. 18F FDG uptake in the large arteries: a correlation study with the atherogenic risk factors. *Seminars in nuclear medicine* 2002;**32**(1): 70-76.
213. Yun M, Yeh D, Araujo LI, Jang S, Newberg A, Alavi A. F-18 FDG uptake in the large arteries: a new observation. *Clin Nucl Med* 2001;**26**(4): 314-319.
214. Ben-Haim S, Kupzov E, Tamir A, Israel O. Evaluation of 18F-FDG uptake and arterial wall calcifications using 18F-FDG PET/CT. *J Nucl Med* 2004;**45**(11): 1816-1821.
215. Tatsumi M, Cohade C, Nakamoto Y, Wahl RL. Fluorodeoxyglucose uptake in the aortic wall at PET/CT: possible finding for active atherosclerosis. *Radiology* 2003;**229**(3): 831-837.
216. Wu YW, Kao HL, Chen MF, Lee BC, Tseng WY, Jeng JS, Tzen KY, Yen RF, Huang PJ, Yang WS. Characterization of plaques using 18F-FDG PET/CT in patients with carotid atherosclerosis and correlation with matrix metalloproteinase-1. *J Nucl Med* 2007;**48**(2): 227-233.
217. Tahara N, Kai H, Ishibashi M, Nakaura H, Kaida H, Baba K, Hayabuchi N, Imaizumi T. Simvastatin attenuates plaque inflammation: evaluation by fluorodeoxyglucose positron emission tomography. *J Am Coll Cardiol* 2006;**48**(9): 1825-1831.
218. Lee SJ, On YK, Lee EJ, Choi JY, Kim BT, Lee KH. Reversal of vascular 18F-FDG uptake with plasma high-density lipoprotein elevation by atherogenic risk reduction. *J Nucl Med* 2008;**49**(8): 1277-1282.
219. Tawakol A, Migrino RQ, Bashian GG, Bedri S, Vermynen D, Cury RC, Yates D, LaMuraglia GM, Furie K, Houser S, Gewirtz H, Muller JE, Brady TJ, Fischman AJ. In vivo 18F-fluorodeoxyglucose positron emission tomography imaging provides a noninvasive measure of carotid plaque inflammation in patients. *Journal of the American College of Cardiology* 2006;**48**(9): 1818-1824.
220. Menezes LJ, Kotze CW, Agu O, Richards T, Brookes J, Goh VJ, Rodriguez-Justo M, Endozo R, Harvey R, Yusuf SW, Ell PJ, Groves AM. Investigating vulnerable atheroma using combined (18)F-FDG PET/CT angiography of carotid plaque with immunohistochemical validation. *J Nucl Med* 2011;**52**(11): 1698-1703.

221. Courtois A, Nusgens BV, Hustinx R, Namur G, Gomez P, Somja J, Defraigne JO, Delvenne P, Michel JB, Colige AC, Sakalihan N. 18F-FDG uptake assessed by PET/CT in abdominal aortic aneurysms is associated with cellular and molecular alterations prefacing wall deterioration and rupture. *Journal of nuclear medicine : official publication, Society of Nuclear Medicine* 2013;**54**(10): 1740-1747.
222. Reeps C, Essler M, Pelisek J, Seidl S, Eckstein HH, Krause BJ. Increased 18F-fluorodeoxyglucose uptake in abdominal aortic aneurysms in positron emission/computed tomography is associated with inflammation, aortic wall instability, and acute symptoms. *Journal of vascular surgery* 2008;**48**(2): 417-423; discussion 424.
223. Rudd JH, Myers KS, Bansilal S, Machac J, Pinto CA, Tong C, Rafique A, Hargeaves R, Farkouh M, Fuster V, Fayad ZA. Atherosclerosis inflammation imaging with 18F-FDG PET: carotid, iliac, and femoral uptake reproducibility, quantification methods, and recommendations. *Journal of nuclear medicine : official publication, Society of Nuclear Medicine* 2008;**49**(6): 871-878.
224. Mizoguchi M, Tahara N, Tahara A, Nitta Y, Kodama N, Oba T, Mawatari K, Yasukawa H, Kaida H, Ishibashi M, Hayabuchi N, Harada H, Ikeda H, Yamagishi S, Imaizumi T. Pioglitazone attenuates atherosclerotic plaque inflammation in patients with impaired glucose tolerance or diabetes a prospective, randomized, comparator-controlled study using serial FDG PET/CT imaging study of carotid artery and ascending aorta. *JACC Cardiovascular imaging* 2011;**4**(10): 1110-1118.
225. Fayad ZA, Mani V, Woodward M, Kallend D, Abt M, Burgess T, Fuster V, Ballantyne CM, Stein EA, Tardif JC, Rudd JH, Farkouh ME, Tawakol A, dal PI. Safety and efficacy of dalcetrapib on atherosclerotic disease using novel non-invasive multimodality imaging (dal-PLAQUE): a randomised clinical trial. *Lancet* 2011;**378**(9802): 1547-1559.
226. Folco EJ, Sheikine Y, Rocha VZ, Christen T, Shvartz E, Sukhova GK, Di Carli MF, Libby P. Hypoxia but not inflammation augments glucose uptake in human macrophages: Implications for imaging atherosclerosis with 18fluorine-labeled 2-deoxy-D-glucose positron emission tomography. *J Am Coll Cardiol* 2011;**58**(6): 603-614.
227. Perrone-Filardi P, Dellegrottaglie S, Rudd JH, Costanzo P, Marciano C, Vassallo E, Marsico F, Ruggiero D, Petretta MP, Chiariello M, Cuocolo A. Molecular imaging of atherosclerosis in translational medicine. *Eur J Nucl Med Mol Imaging* 2011;**38**(5): 969-975.
228. Nahrendorf M, Keliher E, Marinelli B, Leuschner F, Robbins CS, Gerszten RE, Pittet MJ, Swirski FK, Weissleder R. Detection of macrophages in aortic aneurysms by nanoparticle positron emission tomography-computed tomography. *Arteriosclerosis, thrombosis, and vascular biology* 2011;**31**(4): 750-757.
229. Shim CY, Lindner JR. Cardiovascular Molecular Imaging with Contrast Ultrasound: Principles and Applications. *Korean circulation journal* 2014;**44**(1): 1-9.
230. Lindner JR. Microbubbles in medical imaging: current applications and future directions. *Nature reviews Drug discovery* 2004;**3**(6): 527-532.
231. Lindner JR, Song J, Jayaweera AR, Sklenar J, Kaul S. Microvascular rheology of Definity microbubbles after intra-arterial and intravenous administration. *Journal of the American Society of Echocardiography : official publication of the American Society of Echocardiography* 2002;**15**(5): 396-403.
232. Porter TR, Xie F, Silver M, Kricsfeld D, O'Leary E. Real-time perfusion imaging with low mechanical index pulse inversion Doppler imaging. *J Am Coll Cardiol* 2001;**37**(3): 748-753.

233. Fleiner M, Kummer M, Mirlacher M, Sauter G, Cathomas G, Krapf R, Biedermann BC. Arterial neovascularization and inflammation in vulnerable patients: early and late signs of symptomatic atherosclerosis. *Circulation* 2004;**110**(18): 2843-2850.
234. Staub D, Schinkel AF, Coll B, Coli S, van der Steen AF, Reed JD, Krueger C, Thomenius KE, Adam D, Sijbrands EJ, ten Cate FJ, Feinstein SB. Contrast-enhanced ultrasound imaging of the vasa vasorum: from early atherosclerosis to the identification of unstable plaques. *JACC Cardiovascular imaging* 2010;**3**(7): 761-771.
235. Vela D, Buja LM, Madjid M, Burke A, Naghavi M, Willerson JT, Casscells SW, Litovsky S. The role of periadventitial fat in atherosclerosis. *Archives of pathology & laboratory medicine* 2007;**131**(3): 481-487.
236. Lindner JR. Contrast ultrasound molecular imaging of inflammation in cardiovascular disease. *Cardiovascular research* 2009;**84**(2): 182-189.
237. Tang TY, Muller KH, Graves MJ, Li ZY, Walsh SR, Young V, Sadat U, Howarth SP, Gillard JH. Iron oxide particles for atheroma imaging. *Arterioscler Thromb Vasc Biol* 2009;**29**(7): 1001-1008.
238. Vucic E, Sanders HM, Arena F, Terreno E, Aime S, Nicolay K, Leupold E, Dathe M, Sommerdijk NA, Fayad ZA, Mulder WJ. Well-defined, multifunctional nanostructures of a paramagnetic lipid and a lipopeptide for macrophage imaging. *J Am Chem Soc* 2009;**131**(2): 406-407.
239. Jung CW, Jacobs P. Physical and chemical properties of superparamagnetic iron oxide MR contrast agents: ferumoxides, ferumoxtran, ferumoxsil. *Magnetic resonance imaging* 1995;**13**(5): 661-674.
240. Ruehm SG, Corot C, Vogt P, Kolb S, Debatin JF. Magnetic resonance imaging of atherosclerotic plaque with ultrasmall superparamagnetic particles of iron oxide in hyperlipidemic rabbits. *Circulation* 2001;**103**(3): 415-422.
241. Schmitz SA, Coupland SE, Gust R, Winterhalter S, Wagner S, Kresse M, Semmler W, Wolf KJ. Superparamagnetic iron oxide-enhanced MRI of atherosclerotic plaques in Watanabe hereditary hyperlipidemic rabbits. *Invest Radiol* 2000;**35**(8): 460-471.
242. Kooi ME, Cappendijk VC, Cleutjens KB, Kessels AG, Kitslaar PJ, Borgers M, Frederik PM, Daemen MJ, van Engelsehoven JM. Accumulation of ultrasmall superparamagnetic particles of iron oxide in human atherosclerotic plaques can be detected by in vivo magnetic resonance imaging. *Circulation* 2003;**107**(19): 2453-2458.
243. Trivedi RA, Mallawarachi C, JM UK-I, Graves MJ, Horsley J, Goddard MJ, Brown A, Wang L, Kirkpatrick PJ, Brown J, Gillard JH. Identifying inflamed carotid plaques using in vivo USPIO-enhanced MR imaging to label plaque macrophages. *Arterioscler Thromb Vasc Biol* 2006;**26**(7): 1601-1606.
244. Sadat U, Taviani V, Patterson AJ, Young VE, Graves MJ, Teng Z, Tang TY, Gillard JH. Ultrasmall superparamagnetic iron oxide-enhanced magnetic resonance imaging of abdominal aortic aneurysms--a feasibility study. *European journal of vascular and endovascular surgery : the official journal of the European Society for Vascular Surgery* 2011;**41**(2): 167-174.
245. Richards JM, Semple SI, MacGillivray TJ, Gray C, Langrish JP, Williams M, Dweck M, Wallace W, McKillop G, Chalmers RT, Garden OJ, Newby DE. Abdominal aortic aneurysm growth predicted by uptake of ultrasmall superparamagnetic particles of iron oxide: a pilot study. *Circulation Cardiovascular imaging* 2011;**4**(3): 274-281.
246. Osei-Hwedie DO, Amar M, Sviridov D, Remaley AT. Apolipoprotein mimetic peptides: Mechanisms of action as anti-atherogenic agents. *Pharmacology & therapeutics* 2011;**130**(1): 83-91.

247. Briley-Saebo KC, Shaw PX, Mulder WJ, Choi SH, Vucic E, Aguinaldo JG, Witztum JL, Fuster V, Tsimikas S, Fayad ZA. Targeted molecular probes for imaging atherosclerotic lesions with magnetic resonance using antibodies that recognize oxidation-specific epitopes. *Circulation* 2008;**117**(25): 3206-3215.
248. Flacke S, Fischer S, Scott MJ, Fuhrhop RJ, Allen JS, McLean M, Winter P, Sicard GA, Gaffney PJ, Wickline SA, Lanza GM. Novel MRI contrast agent for molecular imaging of fibrin: implications for detecting vulnerable plaques. *Circulation* 2001;**104**(11): 1280-1285.
249. Yu X, Song SK, Chen J, Scott MJ, Fuhrhop RJ, Hall CS, Gaffney PJ, Wickline SA, Lanza GM. High-resolution MRI characterization of human thrombus using a novel fibrin-targeted paramagnetic nanoparticle contrast agent. *Magn Reson Med* 2000;**44**(6): 867-872.
250. Caruthers SDS, A.; Pan, D.; Scott, M.J.; Gaffney, P.J.; Wickline, S.A.; Lanza, G.M. A novel targeted iron oxide nanocolloid agent for rapid detection of fibrin clots via T1 and T2 weighted MRI. *Journal of Cardiovascular Magnetic Resonance* 2008;**10**(1): A384.
251. Anderson NG, Butler AP. Clinical applications of spectral molecular imaging: potential and challenges. *Contrast media & molecular imaging* 2014;**9**(1): 3-12.
252. Nutt R. 1999 ICP Distinguished Scientist Award. The history of positron emission tomography. *Molecular imaging and biology : MIB : the official publication of the Academy of Molecular Imaging* 2002;**4**(1): 11-26.
253. Sweet WH. The uses of nuclear disintegration in the diagnosis and treatment of brain tumor. *The New England journal of medicine* 1951;**245**(23): 875-878.
254. Nutt R. For: Is LSO the future of PET? *Eur J Nucl Med Mol Imaging* 2002;**29**(11): 1523-1525.
255. Rennen HJ, Boerman OC, Oyen WJ, Corstens FH. Imaging infection/inflammation in the new millennium. *Eur J Nucl Med* 2001;**28**(2): 241-252.
256. Palestro CJ. In vivo leukocyte labeling: the quest continues. *J Nucl Med* 2007;**48**(3): 332-334.
257. van Eerd JE, Broekema M, Harris TD, Edwards DS, Oyen WJ, Corstens FH, Boerman OC. Imaging of infection and inflammation with an improved 99mTc-labeled LTB4 antagonist. *J Nucl Med* 2005;**46**(9): 1546-1551.
258. Goldsmith SJ, Vallabhajosula S. Clinically proven radiopharmaceuticals for infection imaging: mechanisms and applications. *Seminars in nuclear medicine* 2009;**39**(1): 2-10.
259. Zhuang H, Duarte PS, Pourdehand M, Shnier D, Alavi A. Exclusion of chronic osteomyelitis with F-18 fluorodeoxyglucose positron emission tomographic imaging. *Clin Nucl Med* 2000;**25**(4): 281-284.
260. Aziz K, Berger K, Claycombe K, Huang R, Patel R, Abela GS. Noninvasive detection and localization of vulnerable plaque and arterial thrombosis with computed tomography angiography/positron emission tomography. *Circulation* 2008;**117**(16): 2061-2070.
261. Calcagno C, Cornily JC, Hyafil F, Rudd JH, Briley-Saebo KC, Mani V, Goldschlager G, Machac J, Fuster V, Fayad ZA. Detection of neovessels in atherosclerotic plaques of rabbits using dynamic contrast enhanced MRI and 18F-FDG PET. *Arterioscler Thromb Vasc Biol* 2008;**28**(7): 1311-1317.
262. Wright EM, Hirayama BA, Loo DF. Active sugar transport in health and disease. *Journal of internal medicine* 2007;**261**(1): 32-43.
263. Joshi F, Rosenbaum D, Bordes S, Rudd JH. Vascular imaging with positron emission tomography. *Journal of internal medicine* 2011;**270**(2): 99-109.

264. Reivich M, Alavi A, Wolf A, Fowler J, Russell J, Arnett C, MacGregor RR, Shiue CY, Atkins H, Anand A, et al. Glucose metabolic rate kinetic model parameter determination in humans: the lumped constants and rate constants for [18F]fluorodeoxyglucose and [11C]deoxyglucose. *J Cereb Blood Flow Metab* 1985;**5**(2): 179-192.
265. Pedersen SF, Graebe M, Fisker Hag AM, Hojgaard L, Sillesen H, Kjaer A. Gene expression and 18FDG uptake in atherosclerotic carotid plaques. *Nucl Med Commun* 2010;**31**(5): 423-429.
266. Leppanen O, Bjornheden T, Evaldsson M, Boren J, Wiklund O, Levin M. ATP depletion in macrophages in the core of advanced rabbit atherosclerotic plaques in vivo. *Atherosclerosis* 2006;**188**(2): 323-330.
267. Deichen JT, Prante O, Gack M, Schmiedehausen K, Kuwert T. Uptake of [18F]fluorodeoxyglucose in human monocyte-macrophages in vitro. *Eur J Nucl Med Mol Imaging* 2003;**30**(2): 267-273.
268. Mamede M, Higashi T, Kitaichi M, Ishizu K, Ishimori T, Nakamoto Y, Yanagihara K, Li M, Tanaka F, Wada H, Manabe T, Saga T. [18F]FDG uptake and PCNA, Glut-1, and Hexokinase-II expressions in cancers and inflammatory lesions of the lung. *Neoplasia* 2005;**7**(4): 369-379.
269. Newsholme P, Curi R, Gordon S, Newsholme EA. Metabolism of glucose, glutamine, long-chain fatty acids and ketone bodies by murine macrophages. *Biochem J* 1986;**239**(1): 121-125.
270. Zhao S, Kuge Y, Tsukamoto E, Mochizuki T, Kato T, Hikosaka K, Nakada K, Hosokawa M, Kohanawa M, Tamaki N. Fluorodeoxyglucose uptake and glucose transporter expression in experimental inflammatory lesions and malignant tumours: effects of insulin and glucose loading. *Nucl Med Commun* 2002;**23**(6): 545-550.
271. Zhuang HM, Cortes-Blanco A, Pourdehnad M, Adam LE, Yamamoto AJ, Martinez-Lazaro R, Lee JH, Loman JC, Rossman MD, Alavi A. Do high glucose levels have differential effect on FDG uptake in inflammatory and malignant disorders? *Nucl Med Commun* 2001;**22**(10): 1123-1128.
272. Avril N, Bense S, Ziegler SI, Dose J, Weber W, Laubenbacher C, Romer W, Janicke F, Schwaiger M. Breast imaging with fluorine-18-FDG PET: quantitative image analysis. *J Nucl Med* 1997;**38**(8): 1186-1191.
273. Maschauer S, Prante O, Hoffmann M, Deichen JT, Kuwert T. Characterization of 18F-FDG uptake in human endothelial cells in vitro. *J Nucl Med* 2004;**45**(3): 455-460.
274. DeGrado TR, Baldwin SW, Wang S, Orr MD, Liao RP, Friedman HS, Reiman R, Price DT, Coleman RE. Synthesis and evaluation of (18)F-labeled choline analogs as oncologic PET tracers. *J Nucl Med* 2001;**42**(12): 1805-1814.
275. Hara T. 18F-fluorocholine: a new oncologic PET tracer. *J Nucl Med* 2001;**42**(12): 1815-1817.
276. Boggs KP, Rock CO, Jackowski S. Lysophosphatidylcholine and 1-O-octadecyl-2-O-methyl-rac-glycero-3-phosphocholine inhibit the CDP-choline pathway of phosphatidylcholine synthesis at the CTP:phosphocholine cytidyltransferase step. *The Journal of biological chemistry* 1995;**270**(13): 7757-7764.
277. Haeffner EW. Studies on choline permeation through the plasma membrane and its incorporation into phosphatidyl choline of Ehrlich-Lettre-ascites tumor cells in vitro. *Eur J Biochem* 1975;**51**(1): 219-228.
278. Matter CM, Wyss MT, Meier P, Spath N, von Lukowicz T, Lohmann C, Weber B, Ramirez de Molina A, Lacal JC, Ametamey SM, von Schulthess GK, Luscher TF,

- Kaufmann PA, Buck A. 18F-choline images murine atherosclerotic plaques ex vivo. *Arterioscler Thromb Vasc Biol* 2006;**26**(3): 584-589.
279. Kato K, Schober O, Ikeda M, Schafers M, Ishigaki T, Kies P, Naganawa S, Stegger L. Evaluation and comparison of 11C-choline uptake and calcification in aortic and common carotid arterial walls with combined PET/CT. *Eur J Nucl Med Mol Imaging* 2009;**36**(10): 1622-1628.
280. Velikyan I, Sundberg AL, Lindhe O, Hoglund AU, Eriksson O, Werner E, Carlsson J, Bergstrom M, Langstrom B, Tolmachev V. Preparation and evaluation of (68)Ga-DOTA-hEGF for visualization of EGFR expression in malignant tumors. *J Nucl Med* 2005;**46**(11): 1881-1888.
281. Lundqvist H, Tolmachev V. Targeting peptides and positron emission tomography. *Biopolymers* 2002;**66**(6): 381-392.
282. Ain KB, Taylor KD, Tofiq S, Venkataraman G. Somatostatin receptor subtype expression in human thyroid and thyroid carcinoma cell lines. *The Journal of clinical endocrinology and metabolism* 1997;**82**(6): 1857-1862.
283. Fani M, Andre JP, Maecke HR. 68Ga-PET: a powerful generator-based alternative to cyclotron-based PET radiopharmaceuticals. *Contrast media & molecular imaging* 2008;**3**(2): 67-77.
284. Middendorp M, Selkinski I, Happel C, Kranert WT, Grunwald F. Comparison of positron emission tomography with [(18)F]FDG and [(68)Ga]DOTATOC in recurrent differentiated thyroid cancer: preliminary data. *The quarterly journal of nuclear medicine and molecular imaging : official publication of the Italian Association of Nuclear Medicine* 2010;**54**(1): 76-83.
285. Pool SE, Krenning EP, Koning GA, van Eijck CH, Teunissen JJ, Kam B, Valkema R, Kwekkeboom DJ, de Jong M. Preclinical and clinical studies of peptide receptor radionuclide therapy. *Seminars in nuclear medicine* 2010;**40**(3): 209-218.
286. Rodrigues M, Traub-Weidinger T, Leimer M, Li S, Andreae F, Angelberger P, Dudczak R, Virgolini I. Value of 111In-DOTA-lanreotide and 111In-DOTA-DPhe1-Tyr3-octreotide in differentiated thyroid cancer: results of in vitro binding studies and in vivo comparison with 18F-FDG PET. *Eur J Nucl Med Mol Imaging* 2005;**32**(10): 1144-1151.
287. Rizzello A, Di Pierro D, Lodi F, Trespidi S, Cicoria G, Pancaldi D, Nanni C, Marengo M, Marzola MC, Al-Nahhas A, Rubello D, Boschi S. Synthesis and quality control of 68Ga citrate for routine clinical PET. *Nucl Med Commun* 2009;**30**(7): 542-545.
288. Bird JL, Izquierdo-Garcia D, Davies JR, Rudd JH, Probst KC, Figg N, Clark JC, Weissberg PL, Davenport AP, Warburton EA. Evaluation of translocator protein quantification as a tool for characterising macrophage burden in human carotid atherosclerosis. *Atherosclerosis* 2010;**210**(2): 388-391.
289. Tegler G, Sorensen J, Ericson K, Bjorck M, Wanhainen A. 4D-PET/CT with [(11)C]-PK11195 and [(11)C]-(D)-deprenyl does not identify the chronic inflammation in asymptomatic abdominal aortic aneurysms. *Eur J Vasc Endovasc Surg* 2013;**45**(4): 351-356.
290. Pugliese F, Gaemperli O, Kinderlerer AR, Lamare F, Shalhoub J, Davies AH, Rimoldi OE, Mason JC, Camici PG. Imaging of vascular inflammation with [11C]-PK11195 and positron emission tomography/computed tomography angiography. *J Am Coll Cardiol* 2010;**56**(8): 653-661.
291. Tahara N, Mukherjee J, de Haas HJ, Petrov AD, Tawakol A, Haider N, Tahara A, Constantinescu CC, Zhou J, Boersma HH, Imaizumi T, Nakano M, Finn A, Fayad Z,

- Virmani R, Fuster V, Bosca L, Narula J. 2-deoxy-2-[F]fluoro-d-mannose positron emission tomography imaging in atherosclerosis. *Nat Med*.
292. Tahara N, Mukherjee J, de Haas HJ, Petrov AD, Tawakol A, Haider N, Tahara A, Constantinescu CC, Zhou J, Boersma HH, Imaizumi T, Nakano M, Finn A, Fayad Z, Virmani R, Fuster V, Bosca L, Narula J. 2-deoxy-2-[(18)F]fluoro-d-mannose positron emission tomography imaging in atherosclerosis. *Nature medicine* 2014;**20**(2): 215-219.
293. Hartung D, Petrov A, Haider N, Fujimoto S, Blankenberg F, Fujimoto A, Virmani R, Kolodgie FD, Strauss HW, Narula J. Radiolabeled Monocyte Chemoattractant Protein 1 for the detection of inflammation in experimental atherosclerosis. *J Nucl Med* 2007;**48**(11): 1816-1821.
294. Kelly KA, Allport JR, Tsourkas A, Shinde-Patil VR, Josephson L, Weissleder R. Detection of vascular adhesion molecule-1 expression using a novel multimodal nanoparticle. *Circ Res* 2005;**96**(3): 327-336.
295. Nahrendorf M, Jaffer FA, Kelly KA, Sosnovik DE, Aikawa E, Libby P, Weissleder R. Noninvasive vascular cell adhesion molecule-1 imaging identifies inflammatory activation of cells in atherosclerosis. *Circulation* 2006;**114**(14): 1504-1511.
296. Broisat A, Hernot S, Toczek J, De Vos J, Riou LM, Martin S, Ahmadi M, Thielens N, Wernery U, Cavelliers V, Muyldermans S, Lahoutte T, Fagret D, Ghezzi C, Devoogdt N. Nanobodies targeting mouse/human VCAM1 for the nuclear imaging of atherosclerotic lesions. *Circ Res* 2012;**110**(7): 927-937.
297. Ishino S, Mukai T, Kuge Y, Kume N, Ogawa M, Takai N, Kamihashi J, Shiomi M, Minami M, Kita T, Saji H. Targeting of lectinlike oxidized low-density lipoprotein receptor 1 (LOX-1) with 99mTc-labeled anti-LOX-1 antibody: potential agent for imaging of vulnerable plaque. *J Nucl Med* 2008;**49**(10): 1677-1685.
298. Nishigori K, Temma T, Yoda K, Onoe S, Kondo N, Shiomi M, Ono M, Saji H. Radioiodinated peptide probe for selective detection of oxidized low density lipoprotein in atherosclerotic plaques. *Nucl Med Biol* 2013;**40**(1): 97-103.
299. Fujimoto S, Hartung D, Ohshima S, Edwards DS, Zhou J, Yalamanchili P, Azure M, Fujimoto A, Isobe S, Matsumoto Y, Boersma H, Wong N, Yamazaki J, Narula N, Petrov A, Narula J. Molecular imaging of matrix metalloproteinase in atherosclerotic lesions: resolution with dietary modification and statin therapy. *J Am Coll Cardiol* 2008;**52**(23): 1847-1857.
300. Kaijzel EL, van Heijningen PM, Wielopolski PA, Vermeij M, Koning GA, van Cappellen WA, Que I, Chan A, Dijkstra J, Ramnath NW, Hawinkels LJ, Bernsen MR, Lowik CW, Essers J. Multimodality imaging reveals a gradual increase in matrix metalloproteinase activity at aneurysmal lesions in live fibulin-4 mice. *Circulation Cardiovascular imaging* 2010;**3**(5): 567-577.
301. Amirbekian V, Aguinaldo JG, Amirbekian S, Hyafil F, Vucic E, Sirol M, Weinreb DB, Le Greneur S, Lancelot E, Corot C, Fisher EA, Galis ZS, Fayad ZA. Atherosclerosis and matrix metalloproteinases: experimental molecular MR imaging in vivo. *Radiology* 2009;**251**(2): 429-438.
302. Razavian M, Zhang J, Nie L, Tavakoli S, Razavian N, Dobrucki LW, Sinusas AJ, Edwards DS, Azure M, Sadeghi MM. Molecular imaging of matrix metalloproteinase activation to predict murine aneurysm expansion in vivo. *Journal of nuclear medicine : official publication, Society of Nuclear Medicine* 2010;**51**(7): 1107-1115.
303. Haider N, Hartung D, Fujimoto S, Petrov A, Kolodgie FD, Virmani R, Ohshima S, Liu H, Zhou J, Fujimoto A, Tahara A, Hofstra L, Narula N, Reutelingsperger C, Narula J. Dual molecular imaging for targeting metalloproteinase activity and apoptosis

- in atherosclerosis: molecular imaging facilitates understanding of pathogenesis. *J Nucl Cardiol* 2009;**16**(5): 753-762.
304. Klink A, Hyafil F, Rudd J, Faries P, Fuster V, Mallat Z, Meilhac O, Mulder WJ, Michel JB, Ramirez F, Storm G, Thompson R, Turnbull IC, Egado J, Martin-Ventura JL, Zaragoza C, Letourneur D, Fayad ZA. Diagnostic and therapeutic strategies for small abdominal aortic aneurysms. *Nature reviews Cardiology* 2011;**8**(6): 338-347.
305. Isobe S, Tsimikas S, Zhou J, Fujimoto S, Sarai M, Branks MJ, Fujimoto A, Hofstra L, Reutelingsperger CP, Murohara T, Virmani R, Kolodgie FD, Narula N, Petrov A, Narula J. Noninvasive imaging of atherosclerotic lesions in apolipoprotein E-deficient and low-density-lipoprotein receptor-deficient mice with annexin A5. *J Nucl Med* 2006;**47**(9): 1497-1505.
306. Burtea C, Laurent S, Lancelot E, Ballet S, Murariu O, Rousseaux O, Port M, Vander Elst L, Corot C, Muller RN. Peptidic targeting of phosphatidylserine for the MRI detection of apoptosis in atherosclerotic plaques. *Mol Pharm* 2009;**6**(6): 1903-1919.
307. Moreno PR, Purushothaman KR, Fuster V, Echeverri D, Trusczyńska H, Sharma SK, Badimon JJ, O'Connor WN. Plaque neovascularization is increased in ruptured atherosclerotic lesions of human aorta: implications for plaque vulnerability. *Circulation* 2004;**110**(14): 2032-2038.
308. Haubner R, Weber WA, Beer AJ, Vabuliene E, Reim D, Sarbia M, Becker KF, Goebel M, Hein R, Wester HJ, Kessler H, Schwaiger M. Noninvasive visualization of the activated $\alpha v \beta 3$ integrin in cancer patients by positron emission tomography and [^{18}F]Galacto-RGD. *PLoS Med* 2005;**2**(3): e70.
309. Saraste A, Laitinen I, Weidl E, Wildgruber M, Weber AW, Nekolla SG, Holzlwimmer G, Esposito I, Walch A, Leppanen P, Lisinen I, Lippa PB, Yla-Herttuala S, Wester HJ, Knuuti J, Schwaiger M. Diet intervention reduces uptake of $\alpha v \beta 3$ integrin-targeted PET tracer ^{18}F -galacto-RGD in mouse atherosclerotic plaques. *J Nucl Cardiol* 2012;**19**(4): 775-784.
310. Tedesco MM, Terashima M, Blankenberg FG, Levashova Z, Spin JM, Backer MV, Backer JM, Sho M, Sho E, McConnell MV, Dalman RL. Analysis of in situ and ex vivo vascular endothelial growth factor receptor expression during experimental aortic aneurysm progression. *Arteriosclerosis, thrombosis, and vascular biology* 2009;**29**(10): 1452-1457.
311. Gawaz M, Konrad I, Hauser AI, Sauer S, Li Z, Wester HJ, Bengel FM, Schwaiger M, Schomig A, Massberg S, Haubner R. Non-invasive imaging of glycoprotein VI binding to injured arterial lesions. *Thrombosis and haemostasis* 2005;**93**(5): 910-913.
312. Dweck MR, Chow MW, Joshi NV, Williams MC, Jones C, Fletcher AM, Richardson H, White A, McKillop G, van Beek EJ, Boon NA, Rudd JH, Newby DE. Coronary arterial ^{18}F -sodium fluoride uptake: a novel marker of plaque biology. *J Am Coll Cardiol* 2012;**59**(17): 1539-1548.
313. Thie JA. Understanding the standardized uptake value, its methods, and implications for usage. *J Nucl Med* 2004;**45**(9): 1431-1434.
314. Eckelman WC, Tatum JL, Kurdziel KA, Croft BY. Quantitative analysis of tumor biochemistry using PET and SPECT. *Nucl Med Biol* 2000;**27**(7): 633-635.
315. Boucek JA, Francis RJ, Jones CG, Khan N, Turlach BA, Green AJ. Assessment of tumour response with (^{18}F)-fluorodeoxyglucose positron emission tomography using three-dimensional measures compared to SUVmax--a phantom study. *Physics in medicine and biology* 2008;**53**(16): 4213-4230.

316. Rudd JH, Myers KS, Bansilal S, Machac J, Woodward M, Fuster V, Farkouh ME, Fayad ZA. Relationships among regional arterial inflammation, calcification, risk factors, and biomarkers: a prospective fluorodeoxyglucose positron-emission tomography/computed tomography imaging study. *Circulation Cardiovascular imaging* 2009;**2**(2): 107-115.
317. Adams MC, Turkington TG, Wilson JM, Wong TZ. A systematic review of the factors affecting accuracy of SUV measurements. *AJR Am J Roentgenol* 2010;**195**(2): 310-320.
318. Both M, Ahmadi-Simab K, Reuter M, Dourvos O, Fritzer E, Ullrich S, Gross WL, Heller M, Bahre M. MRI and FDG-PET in the assessment of inflammatory aortic arch syndrome in complicated courses of giant cell arteritis. *Annals of the rheumatic diseases* 2008;**67**(7): 1030-1033.
319. Rudd JH, Hyafil F, Fayad ZA. Inflammation imaging in atherosclerosis. *Arterioscler Thromb Vasc Biol* 2009;**29**(7): 1009-1016.
320. Bucierius J, Mani V, Moncrieff C, Machac J, Fuster V, Farkouh ME, Tawakol A, Rudd JH, Fayad ZA. Optimizing (18)F-FDG PET/CT imaging of vessel wall inflammation: the impact of (18)F-FDG circulation time, injected dose, uptake parameters, and fasting blood glucose levels. *European journal of nuclear medicine and molecular imaging* 2014;**41**(2): 369-383.
321. Thie JA. A simple interpretation of fractal analysis of images. *Journal of nuclear medicine : official publication, Society of Nuclear Medicine* 2004;**45**(4): 724.
322. Hoffman EJ, Huang SC, Phelps ME. Quantitation in positron emission computed tomography: 1. Effect of object size. *J Comput Assist Tomogr* 1979;**3**(3): 299-308.
323. Astrand H, Ryden-Ahlgren A, Sandgren T, Lanne T. Age-related increase in wall stress of the human abdominal aorta: an in vivo study. *J Vasc Surg* 2005;**42**(5): 926-931.
324. Johansson G, Nydahl S, Olofsson P, Swedenborg J. Survival in patients with abdominal aortic aneurysms. Comparison between operative and nonoperative management. *European journal of vascular surgery* 1990;**4**(5): 497-502.
325. Sterpetti AV, Cavallaro A, Cavallari N, Allegrucci P, Tamburelli A, Agosta F, Bartoli S. Factors influencing the rupture of abdominal aortic aneurysms. *Surgery, gynecology & obstetrics* 1991;**173**(3): 175-178.
326. Fillinger MF, Marra SP, Raghavan ML, Kennedy FE. Prediction of rupture risk in abdominal aortic aneurysm during observation: wall stress versus diameter. *J Vasc Surg* 2003;**37**(4): 724-732.
327. Lindholt JS, Vammen S, Fasting H, Henneberg EW, Heickendorff L. The plasma level of matrix metalloproteinase 9 may predict the natural history of small abdominal aortic aneurysms. A preliminary study. *Eur J Vasc Endovasc Surg* 2000;**20**(3): 281-285.
328. Schirmer M, Duftner C, Seiler R, Dejaco C, Fraedrich G. Abdominal aortic aneurysms: an underestimated type of immune-mediated large vessel arteritis? *Current opinion in rheumatology* 2006;**18**(1): 48-53.
329. Tawakol A, Migrino RQ, Hoffmann U, Abbara S, Houser S, Gewirtz H, Muller JE, Brady TJ, Fischman AJ. Noninvasive in vivo measurement of vascular inflammation with F-18 fluorodeoxyglucose positron emission tomography. *J Nucl Cardiol* 2005;**12**(3): 294-301.
330. Sakalihasan N, Hustinx R, Limet R. Contribution of PET scanning to the evaluation of abdominal aortic aneurysm. *Semin Vasc Surg* 2004;**17**(2): 144-153.

331. von Schulthess GK, Steinert HC, Hany TF. Integrated PET/CT: current applications and future directions. *Radiology* 2006;**238**(2): 405-422.
332. Sayed S, Choke E, Helme S, Dawson J, Morgan R, Belli A, Loosemore T, Thompson MM. Endovascular stent graft repair of mycotic aneurysms of the thoracic aorta. *The Journal of cardiovascular surgery* 2005;**46**(2): 155-161.
333. Kuehl H, Eggebrecht H, Boes T, Antoch G, Rosenbaum S, Ladd S, Bockisch A, Barkhausen J, Erbel R. Detection of inflammation in patients with acute aortic syndrome: comparison of FDG-PET/CT imaging and serological markers of inflammation. *Heart* 2008;**94**(11): 1472-1477.
334. Rappeport ED, Loft A, Berthelsen AK, von der Recke P, Larsen PN, Mogensen AM, Wettergren A, Rasmussen A, Hillingsoe J, Kirkegaard P, Thomsen C. Contrast-enhanced FDG-PET/CT vs. SPIO-enhanced MRI vs. FDG-PET vs. CT in patients with liver metastases from colorectal cancer: a prospective study with intraoperative confirmation. *Acta radiologica* 2007;**48**(4): 369-378.
335. Takahashi M, Momose T, Kameyama M, Ohtomo K. Abnormal accumulation of [18F]fluorodeoxyglucose in the aortic wall related to inflammatory changes: three case reports. *Ann Nucl Med* 2006;**20**(5): 361-364.
336. Baud JM, Mas D, Pichot O, Laroche JP, Viard A, Crevillier M, Giraud M, Ledemey M. [Criteria for quantification and characterization of aneurysms of the abdominal aorta using ultrasonography. The AFFCA study. French Association of Continuous Education in Angiology]. *Journal des maladies vasculaires* 1997;**22**(5): 313-320.
337. Mochizuki T, Tsukamoto E, Kuge Y, Kanegae K, Zhao S, Hikosaka K, Hosokawa M, Kohanawa M, Tamaki N. FDG uptake and glucose transporter subtype expressions in experimental tumor and inflammation models. *J Nucl Med* 2001;**42**(10): 1551-1555.
338. Bergqvist D. Management of small abdominal aortic aneurysms. *Br J Surg* 1999;**86**(4): 433-434.
339. Baxter BT, Terrin MC, Dalman RL. Medical management of small abdominal aortic aneurysms. *Circulation* 2008;**117**(14): 1883-1889.
340. Fillinger M. Who should we operate on and how do we decide: predicting rupture and survival in patients with aortic aneurysm. *Semin Vasc Surg* 2007;**20**(2): 121-127.
341. McMillan WD, Pearce WH. Inflammation and cytokine signaling in aneurysms. *Annals of vascular surgery* 1997;**11**(5): 540-545.
342. Ogawa M, Magata Y, Kato T, Hatano K, Ishino S, Mukai T, Shiomi M, Ito K, Saji H. Application of 18F-FDG PET for monitoring the therapeutic effect of anti-inflammatory drugs on stabilization of vulnerable atherosclerotic plaques. *J Nucl Med* 2006;**47**(11): 1845-1850.
343. Rudd JH, Elkhawad M, Fayad ZA. Vascular imaging with 18F-FDG PET/CT: optimal 18F-FDG circulation time? *Journal of nuclear medicine : official publication, Society of Nuclear Medicine* 2009;**50**(9): 1560; author reply 1560-1561.
344. Tahara N, Imaizumi T, Virmani R, Narula J. Clinical feasibility of molecular imaging of plaque inflammation in atherosclerosis. *J Nucl Med* 2009;**50**(3): 331-334.
345. Blockmans D, Stroobants S, Maes A, Mortelmans L. Positron emission tomography in giant cell arteritis and polymyalgia rheumatica: evidence for inflammation of the aortic arch. *Am J Med* 2000;**108**(3): 246-249.
346. The NHS AAA Screening Programme Annual Report, 2009-10. http://aaa.screening.nhs.uk/annual_report. [November 1 2013].

347. Thapar A, Cheal D, Hopkins T, Ward S, Shalhoub J, Yusuf SW. Internal or external wall diameter for abdominal aortic aneurysm screening? *Annals of the Royal College of Surgeons of England* 2010;**92**(6): 503-505.
348. Menezes LJ, Kotze CW, Hutton BF, Endozo R, Dickson JC, Cullum I, Yusuf SW, Ell PJ, Groves AM. Vascular inflammation imaging with 18F-FDG PET/CT: when to image? *Journal of nuclear medicine : official publication, Society of Nuclear Medicine* 2009;**50**(6): 854-857.
349. Rudd JH, Narula J, Strauss HW, Virmani R, Machac J, Klimas M, Tahara N, Fuster V, Warburton EA, Fayad ZA, Tawakol AA. Imaging atherosclerotic plaque inflammation by fluorodeoxyglucose with positron emission tomography: ready for prime time? *J Am Coll Cardiol* 2010;**55**(23): 2527-2535.
350. Shankar LK, Hoffman JM, Bacharach S, Graham MM, Karp J, Lammertsma AA, Larson S, Mankoff DA, Siegel BA, Van den Abbeele A, Yap J, Sullivan D. Consensus recommendations for the use of 18F-FDG PET as an indicator of therapeutic response in patients in National Cancer Institute Trials. *J Nucl Med* 2006;**47**(6): 1059-1066.
351. Chaikof EL, Brewster DC, Dalman RL, Makaroun MS, Illig KA, Sicard GA, Timaran CH, Upchurch GR, Jr., Veith FJ, Society for Vascular S. The care of patients with an abdominal aortic aneurysm: the Society for Vascular Surgery practice guidelines. *J Vasc Surg* 2009;**50**(4 Suppl): S2-49.
352. Kotze CW, Menezes LJ, Endozo R, Groves AM, Ell PJ, Yusuf SW. Increased metabolic activity in abdominal aortic aneurysm detected by 18F-fluorodeoxyglucose (18F-FDG) positron emission tomography/computed tomography (PET/CT). *Eur J Vasc Endovasc Surg* 2009;**38**(1): 93-99.
353. Truijers M, Kurvers HA, Bredie SJ, Oyen WJ, Blankensteijn JD. In vivo imaging of abdominal aortic aneurysms: increased FDG uptake suggests inflammation in the aneurysm wall. *Journal of endovascular therapy : an official journal of the International Society of Endovascular Specialists* 2008;**15**(4): 462-467.
354. Menezes LJ, Kayani I, Ben-Haim S, Hutton B, Ell PJ, Groves AM. What is the natural history of 18F-FDG uptake in arterial atheroma on PET/CT? Implications for imaging the vulnerable plaque. *Atherosclerosis* 2010;**211**(1): 136-140.
355. Taggart DR, Han MM, Quach A, Groshen S, Ye W, Villablanca JG, Jackson HA, Mari Aparici C, Carlson D, Maris J, Hawkins R, Matthay KK. Comparison of iodine-123 metaiodobenzylguanidine (MIBG) scan and [18F]fluorodeoxyglucose positron emission tomography to evaluate response after iodine-131 MIBG therapy for relapsed neuroblastoma. *J Clin Oncol* 2009;**27**(32): 5343-5349.
356. Zhu AX, Meyerhardt JA, Blaszkowsky LS, Kambadakone AR, Muzikansky A, Zheng H, Clark JW, Abrams TA, Chan JA, Enzinger PC, Bhargava P, Kwak EL, Allen JN, Jain SR, Stuart K, Horgan K, Sheehan S, Fuchs CS, Ryan DP, Sahani DV. Efficacy and safety of gemcitabine, oxaliplatin, and bevacizumab in advanced biliary-tract cancers and correlation of changes in 18-fluorodeoxyglucose PET with clinical outcome: a phase 2 study. *The lancet oncology* 2010;**11**(1): 48-54.
357. Kato K, Nishio A, Kato N, Usami H, Fujimaki T, Murohara T. Uptake of 18F-FDG in acute aortic dissection: a determinant of unfavorable outcome. *Journal of nuclear medicine : official publication, Society of Nuclear Medicine* 2010;**51**(5): 674-681.
358. Reeps C, Pelisek J, Bundschuh RA, Gurdan M, Zimmermann A, Ockert S, Dobritz M, Eckstein HH, Essler M. Imaging of acute and chronic aortic dissection by 18F-FDG PET/CT. *J Nucl Med* 2010;**51**(5): 686-691.

359. Rudd JH, Myers KS, Bansilal S, Machac J, Rafique A, Farkouh M, Fuster V, Fayad ZA. (18)Fluorodeoxyglucose positron emission tomography imaging of atherosclerotic plaque inflammation is highly reproducible: implications for atherosclerosis therapy trials. *J Am Coll Cardiol* 2007;**50**(9): 892-896.
360. Rudd JH, Machac J, Fayad ZA. Simvastatin and plaque inflammation. *J Am Coll Cardiol* 2007;**49**(19): 1991; author reply 1991-1992.
361. Blockmans D, Coudyzer W, Vanderschueren S, Stroobants S, Loeckx D, Heye S, De Ceuninck L, Marchal G, Bobbaers H. Relationship between fluorodeoxyglucose uptake in the large vessels and late aortic diameter in giant cell arteritis. *Rheumatology* 2008;**47**(8): 1179-1184.
362. Speelman L, Bosboom EM, Schurink GW, Buth J, Breeuwer M, Jacobs MJ, van de Vosse FN. Initial stress and nonlinear material behavior in patient-specific AAA wall stress analysis. *J Biomech* 2009;**42**(11): 1713-1719.
363. Tsai TT, Nienaber CA, Eagle KA. Acute aortic syndromes. *Circulation* 2005;**112**(24): 3802-3813.
364. Golledge J, Muller J, Daugherty A, Norman P. Abdominal aortic aneurysm: pathogenesis and implications for management. *Arterioscler Thromb Vasc Biol* 2006;**26**(12): 2605-2613.
365. Kotze CW, Groves AM, Menezes LJ, Harvey R, Endozo R, Kayani IA, Ell PJ, Yusuf SW. What is the relationship between (1)(8)F-FDG aortic aneurysm uptake on PET/CT and future growth rate? *Eur J Nucl Med Mol Imaging* 2011;**38**(8): 1493-1499.
366. Garcia G, Maiora J, Tapia A, De Blas M. Evaluation of texture for classification of abdominal aortic aneurysm after endovascular repair. *J Digit Imaging* 2012;**25**(3): 369-376.
367. Acharya UR, Sree SV, Mookiah MR, Saba L, Gao H, Mallarini G, Suri JS. Computed tomography carotid wall plaque characterization using a combination of discrete wavelet transform and texture features: A pilot study. *Proc Inst Mech Eng H* 2013;**227**(6): 643-654.
368. Ganeshan B, Goh V, Mandeville HC, Ng QS, Hoskin PJ, Miles KA. Non-small cell lung cancer: histopathologic correlates for texture parameters at CT. *Radiology* 2013;**266**(1): 326-336.
369. Ganeshan B, Panayiotou E, Burnand K, Dizdarevic S, Miles K. Tumour heterogeneity in non-small cell lung carcinoma assessed by CT texture analysis: a potential marker of survival. *European radiology* 2012;**22**(4): 796-802.
370. Babikir S GB, Groves A.M, Kayani I. . Texture analysis of Lymphoma on unenhanced computed tomography: initial evidence for a relationship with tumour glucose metabolism, stage, end of treatment status and survival. In: European Society of Radiology. Vienna, Austria.; 2013.
371. Ng F, Ganeshan B, Kozarski R, Miles KA, Goh V. Assessment of primary colorectal cancer heterogeneity by using whole-tumor texture analysis: contrast-enhanced CT texture as a biomarker of 5-year survival. *Radiology* 2013;**266**(1): 177-184.
372. Bezy-Wendling J, Kretowski M, Rolland Y, Le Bidon W. Toward a better understanding of texture in vascular CT scan simulated images. *IEEE Trans Biomed Eng* 2001;**48**(1): 120-124.
373. Ganeshan B, Miles KA, Young RC, Chatwin CR. Hepatic enhancement in colorectal cancer: texture analysis correlates with hepatic hemodynamics and patient survival. *Acad Radiol* 2007;**14**(12): 1520-1530.
374. Ganeshan B, Miles KA, Young RC, Chatwin CR. In search of biologic correlates for liver texture on portal-phase CT. *Acad Radiol* 2007;**14**(9): 1058-1068.

375. Ganeshan B, Abaleke S, Young RC, Chatwin CR, Miles KA. Texture analysis of non-small cell lung cancer on unenhanced computed tomography: initial evidence for a relationship with tumour glucose metabolism and stage. *Cancer Imaging* 2010;**10**: 137-143.
376. Miles KA, Ganeshan B, Hayball MP. CT texture analysis using the filtration-histogram method: what do the measurements mean? *Cancer Imaging* 2013;**13**(3): 400-406.
377. Kakkos SK, Stevens JM, Nicolaides AN, Kyriacou E, Pattichis CS, Geroulakos G, Thomas D. Texture analysis of ultrasonic images of symptomatic carotid plaques can identify those plaques associated with ipsilateral embolic brain infarction. *Eur J Vasc Endovasc Surg* 2007;**33**(4): 422-429.
378. Madycki G, Staszkiwicz W, Gabrusiewicz A. Carotid plaque texture analysis can predict the incidence of silent brain infarcts among patients undergoing carotid endarterectomy. *Eur J Vasc Endovasc Surg* 2006;**31**(4): 373-380.
379. Bural GG, Torigian DA, Chamroonrat W, Alkhalaf K, Houseni M, El-Haddad G, Alavi A. Quantitative assessment of the atherosclerotic burden of the aorta by combined FDG-PET and CT image analysis: a new concept. *Nucl Med Biol* 2006;**33**(8): 1037-1043.
380. Ganeshan B ZZ, Goh VJ, Lambrou T, Engledow A, Rodriguez-Justo J, PeckJ, Meagher M, Shastry M, Taylor SA, Halligan S, Ell PJ, Miles KA, Groves AM. Quantitative imaging biomarkers from PET-CT as potential correlates for angiogenesis and hypoxia in colorectal cancer. In: European Society of Radiology. Vienna, Austria; 2012.
381. Gourtsoyianni S LG, Khan A, Glynne- Jones R, Ganeshan B, Miles K, Goh V. . Reproducibility of MRI texture analysis in primary rectal cancer. In: European Society of Radiology. Vienna, Austria.; 2013.
382. Bjornheden T, Levin M, Evaldsson M, Wiklund O. Evidence of hypoxic areas within the arterial wall in vivo. *Arterioscler Thromb Vasc Biol* 1999;**19**(4): 870-876.
383. Sluimer JC, Daemen MJ. Novel concepts in atherogenesis: angiogenesis and hypoxia in atherosclerosis. *J Pathol* 2009;**218**(1): 7-29.
384. Thompson MM, Jones L, Nasim A, Sayers RD, Bell PR. Angiogenesis in abdominal aortic aneurysms. *Eur J Vasc Endovasc Surg* 1996;**11**(4): 464-469.
385. Ganeshan B, Miles KA. Quantifying tumour heterogeneity with CT. *Cancer Imaging* 2013;**13**: 140-149.
386. Miles KA, Ganeshan B, Griffiths MR, Young RC, Chatwin CR. Colorectal cancer: texture analysis of portal phase hepatic CT images as a potential marker of survival. *Radiology* 2009;**250**(2): 444-452.
387. Bergqvist D. Pharmacological interventions to attenuate the expansion of abdominal aortic aneurysm (AAA) - a systematic review. *Eur J Vasc Endovasc Surg* 2011;**41**(5): 663-667.
388. Goh V, Ganeshan B, Nathan P, Juttla JK, Vinayan A, Miles KA. Assessment of response to tyrosine kinase inhibitors in metastatic renal cell cancer: CT texture as a predictive biomarker. *Radiology* 2011;**261**(1): 165-171.
389. Thubrikar MJ, Labrosse M, Robicsek F, Al-Soudi J, Fowler B. Mechanical properties of abdominal aortic aneurysm wall. *J Med Eng Technol* 2001;**25**(4): 133-142.
390. Rakebrandt F, Crawford DC, Havard D, Coleman D, Woodcock JP. Relationship between ultrasound texture classification images and histology of atherosclerotic plaque. *Ultrasound Med Biol* 2000;**26**(9): 1393-1402.
391. Hovsepian DM, Ziporin SJ, Sakurai MK, Lee JK, Curci JA, Thompson RW. Elevated plasma levels of matrix metalloproteinase-9 in patients with abdominal aortic

- aneurysms: a circulating marker of degenerative aneurysm disease. *J Vasc Interv Radiol* 2000;**11**(10): 1345-1352.
392. Juvonen J, Surcel HM, Satta J, Teppo AM, Bloigu A, Syrjala H, Airaksinen J, Leinonen M, Saikku P, Juvonen T. Elevated circulating levels of inflammatory cytokines in patients with abdominal aortic aneurysm. *Arterioscler Thromb Vasc Biol* 1997;**17**(11): 2843-2847.
393. Petersen E, Gineitis A, Wagberg F, Angquist KA. Serum levels of elastin-derived peptides in patients with ruptured and asymptomatic abdominal aortic aneurysms. *Eur J Vasc Endovasc Surg* 2001;**22**(1): 48-52.
394. Golledge J, Tsao PS, Dalman RL, Norman PE. Circulating markers of abdominal aortic aneurysm presence and progression. *Circulation* 2008;**118**(23): 2382-2392.
395. Tahara N, Kai H, Yamagishi S, Mizoguchi M, Nakaura H, Ishibashi M, Kaida H, Baba K, Hayabuchi N, Imaizumi T. Vascular inflammation evaluated by [18F]-fluorodeoxyglucose positron emission tomography is associated with the metabolic syndrome. *J Am Coll Cardiol* 2007;**49**(14): 1533-1539.
396. Domanovits H, Schillinger M, Mullner M, Holzenbein T, Janata K, Bayegan K, Laggner AN. Acute phase reactants in patients with abdominal aortic aneurysm. *Atherosclerosis* 2002;**163**(2): 297-302.
397. Eugster T, Huber A, Obeid T, Schwegler I, Gurke L, Stierli P. Aminoterminal propeptide of type III procollagen and matrix metalloproteinases-2 and -9 failed to serve as serum markers for abdominal aortic aneurysm. *Eur J Vasc Endovasc Surg* 2005;**29**(4): 378-382.
398. Freestone T, Turner RJ, Coady A, Higman DJ, Greenhalgh RM, Powell JT. Inflammation and matrix metalloproteinases in the enlarging abdominal aortic aneurysm. *Arterioscler Thromb Vasc Biol* 1995;**15**(8): 1145-1151.
399. Norman P, Spencer CA, Lawrence-Brown MM, Jamrozik K. C-reactive protein levels and the expansion of screen-detected abdominal aortic aneurysms in men. *Circulation* 2004;**110**(7): 862-866.
400. Lindholt JS, Erlandsen EJ, Henneberg EW. Cystatin C deficiency is associated with the progression of small abdominal aortic aneurysms. *Br J Surg* 2001;**88**(11): 1472-1475.
401. De Haro J, Acin F, Bleda S, Varela C, Medina FJ, Esparza L. Prediction of asymptomatic abdominal aortic aneurysm expansion by means of rate of variation of C-reactive protein plasma levels. *J Vasc Surg* 2012;**56**(1): 45-52.
402. Vainas T. Serum C-Reactive Protein Level Is Associated With Abdominal Aortic Aneurysm Size and May Be Produced by Aneurysmal Tissue. *Circulation* 2003;**107**(8): 1103-1105.
403. Libby P. Inflammation in atherosclerosis. *Nature* 2002;**420**(6917): 868-874.
404. Libby P, Sukhova G, Lee RT, Galis ZS. Cytokines regulate vascular functions related to stability of the atherosclerotic plaque. *J Cardiovasc Pharmacol* 1995;**25** Suppl 2: S9-12.
405. King VL, Lin AY, Kristo F, Anderson TJ, Ahluwalia N, Hardy GJ, Owens AP, 3rd, Howatt DA, Shen D, Tager AM, Luster AD, Daugherty A, Gerszten RE. Interferon-gamma and the interferon-inducible chemokine CXCL10 protect against aneurysm formation and rupture. *Circulation* 2009;**119**(3): 426-435.
406. Shapiro SD, Campbell EJ, Kobayashi DK, Welgus HG. Immune modulation of metalloproteinase production in human macrophages. Selective pretranslational suppression of interstitial collagenase and stromelysin biosynthesis by interferon-gamma. *J Clin Invest* 1990;**86**(4): 1204-1210.

407. Xie B, Dong Z, Fidler IJ. Regulatory mechanisms for the expression of type IV collagenases/gelatinases in murine macrophages. *J Immunol* 1994;**152**(7): 3637-3644.
408. Amento EP, Ehsani N, Palmer H, Libby P. Cytokines and growth factors positively and negatively regulate interstitial collagen gene expression in human vascular smooth muscle cells. *Arterioscler Thromb* 1991;**11**(5): 1223-1230.
409. Li X, Samnick S, Lapa C, Israel I, Buck AK, Kreissl MC, Bauer W. 68Ga-DOTATATE PET/CT for the detection of inflammation of large arteries: correlation with 18F-FDG, calcium burden and risk factors. *EJNMMI research* 2012;**2**(1): 52.
410. Ohtsuka T, Hamada M, Hiasa G, Sasaki O, Suzuki M, Hara Y, Shigematsu Y, Hiwada K. Effect of beta-blockers on circulating levels of inflammatory and anti-inflammatory cytokines in patients with dilated cardiomyopathy. *J Am Coll Cardiol* 2001;**37**(2): 412-417.
411. Peng H, Carretero OA, Vuljaj N, Liao TD, Motivala A, Peterson EL, Rhaleb NE. Angiotensin-converting enzyme inhibitors: a new mechanism of action. *Circulation* 2005;**112**(16): 2436-2445.
412. Glasser SP, Selwyn AP, Ganz P. Atherosclerosis: risk factors and the vascular endothelium. *American heart journal* 1996;**131**(2): 379-384.
413. Asthana A, Johnson HM, Piper ME, Fiore MC, Baker TB, Stein JH. Effects of smoking intensity and cessation on inflammatory markers in a large cohort of active smokers. *American heart journal* 2010;**160**(3): 458-463.
414. Hastie CE, Haw S, Pell JP. Impact of smoking cessation and lifetime exposure on C-reactive protein. *Nicotine Tob Res* 2008;**10**(4): 637-642.
415. Rahman MS, Storrar N, Anderson LJ. FDG-PET/CT in the diagnosis of aortitis in fever of unknown origin with severe aortic incompetence. *Heart* 2013;**99**(6): 435-436.